Lost in Starvation: How the interplay between physiology and ecology impacts bacterial persistence in a patchy landscape

by

Elise Ledieu-Dherbécourt

Master of Engineering, École supérieure d'électricité (2015)
Master of Science, Eidgenössische Technische Hochschule Zürich (2015)

Submitted to the Department of Civil and Environmental Engineering
in partial fulfillment of the requirements for the degree of

Doctor of Philosophy in Civil and Environmental Engineering

at the

MASSACHUSETTS INSTITUTE OF TECHNOLOGY

September 2022

Author .....
Department of Civil and Environmental Engineering
August 12, 2022

Certified by .....
Otto X. Cordero
Associate Professor
Thesis Supervisor

Accepted by .....
Colette L. Heald
Professor of Civil and Environmental Engineering
Chairman, Graduate Program Committee

Lost in Starvation: How the interplay between physiology and ecology impacts bacterial persistence in a patchy landscape

by

Elise Ledieu-Dherbécourt

Submitted to the Department of Civil and Environmental Engineering
on August 12, 2022, in partial fulfillment of the
requirements for the degree of
Doctor of Philosophy in Civil and Environmental Engineering

Abstract

Heterotrophic marine bacteria navigate a heterogeneous landscape of resources. Bacterial populations cycle through periods of feasting when attached to nutrient particles and periods of famine when foraging between hotspots; thus, bacterial physiological states and ecological processes are intertwined. The stress response to nutrient limitation appears within three hours, while the encounter time to new particles has been estimated to happen on the scale of days. Therefore, it is unclear how the phenotypic changes undergone by bacteria during starvation affect their ability to search for and acquire nutrients. Here, we quantified the physiological responses of the marine heterotroph *Vibrio coralliilyticus* to carbon and nitrogen starvation and its subsequent success at foraging in a landscape of resource particles. We compare the foraging success of different bacterial populations in terms of the minimum number of particles needed for ten percent of such a population to encounter any particle. We parametrize a model of bacterial foraging during starvation superposing multiple Poisson processes using measurements of viability, motility, attachment, and renewed growth observed for *Vibrio coralliilyticus* over several days of carbon and nitrogen limitation. We find that motility loss, bacterial persistence, and reductive cellular division are key behaviours determining foraging success. While motility loss increases the number of particles required for successful foraging in a population, bacterial persistence relaxes that constraint. Heightened reductive division accelerates the speed at which the first ten percent of the initial bacterial population achieves a particle encounter. This work provides a quantitative estimate of the influence of nutrient-limited phenotypes on bacterial foraging success in a marine environment.

Thesis Supervisor: Otto X. Cordero
Title: Associate Professor

La douleur me guette, tapie dans mon futur, camouflée dans les souvenirs ; elle m'attend pour me trapper mais je la contournerai et me défendrai hardiment. Je chasserai de moi jusqu'à la moindre image. Mais sous les cendres, l'inévitable espérance tiendra bon. Je ne sais d'où viendra le souffle qui l'attisera. Je ne sais vers quoi elle me poussera. Je la sens. Dans mon ensevelissement je la sens. Indistincte, informe, impalpable mais présente. Je me retire en moi mais je n'y mourrai pas.

Excerpt of Elise ou la vraie vie by Claire Etcherelli

Pour René et Marie-Louise

Pour Lara

Acknowledgments

First and foremost, I want to thank my PI, Otto Cordero, for giving me the opportunity to embark on this adventure. You have given me a precious space to grow as a scientist and explore the fascinating world of microbial ecology. I also want to acknowledge the dedicated time and helpful feedback by all my committee members across the years, in particular by Jeff Gore, Martin Polz, Katharina Ribbeck, Andrew Babbin, and my committee chair, Mick Follows.

This thesis would not have seen the light of days, if it was not for the critical feedback of Julia Schwartzman, for the corrections of Rachel Szabo, Rachel Gregor, Patrizia Stadler and Matti Grakla, for the well-timed coffees with Gabriel Leventhal, and for the many pieces of advice of Manoshi Datta. I have had the privilege to be surrounded by many great scientists in the last seven years in the Cordero lab. Thank you to all the past and present lab members for building such a vibrant community: Tim Enke, Lei Ma, XiaoYu Shan, Rachel Szabo, Annika Gomez, Gabriel Vercelli, Teja Jammalamadaka, Manoshi Datta, Gabriel Leventhal, Rachel Gregor, Leonora Bittleson, Shaul Pollak, Matti Gralka, Stefany Moreno Gamez, Akshit Goyal, Andreas Sichert, Ali Ebrahimi, Julia Schwartzman, Patrizia Stadler, Jose Saavedra, Matthew Metzger, Luis Valentin, Lu Lu, Philip Wasson, Tao Wu, Yuya Sato, Julien Barrere, Désirée Schmitz, Jingqiu Liao, Craig McLean, Jakob Russel, Lauren McLean, Denise Stewart. I also want to reckognize the work of Lauren, Denise, Jose, and Patti for enabling us to do our best science.

This work has been nourished by the many interactions mediated by the PriME collaboration, supported by the Simons Foundation. Special thanks to Johannes Keegstra for many discussions and his enthusiasm for this research question ; Tolga Caglar, Ben Roller, Noelle Norris, Jonasz Slomka for their feedback and help on this project. I also want to acknowledge my collaborators within MIT for providing me with their expertise in new techniques and discplines: Nate Cermak, Scott Manalis and especially Yanqi Wu; Rami Abi-Akl and Tal Cohen.

As a graduate student, I was fortunate enough to attend classes by Alan Grossman,

Greg Fournier, Daniel Rothman, Dave Des Marais, and Serguei Saavedra. These lectures were candy for the brain. I'll also fondly remember being a teaching assistant for Prof. Harry Hemond. Thank you all!

It takes a village to make a thesis a reality: I am grateful for all the support of the administrators in the Civil and Engineering department of MIT. Special thanks to Jay Matthews, Eileen Covey, Kiley Clapper, Sarah Smith, Max Martelli, and John McFarlane. The friendly faces of Parsons, Pierce and other MIT/Harvard buildings were a reason to go to work everyday: thank you to Adam, Affi, Aimee, Akshay, Alexandre, Allie, Ana, Anastasia, Andrew, Anne, Benjamin, Beth, Brad, Charles, Charlotte, Chika, Dana, Danielle, Davide, Eeshan, Estelle, Francisco, Gonzo, Halina, Harry, Hayley, Isabelle, Ishan, Jackie, Jean, Joleen, Josh, Jérome, Katya, KellyAnn, Kerrin, Kevin, Laélia, Layla, Lena, Lily, Lucie, Malivai, Martin, Mason, Michel, Miles, Moni, Morgan, Neo, Rami, Raphael, Ray, Richard, Rim, Sarah, Saviz, Shahd, Sid, Sophie, Stefan, Sébastien, Tanush, Victor, Vie and, of course, to the French crew: Marianne, Julien, Baptiste, Maxime, Timothée. I also had the privilege of meeting extraordinary people across MIT through my involvement in extracurricular activities. Thanks to the teams of the European Club, MIT Off-Campus Housing, the French Club, the Muddy Charles and especially the REFS community. It was rewarding to learn and work alongside you.

I found the fighting spirit needed to complete this thesis in the many sports I practiced during my time in Boston. I am especially obliged to my coaches (Sima in waterpolo ; Tony and Max in volleyball ; Amir, Flavi, and Bruna in team handball ; Christine, Glenn, and John in rowing) for showing me that leadership can take many different forms. You have pushed me to become better one practice at a time. Shout-out to my amazing teammates with whom I have shared sweat, tears, dance moves, and laughters. I appreciate y'all from the Boston Team Handball family, from the MIT Women Volleyball Club, and from the MIT Rowing club travelling crews.

I also want to acknowledge the impact of the people I met along the way: thanks to my roommates (Simon, Affi, Mansi, Nielsen, Jeremy, Nicolas, Alex, Brendan, Seth, Olivia) for creating many little homes with me ; Anne and Zaza for being a safe space

in dire times ; the Watertown crew (Olivia, Joe, Justin, Ryan) for being a peaceful retreat ; Nick for his support at the finish line.

I am also so grateful to have found my special people here in Boston: Sam Turton for growing wiser together, Rachel Szabo for personifying ineffable heart, Simon Batzner for chilling, Tanush Jagdish for being a kindred soul, Leilani Gilpin for being my forever captain, Muriel Rambeloarison for vibing in parallel conversations, Marianne Acker for being a fellow life adventurer, Timothée Jamin for being a thoughtful devil's advocate, Benjamin Jacot for honouring me with the title of friend. *A vous, je ne dis rien, car vous savez déjà tout.* I thank you all so much for being amazing partners in this grad school journey. You made this whole experience worth it.

I also want to thank the family I choose over and over again. Your support throughout the years has been a source of joy and strength. Ania, Shirou, Mémo, Régi, Mathieu, Sarah, Odile D, Claire, Laureline, Valériane, Odile P, Léonard, Jordan, Louise, Vincent, Marc, Réa, Bertrand, Ginie : You keep showing me that friendship transcends time, space, and oceans.

I would not have done any of this without the love and support of my family, especially my very cool mother, Kiki, and my very swell brother, Titus. Thank you for being beacons of resilience. There is never a dull moment with you around. I also want to thank my grandparents, Pépé, Mémé, and Mamie for teaching me how to appreciate the simple joys of life ; my parents for, each in their own ways, pushing me towards new intellectual horizons ; my parrain Christian and my aunt Brigitte for all the gut-wrenching belly laughters.

Finally, to you, the reader of this thesis, thank you. My work will not have been in vain.

Contents

List of Figures

List of Tables

Chapter 1

Introduction

1.1 Background

1.1.1 Marine bacteria live in patchy landscapes

The different scales of patchiness

As microbes live in a natural environment, notably in the oceans, they experience a set of conditions specific to their localization. On a worldwide scale, oceans present a heterogeneous distribution of resources that arise from biogeochemical cycles and physical properties. Global phenomena such as ocean acidification exhibit spatial and temporal patterning due to water circulation and seasonal changes in biochemical processes, for example, affected by temperature [39]. These large-scale variations create gradients of nutrients that constrain the bacterial life observed within each body of water. Microbes then exhibit growth and perform certain functions such as primary production and bacterial secondary production given their surrounding nutritional space. For example, productivity in some of the mixed layer in the Atlantic ocean is primarily limited by nitrogen, due to the low concentrations of nitrate [115]. Resource heterogeneity creates different milieus to which microbes need to adapt.

These different physicochemical conditions in oceans have been extensively sampled on different spatial and temporal scales. Their association with biological data casts light on the diverse roles of oceanic microbial life and their efficiency at fulfilling

their function [37]. The horizontal resolution of biological measurements coupled with geochemical variables is on the order of magnitude of kilometers or tens of meters in the best-case scenario with a sample size for biological data of the order of liters. [61] [99] [29] These studies provide new insights on the ecology of microbes by linking metagenomics and proteomics data to the environmental variables. Complementary experiments such as addition of selected nutrients to a sample also allow to determine which factors contribute to a resurgence of bacterial growth. [174]

However, this scale of spatial patterning does not correspond to the range of conditions a microbe experiences within its life cycle. As a limit-case example, the sulfur-oxidizing bacterium *Thiovulum majus* isolated in the swamp ecosystems exhibits speeds up to 650 micrometers per second. [51] [46] At the best of their abilities, when presented with a gradient they respond to, they can move two meters away from their starting point within an hour. For the fastest marine algorithm *Vibrio alginolyticus*, this estimate drops to less than a meter per hour. [156]. These approximations also do not consider the physical flow that surrounds microbes. On top of that, most microbes do not have motile properties and move via Brownian motion within water. Through their mobility, microbial populations have the opportunity to disperse within the oceans over long timescales and contribute to the homogenization of the ocean biosphere. [109] However, even motile marine microbes only end up exploring volumes of up to 0.8 milliliters within a day [161]. The scale at which a bacterium experiences its environment is relative to its size and its ability to move against the flow. The resolution of the methods used to sample and observe microbes *in situ* on a global level does not capture this microbial microenvironment.

At this finer scale, there exist hotspots of nutrients due the presence of structures that are bigger than a typical bacterial cell size (about one micrometer in length). These structures can be bigger organisms such as zooplankton or diatoms that can leak resources to their surrounding environment during their apoptosis [155]. This phenomenon creates gradients that bacteria can navigate. Another structuring factor of the bacterial microenvironment is marine snow [88]. Marine snow consists of particulate organic matter. All in all, bacteria live in and impact a highly heteroge-

neous environment where nutrient concentrations are limited both by global physical processes and by local players [10]

Nutrient patches at the mesoscale

Individual heterotrophic bacteria explore patchy landscapes of resources within the range that they can explore. These ecological patches consist of macroscopic aggregates, rich in various nutrients [7, 146]. They notably concentrate chitin, a non-soluble polysaccharide abundant in the oceans due to its predominance in shell structure [20]. These aggregates also contribute to a vertical flux of particulate organic matter by sinking in the ocean due to their density [147]. Their high concentration of nutrients makes them a sought-out microhabitat for bacteria, as they are more abundant and active on these particles than in the surrounding seawater [136, 152, 78].

In the wide volume that oceans occupy, these particles are not homogeneously distributed and can exhibit different physical properties. For example, the heterogeneity in particle diameters can be described by power-law functions called particle size distributions estimated *in situ* by various experimental methods [96, 134, 159, 62]. These distributions capture both the contribution of small size particles via the exponent and the number of particles. Quantifying these properties leads to better estimates of the processes governing the biological carbon pump, notably of the rate of remineralization [7, 85]. The geographical variation of particle concentrations depends on biophysicochemical processes such as the coagulation of transparent exopolymer particles [103], the rate of particle degradation by the bacterial community [85] and also on the lability of the chemical components of the marine snow [120].

Bacterial populations navigate that local ecosystem of patches and contribute to the degradation of these patches [11]. Bacteria indeed possess the enzymatic machinery to utilize these patches as resources to grow [89, 151]. This biological process leads to the reduction of the organic matter that sinks with particles [192, 120]. Thus, bacteria fulfill an environmental role within the oceanic cycle of organic matter through their colonization of these patches. This ecological function focuses the quantification efforts *in vitro* [34, 44, 43, 137, 5, 168] and *in silico* [42] on the

colonization dynamics on particles. Datta et al. identified successional patterns of bacterial arrival on an enrichment of chitin particles [34], while Pollak and colleagues inferred ecological roles for multiple bacterial types around chitin [137].

However, bacteria have to navigate between particles and forage for these patches [161]. What happens between patches impacts encounter odds and arrival time scales on particles, and thus colonization dynamics [173, 167, 60, 168]. In the process of community assembly on a particle, priority effects which define the advantage for a bacterium earlier without competition can enhance the establishment of one specific bacterial population on a patch [167]. The presence or absence of each bacterial strain also determines the power balance between different bacterial taxa and thus the community function [60, 168]. All these factors also play a part in the persistence of a bacterial population. Even though the landscape of patches is more continuous than meets the eye [11], bacterial populations need to be efficient foragers to hop from one patch to another and benefit from the resources offered by the concentrated nutrient particles.

1.1.2 Nutrient heterogeneity requires bacterial foraging

Particularities of bacterial foraging

Foraging corresponds to the act of searching and finding resources in an heterogeneous environment. Both observations and models of this process take as a starting point either the foraging agent, which can be an animal [19] as well as a bacterium [18], or the utilitarian maximization of resource scavenging through optimal foraging theory [141]. In the former case, the path the foragers follow can be described by a variety of stochastic processes, most of them being a variation of the random walk process [21, 106]. Random walks consist of a succession of steps taken at random within an environment. Another way to formalize random walks is to consider an agent alternating runs (straight lines) and turns at random angles within an environment. This characterization mirrors the way bacteria move through patterns such as run-and-tumble or reverse-and-flick [169, 160]. Bacterial foraging has also been singled out

as a biased random walk thanks to the role of chemotaxis [79, 131]. A chemotactic bacteria can follow environmental chemical cues, such as concentration gradients, by adapting its searching strategy. These motility patterns determine the ability of bacteria to efficiently explore their surrounding environment.

Foraging involves searching for resources but also utilizing them. Another particularity of bacterial foraging stems from the overlap in time scales between bacterial foraging and other processes, such as death and growth [49, 161]. When a bacterium encounters a patch of usable nutrients, bacterial growth leads to a direct increase of the abundance of that bacterial population, which is very different to the case of most animals. For example, birds [14] hop from one patch to another to look for resources to optimize their energy intake under the assumption of a constant number of individuals. However, for bacteria, one of the parameters that optimizes a population's persistence is the number of offspring a bacterium produces from one patch. That variable called the growth return quantifies the increase in bacterial number with respect to the quality of the patch. This return on investment needs to be contrasted with the search time. Unlike for bigger organisms, the bacterial population size is not constant over the foraging process. Thus, investigating foraging requires taking into account the dynamics of the whole foraging population and its competing processes. Yawata et al. developed a theoretical and experimental framework to document the trade-offs between search time and residence time [187]. All in all, bacterial exploration of a patchy landscape makes scavenging a process not only driven by individual cellular properties but also by whole population dynamics.

Bacteria developed strategies to cope with nutrient heterogeneity

Being able to adapt to local nutrient limitations is key for oceanic bacteria to persist. Microbial potential for nutrient acquisition is determinant for their growth and hence for their persistence in the environment [140]. Bacterial cells have developed strategies to get the necessary supply of resources for their growth. These strategies are highly dependent on their abilities to move around. If a bacterium does not have the machinery required to move within its microenvironment, it has to rely on dif-

fusive processes to gather resources. However, if a bacterium is able to propel itself, it can also proactively scavenge for resources it needs when the motility apparatus is functioning. Within the field, there has been an on-going debate on which of these two strategies is the most relevant to study when talking about microbial survival in oceans.

Zehr et al. argued that non-motile cells rely on diffusion of small soluble molecules to fulfill their requirement in resources and see a relatively homogeneous nutrient environment [193]. As more than a quarter of phototrophic bacteria in the ocean are non-motile, they argue that there must be an effective way for these organisms to get the supply of nutrients they need, even though the environment they live in is sparse. Small soluble molecules such as ammonium are subject to diffusive processes that rapidly homogenize the gradients. From these concentrations that are hypothesized to be homogenous on a microenvironment level, the number of molecules present in a cell-sized volume is computed and appears to be enough to sustain cellular growth. Hence, motility is not necessary for cells to survive and strive in an oceanic environment.

Lambert and colleagues challenge the conclusion that non-motile bacteria are dominating the oceanic bacterial processes [98]. Motility is an asset for cells to maximize their nutrient uptake and to reach higher metabolic rates. Even though motile cells build up a relatively low amount of the total bacterial biomass in the ocean, their motility allows them to take full advantage of the heterogeneous environment formed by insoluble materials, notably through chemotaxis. Motile cells are efficient at finding nutrient hotspots. Fast swimmers whose space exploration can be modeled by a random walk find a particle within a day on average. A lucky swimmer belonging to the top 1% of bacteria reaching a nutrient-replete patch does so in less than an hour. Therefore, importantly, persisting as a population within the environment means that some but not all bacteria need to reach nutrient hotspots. On top of that, these calculations do not take into account the ability of cells to move up gradients of nutrients and direct their trajectories towards potential food sources. This ability called chemotaxis dramatically improves the time to reach a patch. The efficiency

of actively foraging for resources is of course linked to the concentration and size of particles. In the worst conditions, bacteria stay in the bulk looking for a hotspot for over a week.

1.1.3 Nutrient limitation dynamically impacts bacterial physiology

When bacteria forage in seawater, they experience an environment depleted in nutrients relative to the abundance of resources on a particle. That same nutrient limitation has the potential to change bacterial phenotypes within a few minutes for the duration of the nutrient deprivation. Bacteria such as *Vibrio spp.* can rapidly adapt to nutrient depletions, as their stringent stress response happens within half an hour [129] and other molecular adjustments can take place throughout the entire duration of starvation [145]. In this section, I explore the changes of important bacterial foraging behaviors, such as viability, motility and attachment, to nutrient deprivation.

The moment a cell leaves a particle and the instant it finds a new patch define sharp transitions of the immediate nutritional surrounding for bacteria. Notably, the way nutrients get depleted matters for cell physiology. In the case of a patchy landscape, I assume that changes in nutrient concentrations are imposed by the environment and not by the cells exhausting the resources. Phenotypes are indeed impacted differently if cells are at an exponential growing phase [41] or at a late stationary phase [135]. For this section, we will focus on sharp transitions in the concentrations that mimic the attachment/detachment process on a particle.

Viability

Starvation of a bacterial population impacts numerous cell properties which are linked to their ability to scavenge for resources. First, cell viability is strongly affected by starvation [127, 125]. Viability is defined here by the ability for cells to regrow on rich media. The percentage of cells that can form colonies again on a rich agar plate

after a starvation treatment drops dramatically to 0% within 80 hours in the case of *Vibrio sp.14* facing a nitrogen limitation [125]. The limiting nutrient matters, as this result differs when it comes to carbon or phosphorus limitation. When considering a population of starved cells, it is expected that the viable portion of the population is decreasing [144]. Bacteria are expected to die at a constant rate, when the transition from the nutrient-rich environment to the nutrient-poor one is sharp.

Contrary to the model organism *E. coli*, marine heterotrophic bacteria such as *Vibrio spp.* are able to undergo reductive division to ultra microcells in a nutrient-limited environment [124, 126]. Here, reductive division is defined as the decrease in cell size happening after a division event. The maximal size of both daughter cells together in that environment is smaller than two times the one of the mother cell. Starved phenotypes of *Vibrio sp.14* are significantly smaller in cell length. These morphological changes in response to starvation happen within the first 100 hours of starvation. It is also notable that this fragmentation of biomass into smaller vessels potentially impacts the abundance of a bacterial population, as more cells are produced even in a nutrient-depleted environment.

Whenever looking into microbial physiology, the nutritional history of each cell matters and impacts the new physiological state of the bacteria. For example, one factor that might play a role in bacterial numbers after a sharp transition is that a bacterium can potentially store carbon-rich compounds within its cytoplasm such as poly-β-hydroxybutyrate [27]. These storage units accumulated during growth on a rich media can be used to sustain a few cell divisions once the cells enter a nutrient-depleted environment [126]. Growth in a nutrient-limited environment can, thus, still happen, even with a doubling time on the scale of days [56]. This additional cellular vitality enabled by storage falls under the umbrella of reductive division defined in the previous paragraph. An increase in the abundance of a bacterial population even in a nutrient-limited environment could significantly influence the foraging fate of a population. These changes in the head count of a bacterial population can be key to determining the persistence of bacteria scavenging for resources, as mentioned in section 1.1.2. It is unclear how much the viability loss and the reductive division

balance each other when it comes to the absolute number of bacteria foraging. The process of foraging happens at a similar time scale to the processes of death and potentially reductive division. The dynamics of cell viability are at odds with the ecological behavior of foraging bacteria. Taking into account the viability under starvation could then influence the search time of hotspots, and also the persistence of a bacterial population.

Even though cell viability is defined as the ability of a bacterium to regrow in rich media, it is notable that some starved, yet viable cells that encounter a particle might not be able to use the resource as well as their non-starved counterparts. The abundance of viable cells does not mirror the ability of bacteria to utilize the particle to divide. Chitin is a complex polysaccharide that requires enzymatic machinery to degrade [71, 137]. However, under nutrient limitation, marine bacteria degrade some of their intracellular proteins, which can lead to the reallocation of metabolic resources towards persistence [91]. The impact on cellular viability on particle colonization does not stop with the bacteria-particle encounter but afterwards, when a bacterium has been able to re-grow on the substrate of interest and recover an exponentially-growing physiological state.

Motility

Nutrient limitation not only affects viability, it also alters motility. A motile bacterium can explore more space during foraging than a non-motile one. That ability is captured by the notion of bacterial diffusivity that is at least three orders of magnitude higher for bacteria exhibiting active motility [86, 98]. As motile bacteria forage through their environment, they survey a nutrient-depleted environment, which can lead to bacteria losing their motile properties. Within 16 days of nutrient limitation, almost all *Vibrio sp. 14* lost their flagellum, which made them unable to be motile [165]. This dramatic change in molecular machinery could lead to a decrease in the motile fraction of a bacterial population while foraging. Motility loss impacts how fast and far bacteria are able to explore their surroundings.

When living in nutrient deplete conditions, the average speed of a motile bacterial

population is slow. Starvation skews the distribution of bacterial speeds within a population towards lower values [186, 113]. As famine influences motile properties, it seems necessary to include speed variations due to starvation within the foraging models, especially because the time scales of the motility decline are relevant to the search for new resources.

If starvation negatively impacts bacterial motility, starved cells also change their chemotactic abilities. Chemotaxis describes the ability of bacteria to direct their movement within a chemical gradient they are experiencing. While foraging for resources, bacteria can bias their random walk towards hotspots by sensing signals from chemo-attractants released at the feasting location [162]. After starvation, cells are more responsive to lower concentrations of chemo-attractant [171, 125, 100]. Chemotaxis relies on bacteria sensing differential concentrations of nutrients in space. Sensing lower concentrations confers a significant advantage in foraging for resources, as it informs about the trade-off between the energy usage required by motile behaviors and the potential growth return.

Attachment

Once a bacterium finds a particle, this encounter needs to become long-lasting through attachment or at least through the absence of detachment. Bacterial strains can exhibit different strategies in terms of attachment strengths [188]. Attachment results from the physical interaction between the cell and the particle, sometimes facilitated by the surrounding fluid [68]. Active attachment also referred to as adhesion can be mediated by molecular mechanisms. This process can be both general [132] or specific to certain substrates such as chitin [138, 114]. The cell membrane and wall play an important role in successful attachment that depends on bacterial physiology.

There is contradicting evidence when it comes to the influence of nutrient deprivation on bacterial stickiness. On the one hand, some *Vibrio* can increase in their adhesion properties by adding to the composition of their cell surface a new polymer [36]. In other cases, changes in the cell membrane's physical properties, such as an increase in hydrophobicity, could mediate an augmentation of bacterial adhesion,

as surveyed by Kjelleberg and Hermansson [92]. On the other hand, Pruzzo et al. showed that long-term exposure to a nutrient-limited environment leads to the decrease by almost half of the adhesive propensities of *Vibrio cholerae* [139]. There is at least strain-level variability between the impact of nutrient limitation on bacterial adhesion to surfaces. In a patchy environment, resource allocation towards surface adhesion becomes a strategy to increase the odds of successful attachment, and thus growth at the moment of encounter.

Individual cellular attachment also depends on the encountered particle and its hospitalibility. The nature of the particle, notably the presence of labile resources, could influence the settlement of a bacteria, as an easily degradable particle can optimize bacterial growth return on the patch. The presence of other degrading bacteria could lead to cooperative efforts in the production of public goods, such as extracellular degradation enzymes [43]. High attachment also inflates the risk for a bacterium to be stuck on a particle without a competitive advantage, be it because of viral infection or bacterial competitors or free-riders [42, 137, 168]. As attachment corresponds to the transition to the next phase of a bacteria's life cycle, it interplays with both the physiology of the arriving bacteria and the microbial ecology on a particle.

1.2 Environmental relevance of bacterial foraging under nutrient starvation

The active search for nutrients by motile bacteria is rewarded by high metabolic activity. This activity is concentrated around particles, which act as hotspots of metabolic activity because of their density in resources. It has been shown that bacterial populations on particulate organic matter are taxonomically different to bacterial populations living in the bulk seawater [50]. If motile cells constitute a low proportion of free-living bacteria, they are overrepresented on particles. As these particles are nutrient rich, it has been shown that cells on particles are more metabolically active

than the free-living cells [143]. Motile cells are the most metabolically active part of the bacterial biomass.

However, motile cells need to forage for resources within a nutrient-depleted environment. They undergo cycles of famine and feast, as Srinivasan et al. described in 1998 [157]. Nutrient starvation induces physiological changes that impact the cell properties and behaviors. The lack of nutrients to feed on is a strain for bacteria, the same way that drought can be a strain to plants. As motility is a cell property that requires energy, it is likely to be impacted by a stressing environment [112]. All the calculations made by Lambert and colleagues concerning motility assume constant speed for all the bacterial population [98]. It is unclear how starvation would influence the average searching time.

Starvation and motility are highly relevant when considering the dynamics of communities in a patchy landscape. The heterogeneity of resources implies that cells undergo phases of nutrient depletion. As phases of abundance are concentrated around hotspots, phases of depletion correspond to phases of scavenging for new resources where bacteria can activate their motile behaviors. So far, the link between motility, starvation and population persistence within a patchy landscape has rarely been explored from an ecological point of view. On the one hand, starvation studies have focused on the change of cellular physiological traits, such as motility, chemotaxis and others [181]. On the other hand, the experimental systems exploring the ecology of bacteria in heterogeneous landscapes have all been primed with cells coming out of the exponential phase [45]. It is unclear how the changes of physiology due to starvation impact the ecological dynamics of a bacterial population in a patchy landscape.

1.3 Contributions

Bacteria explore a heterogeneous landscape. That heterogeneity stems from the presence of nutrient hotspots that bacteria can find through their active motility or their passive diffusion in the water. The time it takes for one bacteria to encounter a par-

ticle depends on its diffusivity and on the particle concentration. Using a theoretical model, Lambert et al. states that the top 10 % of a motile bacterial population can reach a particle within the range of minutes (when chemotaxis is involved) to days (when the particle concentration is low) [98]. The main take-away of this paper is that motile bacteria drive particle colonization, even if they only represent a small fraction of the global population, as they arrive at the particles significantly faster. Their model compares two distinct non-overlapping population types: one motile and one non-motile, as it assumes that these two properties are constant [153]. However, this hypothesis does not take into account that foraging happens within a space of low nutrient availability. Nutrient limitation does not only impact cell viability but also cell motility and cell attachment, which are key parameters to the scavenging of a bacterial population [165] As motile bacteria look for available resources in the ocean, they undergo nutrient limitation, which affects their cell number, their ability to be motile and to attach. For example, both the percentage of motile cells within a population and the bacterial diffusivity of the motile cell fraction dramatically decrease over time [186]. Here, I bridge the gap between microbial physiology and ecology to estimate time scales of particle colonization.

1.3.1 Experimental quantification of bacterial foraging behaviors at single-cell and population levels under nutrient limitation

These dynamic changes of bacterial behaviors at a single-cell level under nutrient deprivation impact the foraging abilities at the bacterial population scale. Bacteria can adopt a wide variety of strategies to be competitive foragers under nutrient limitation. As a single bacterial population aims to persist within a patchy environment, adaptation to a stressful environment can be the source of heterogeneities with a bacterial population [176]. This process is called bet-hedging [57, 116, 52]. No experimental evidence for bet-hedging has been gathered for marine heterotrophic bacteria. So far, measurements made about the impact of nutrient limitation on bacterial behaviours

in marine heterotrophs have been made at the population level, notably all studies conducted at the beginning of the 1990s by Nyström et al. [125, 127, 126]. In this thesis, I leverage the technical improvements made in microfluidic devices, microscopy and computational techniques to get single-cell (when appropriate, single-particle) and population level measurements of these dynamic changes in phenotypic plasticity and explore the population heterogeneity. The time scale for interrogating these phenomena is here on the order of days, as it corresponds to the order of magnitude of time that bacteria scavenge for resources.

1.3.2 Estimations of nutritional requirements and foraging time scales of a bacterial population in a patchy landscape

Once I gather experimental evidence for bacterial behavioral changes due to nutrient limitation, I can use this qualitative and quantitative information to revise the estimations of bacterial foraging time scales. Current approximations for bacterial resource scavenging in the oceans do not consider the impact of nutrient deprivation on bacterial physiology for motile bacteria [98]. In this thesis, I incrementally develop foraging frameworks that account for the phenotypic plasticity. In our stochastic models, foragers explore both a physical space parametrized by the number of particles and a behavioral space constrained by their answer to nutrient limitation. I also seek to connect these ecological models with oceanography measurements by analyzing the feasibility of bacterial colonization for different particle concentrations given their scavenging behaviors.

1.4 Thesis Outline

After this introductory chapter, the second part of this thesis explains the steps followed for the design of the experimental system constrained by the current technical state-of-the-art. The third chapter presents the obtained experimental results, while the fourth one consolidates these into a modeling framework. The fifth chap-

ter expands the scope of this thesis by providing preliminary data that surveys open questions pertaining to the link between ecological and physiological states. The sixth and final chapter discusses the impact of this thesis.

Chapter 2

Experimental Design for Long-Term Nutrient Limitation

This chapter describes the process of designing the experimental set-up used for long-term nutrient limitation and its observation. This work starts with the following question: What is the influence of long-term nutrient limitation on bacterial foraging? To answer this question, I develop an experimental set-up that follows a bacterial strain limited by one nutrient for multiple consecutive days. This framework must also yield consistent results and be flexible enough to observe bacterial behaviors that impact foraging. The first part of the chapter explains the choices linked to long-term starvation, such as the selections of a bacterial strain, a defined media, a specific limiting resource, and a particular physical set-up. The rationale behind each pick and the system's limitations are also explored in this first part. The second half of this chapter focuses on the methods for observing different bacterial behaviors such as viability, motility, attachment, and rescue.

2.1 Long-Term Nutrient Limitation

2.1.1 Strain choice

Microbial diversity provides the reductionist scientist with a vast array of microbes to choose from and many dilemmas. The first step in this important process is establishing selection criteria that fit the experimental design and goals. In this case, I choose to focus on heterotrophic bacteria degrading chitin, an abundant insoluble polymer in the marine environment. The scientific questions require that three selection criteria are met: a bacterial strain's cultivability, its ability to use chitin as a carbon source, and its motility. These criteria can then be evaluated against a strain collection, partially presented in table 2.1. The Cordero lab has established a strain collection from environmental samples [34]. Datta et al. performed an enrichment experiment with particular organic matter, notably with chitin particles, to isolate strains from Nahant beach in Massachusetts. These strains are characterized both genetically (metagenomic data are available) [34, 44] and phenotypically [43, 137]. Early colonizers arrive at particles, as they are motile and can degrade chitin. In contrast, late colonizers are less efficient at foraging for resources and using them. Thus, early colonizers, with their ability to move around and degrade carbon sources, are good model organisms when investigating the impact of nutrient limitation on foraging. They have the most to lose when deprived of nutrients. The search for an ideal model strain therefore focuses on the early colonizer strains, all gram-negative bacteria mainly belonging to the genera *Vibrio* and *Alteromonas*.

Table 2.1: Metadata available about the short-listed strains of this thesis. These data were gathered within the context of [44] and [34] by Tim Enke, Matthew Metzger, and Manoshi Datta

Strain Name	Genus (or higher order when unavailable)	Growth on GlcNAc	Growth on chitin (Halo)	Growth on chitin beads	Chitinase secretion	Motility
1A01	*Vibrio*	+	−	+	+	+
3D05	*Pseudoalteromonas*	+	+	+	+	+
6C06	*Psychromonas*	+	+	+	+	+
6D02	*Alteromonadales*	+	−	+	−	−
6D03	*Vibrionaceae*	+	+	+	+	+

Technical limitations also create another set of criteria to narrow down the search for optimal strains. As chitin is not soluble, the bacteria of choice need to grow within a minimal media composed of N-acetyl-glucosamine (abbreviated GlcNAc), the building block of chitin, as the sole carbon and nitrogen source. The recipe of such a media ideally removes any confounding factors by being strictly composed of known chemicals. I conducted several dual screenings, including different early colonizers with multiple potential limiting resources. These screenings are explored in more detail in part 2.1.2 and further restrained the number of candidates available for our set-up.

At the start of this project, none of these isolates were successfully fluorescently labeled with genetic engineering. Even though this project does not directly rely on the use of genetic modifications, further extensions of the project could require strain engineering. For example, a caveat of not having a labeled strain is that chitin is auto-fluorescent. It is not a given that enough contrast can be achieved to observe the bacterial colonization of a chitin bead by adding a dye that is typically neutral to bacterial metabolism up to a certain concentration threshold. Thus, I also added the fluorescently labeled strain *Vibrio coralliilyticus*, when it became available, as liability management for screening natural isolates to potentially circumvent these drawbacks.

Vibrio coralliilyticus fills all the requirements for a strain of interest, as it is motile

through the use of a single-pole, sheathed flagellum, and it can utilize both N-acetyl-D-glucosamine and chitin [15, 84, 108]. This Gram-negative rod-shaped bacterium is also a pathogen of the coral *Pocillopora damicorni*. This strain has been the focus of many environmental studies because its pathogenicity, linked to extracellular protease production, depends on temperature. This led to the development of genetic tools for this strain, which is rare for a microbe first isolated less than ten years ago [15]. The available constructs range from bright fluorescent labels [148] to a motility knock-out [108]. I also established the time scales of chitin bead colonization for this strain (see Appendix D). This shows that *Vibrio coralliilyticus* visibly colonizes and degrades available particles faster than most other available strains [45]. The hyper-efficiency of this strain to move within the media, degrade complex carbon sources, and colonize particles makes it an ideal candidate for our experimental set-up. *Vibrio coralliilyticus* has the most to lose. Changes in these different phenotypes between starved and exponentially growing are also easier to measure and observe, as the baseline time scales are shorter. Therefore, I chose this bacterial strain for our assays.

2.1.2 Media choice

Limiting Resource

Nutrient limitation is a concept that appears in diverse disciplines such as bacterial physiology [144] and microbial ecology [49]. As this thesis aims at bridging these different kinds of literature, it is important to define nutrient limitation in a way that is both unifying and actionable. Here, I first examine the impact that this definition has on the experimental set-up.

In the lab, there are two major ways to provide bacteria with nutrients. On one hand, bacteria can be cultivated within a closed system. In this case, bacteria are inoculated within a finite pool of resources. Nutrient starvation occurs when one of the resources is depleted. On the other hand, resource supply can be continuous. In this set-up, referred to as a chemostat, nutrient limitation stems from the imbalance between the bacterial demand in certain resources and the supply of those nutrients.

Both these methods lead to nutrient stress, the first one through nutrient depletion and the second one through nutrient imbalance. From a technical standpoint, the chemostat approach has more parameters, such as in and out fluxes, to optimize than a closed batch system set-up. When a bacterial population exhibits a very slow growth, it can be especially challenging to avoid bacterial extinction while maintaining a constant nutrient environment [194]. While those two methods are different, the closed system can be seen as a limit case of a chemostat, where the fluxes are nil. This perspective is particularly relevant when some nutrients are completely depleted in the media, and that inhibits bacterial growth. Keeping that in mind, the most parsimonious experimental step involves describing the effect of nutrient depletion on bacterial phenotypes. The work could later be extended to a chemostat to focus on questions around nutrient pools.

Within the framework of a closed system, when submitting bacteria to nutrient stress, the choice of the limiting resource is key. Each resource is processed through different metabolic pathways, which leads to varied effects on bacterial phenotypes. Removal of all sources of carbon, nitrogen, and phosphorus from the media gives an appreciation for the impact of multiple-nutrient depletion on bacterial behaviors [186, 127]. However, this approach lacks any potential mechanistic insight on nutrient limitation, as it remains unclear which resources are the actual bottlenecks for the observed change in phenotype [125]. The experimental framework presented here stems from a parsimonious approach: the heterotrophic bacteria of choice are starved when they alter their phenotypes due to the depletion of one nutrient.

To select that nutrient of interest, I conducted growth assays while titrating the different nutrients individually. Bacterial concentrations were monitored continuously for up to 48 hours by measuring optical density at 600 nanometers. The artificial seawater media recipe (presented in section B.1) used to first characterize the marine isolates [45] supplies a shortlist of potential limiting nutrients: glucose for carbon limitation, ammonium for nitrogen, phosphate dibasic for phosphorus, and N-acetyl-D-glucosamine for carbon and nitrogen. While keeping all the other nutrients at the concentrations prescribed by the original rich media recipe, I quantified the effect of

reducing the concentration of one of the nutrients of interest by 10-fold dilutions. This screening reveals the impact of varying nutrient concentrations for multiple bacterial strains from the Cordero collection and for the main strain of interest, *Vibrio coralliilyticus*. These bacteria were first revived in marine broth, a very rich media.

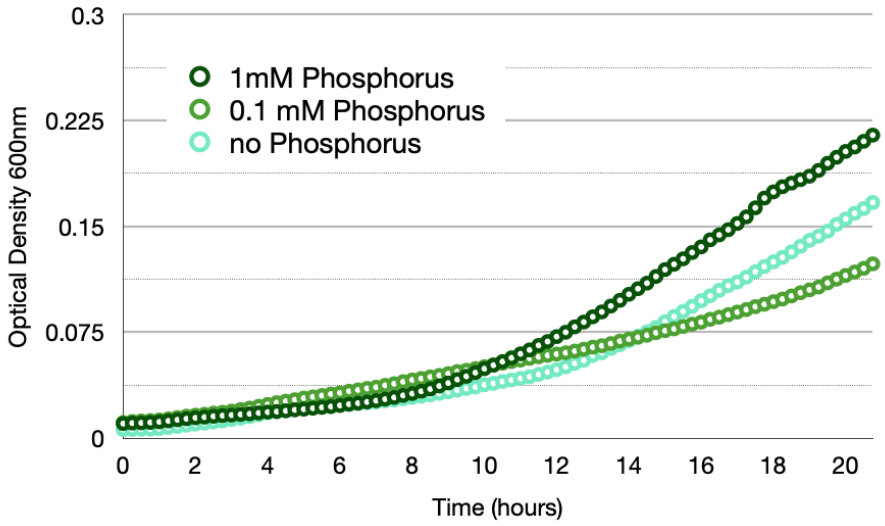

Figure 2-1: Optical density measurement over 21 hours of *Vibrio coralliilyticus* for different concentrations of phosphate with a base media composed of GlcNac and ammonium. Each point is the mean of a technical triplicate.

In our system, the addition of phosphorus in the media influences neither the growth rate nor the growth yield when keeping all the other nutrient concentrations equal. In figure 2-1, the observed optical density after 21 hours is similar for all concentrations of phosphate dibasic and notably for the negative control, where there was no phosphorus added. The kinetic data also vouches for the independence between bacterial growth and phosphorus concentration in the media. A potential limitation to these data is that there could be some phosphate contamination, for example, due to the water used as a base for the media in section 2.1.2. This assumption is further validated by the fact that when cells are washed with the new media before being inoculated in a low phosphate concentration media, they grow faster than cells that have not been washed. Another hypothesis is that these heterotrophic bacteria have a

very flexible phosphorus stoichiometry that allows them to reallocate their phosphorus internally [55]. Their growth then becomes either carbon and/or nitrogen-limited before being phosphorus-limited. On top of the multiple interpretations of such results, there is also a conceptual argument not to consider phosphorus limitation. Within the chitin particle system, heterotrophic bacteria navigate a patchy landscape of carbon and nitrogen-rich particles. The highest differences in concentrations between the patches and their surrounding media are the ones in carbon and nitrogen, as these last two elements are not provided within the surrounding media. This thesis aims to observe nutrient limitation in the context of population cycles of feast and famine [157], which is focused on carbon and nitrogen. For parsimony's sake, I thus chose to discard phosphate limitation from our study.

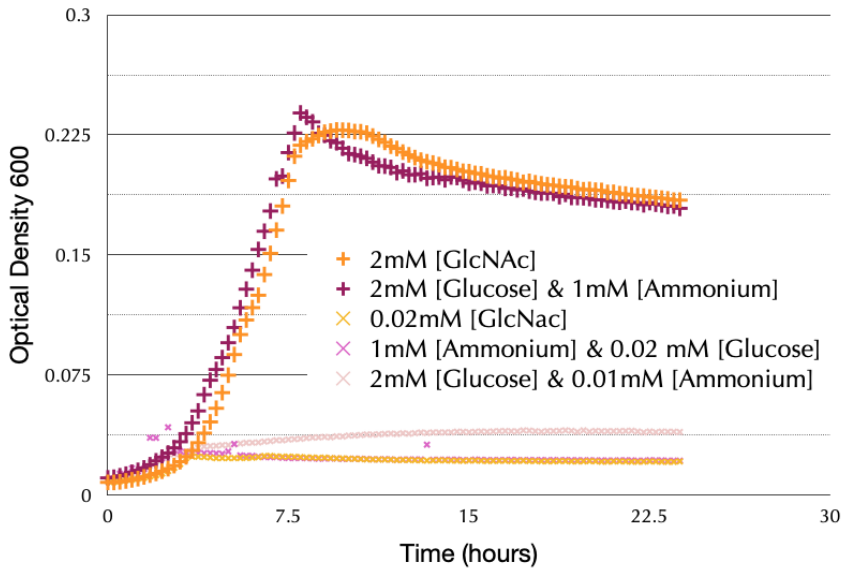

Figure 2-2: Optical density measurement over 23 hours of *Vibrio coralliilyticus* for different concentrations of GlcNAc, ammonium and glucose. Each point is the mean of a technical triplicate.

Another unexpected result from this screening stems from the serial dilution in ammonium when coupled with either glucose as a carbon source or N-acetyl-D-glucosamine as another carbon-nitrogen source. In both cases, high ammonium concentrations (1mM) appear to be toxic as no growth is observed for the first 21 hours,

as shown in figure 2-2. For some model organisms, it has been shown that ammonium-impaired growth is linked to changes in general properties of the medium, such as osmolarity or ionic strength [119]. Variations in ammonium concentration unsurprisingly impact the growth of cells more in glucose than in N-acetyl-D-glucosamine. The latter indeed provides bacteria with both carbon and nitrogen. In the absence of ammonium with that carbon and nitrogen source, cellular growth for *Vibrio coralliilyticus* is still supported. However, in the inoculation with glucose and ammonium, growth rate and yield are optimal for the concentration of ammonium 10-fold lower than the one used in the artificial seawater recipe. A higher ammonium concentration leads to significantly lower growth, as seen in figure 2-3. In this particular screen, ammonium both supplies nitrogen and poisons the cells. The toxicity of ammonium adds a layer of complexity to the interpretation of nutrient starvation.

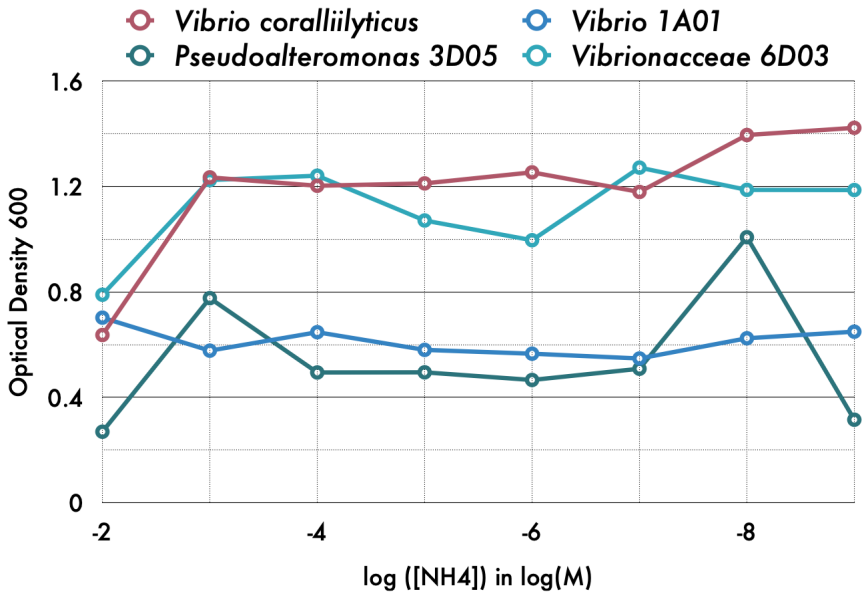

Figure 2-3: Optical density attained after 21 hours by different bacterial strains as a function of the ammonium concentration provided in the original media presented in B.6. Each point is the mean of a technical triplicate.

Carbon concentrations impact both the growth rate and yield. The more carbon, the faster and the more bacteria grow. Kinetic data for *Vibrio coralliilyticus* also

reveals that this bacterial strain resumes growth faster on N-acetyl-glucosamine than on glucose by three hours. The growth yields for both these carbon sources are comparable, as shown in figure 2-4. Another goal for this screening was to establish the minimal carbon concentration that leads to visible optical density changes. That concentration 2mM is an order of magnitude below the controlled artificial seawater medium used as a reference presented in table B.6. That chosen new concentration is the one that will be referred to later as the base medium concentration, whose recipe is in table B.7.

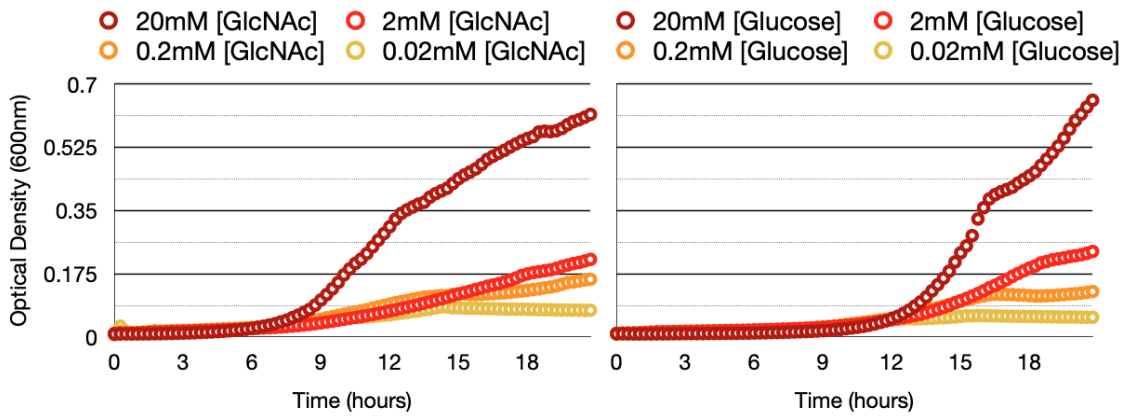

Figure 2-4: Optical density over 21 hours for *Vibrio coralliilyticus* with different concentrations of GlcNAc on the left panel and of glucose on the right panel. The rest of the chemical are given by the original media recipe in table B.6. Each point is the mean of a technical triplicate.

This first screen established two parameters: a carbon base concentration and an optimal concentration in ammonium. Then, six bacterial strains, including *Vibrio coralliilyticus*, were submitted to another growth assay comparing the dynamics under these standard concentrations with the dynamics when one of the nutrients was diluted 10-fold. *Vibrio coralliilyticus* exhibits the fastest growth on the standard media (see section 2.1.1), attaining its maximal bacterial concentration within ten hours for both N-acetyl-D-glucosamine and glucose media. Even though all the selected strains are able to grow on N-acetyl-D-glucosamine, they use glucose as a carbon source with different efficiency. For example, the *Pseudoalteromonas* 3D05 did not exhibit any

growth on glucose, whereas the *Vibrio splendidus* 1A01 grew to a higher yield and faster on the combination of glucose and ammonium than on N-acetyl-D-glucosamine. With that last combined carbon/nitrogen source, *Vibrio splendidus* 1A01 's growth rate shifts after 10 hours, hinting toward more complex degradation dynamics. When confronted with lower carbon and nitrogen concentrations, cells follow similar dynamics for the first few hours and then reach their maximum yield. This observation verifies that cells are alive then and that, even in the presence of submillimolar carbon concentrations, bacteria reach a stationary phase within the first five hours.

After focusing on carbon and nitrogen limitations, I decided to use N-acetyl-D-glucosamine as the primary source for both these nutrients. This way, it avoids the caveat of ammonium toxicity while remaining consistent with our experimental model system of a landscape of chitin beads. N-acetyl-D-glucosamine is indeed the monomer of chitin. Further work could decouple that dual carbon and nitrogen limitation by contrasting the result in this thesis with independent nutrient limitations in both glucose and nitrogen.

Gradual media set-up

After choosing the limiting nutrient of the media, it is essential to determine conditions to start the nutrient limitation in a reproducible manner. Reproducibility comes with high control over the different variables that influence bacterial growth. This part aims at uncovering what happens from the frozen bacterial stock to the inoculation in the nutrient-limited environment.

Cells are first revived from a frozen stock by being streaked on a marine broth plate. Marine broth is a rich media with many resources. Cells form visible colonies within a day. To ensure that bacteria conserve the same physiological state, these colonies can be harvested up to 3 days after the streaking process. Once a colony is picked, it is transferred to 1mL of rich liquid media. Rich liquid media comprises a mix of 10% filter-sterilized marine broth and 90% of base media (see table B.9). That base media emulates seawater while being a highly chemically defined media. Its recipe can be found in the table B.7. It is noticeable that all the major nutrients, such

as carbon, nitrogen, and phosphorus, are supplied in this base media, whose primary source of carbon and nitrogen is N-acetyl-D-glucosamine, abbreviated GlcNAc for the rest of this thesis. The bacteria are incubated in this mixed media for 4 hours. This stage balances the need to jump-start bacterial growth with marine broth, the limitation of potential carry-over nutrients from the rich media, and the exposure of bacteria to the base media.

After being exposed to this mixed media, bacteria are inoculated at various initial bacterial concentrations in the base media. In that milieu, the GlcNAc concentration can support exponential bacterial growth. This incubation lasts around 24 hours at 25°C. In the end, the measurement of optical density gives a first approximation of the number of cells present in each sample. Also, it informs about the physiological state of the sample. The goal here is to select a sample growing up to the same physiological state consistently. This way, the starting condition of the nutrient limitation experiment is reproducible. Then, that sample is diluted to a 0.005 OD in 5 mL of nutrient-limited media. The nutrient-limited media presented in table B.8 is devoid of GlcNAc. The only carbon and nitrogen sources stem from the carry-over of nutrients from the base media. That inoculation corresponds to the time zero of the nutrient limitation set-up.

This set-up is based on the harvesting of exponentially-growing cells. While this setting enhances the experimental reproducibility, it has implications for the carry-over of the limiting nutrient. The Monod growth curve establishes that the limiting nutrient concentration is over a certain threshold when cells grow exponentially at their maximum growth rate. That threshold is strain-specific and can be determined by observing bacterial growth rate at different starting nutrient concentrations. As a result, when sampling from an exponentially growing population of bacteria, the sample will contain some limiting nutrient that has not been completely depleted.

The most common way to eliminate the nutrient carry-over consists in washing the cells [111]. After centrifuging the sample, the supernatant is removed and replaced with the new fresh media. This method eliminates the media variability due to the carry-over of chemicals from the preceding steps. It works for a population of cells

that can form a pellet in these conditions. Two conditions are necessary for this to happen. Firstly, cells have to be in a high enough concentration to create a visible pellet at the bottom of the tube. Secondly, cells also have to have a high enough mass, such that the centrifugal force significantly impacts them. Here, the controlled media in which cells grow exponentially before experiencing nutrient limitation can sustain cell proliferation up to a low density of cells. Optical density measurements at the stationary phase never exceed 0.110. In addition to a low bacterial concentration, cell mass measurements also indicate that *Vibrio coralliilyticus*' biomass is more than two times smaller in that media (around 70 femtograms) than in marine broth (about 200 femtograms). This lower weight makes cells less likely to form a pellet, as the applied centrifugal force depends on their mass. Combined, these factors make it challenging to pellet cells and thus to wash cells before starting the incubation.

Carry-over of nutrients from the controlled media is not avoidable. However, GlcNAc is the only nutrient removed from the limitation media and thus the only one that needs to be quantified. As a first approximation, the concentration of spurious GlcNAc is measured via a reducing sugar assay using a dinitrosalicylic acid reagent [110]. The reagent becomes fluorescent when reacting with reducing sugars. The set-up is first calibrated using serial dilutions of the reducing sugar of interest, GlcNAc, here. The amount of sugar detected in the controlled media at the time of transfer to the GlcNAc free media is below the sensitivity threshold of the assay (5 mM). It is noteworthy that that carry-over nutrient concentration is diluted another time, as it is linked to the volume of bacterial cells transferred into the GlcNAc-free incubation. The amount of this controlled media transferred to the following media constitutes maximally 10% of the final incubation volume. It implies that the maximal concentration of GlcNAc at the start of the nutrient-limited incubation is 0.5 mM.

Other components in the media

The media in which the nutrient limitation takes place lacks GlcNAc. However, GlcNAc is not the only potential provider of carbon and nitrogen sources in this

media. Even though this media is highly defined, it still contains molecules made of carbon and nitrogen. It also relies on using cleaned and purified water coming from the city of Cambridge. This water could include a certain amount of dissolved organic matter even after the purification steps. In this part, I quantify the influence of these factors on bacterial growth (or lack thereof) within the nutrient-limited media.

An unexpected result triggered this investigation for other carbon and nitrogen sources in the media. This result appeared when looking into the influence of bacterial concentration on the dynamics of the number of viable cells. After transferring cells to starvation media (a media without carbon and nitrogen sources), I observe that cells can grow again within the first few days, as exemplified in figure 3-1, at the highest starting concentration of bacteria. One of the hypotheses is that this growth could be due to carry-over GlcNAc from the first incubation media as the cells are not washed. The main argument against growth on carry-over GlcNAc is that cells starting at very low concentrations can grow more than the carry-over GlcNac would allow at such low concentrations, as discussed in the last section. Another assumption is that bacteria can grow on another component of the nutrient-depleted media. To mitigate the effects of potential carry-over nutrients, cells are diluted again in a nutrient-limited milieu after 24 hours. If bacteria can grow on another chemical in the media, the total number of cell divisions within 24 hours would positively correlate with the dilution factor. The higher the bacterial density, the faster a resource is exhausted. The following figure presents the number of bacterial divisions as a function of the dilution factor, as seen in figure 2-5. It is noticeable that there is a positive correlation between these two variables, which hints that cells can grow on something else in the media. The presence of another carbon and nitrogen source in the media does not change long-term starvation results. It has, however, the potential to interplay with reductive division in the short term. Thus, spurious growth in the nutrient-limited media needs to be quantified.

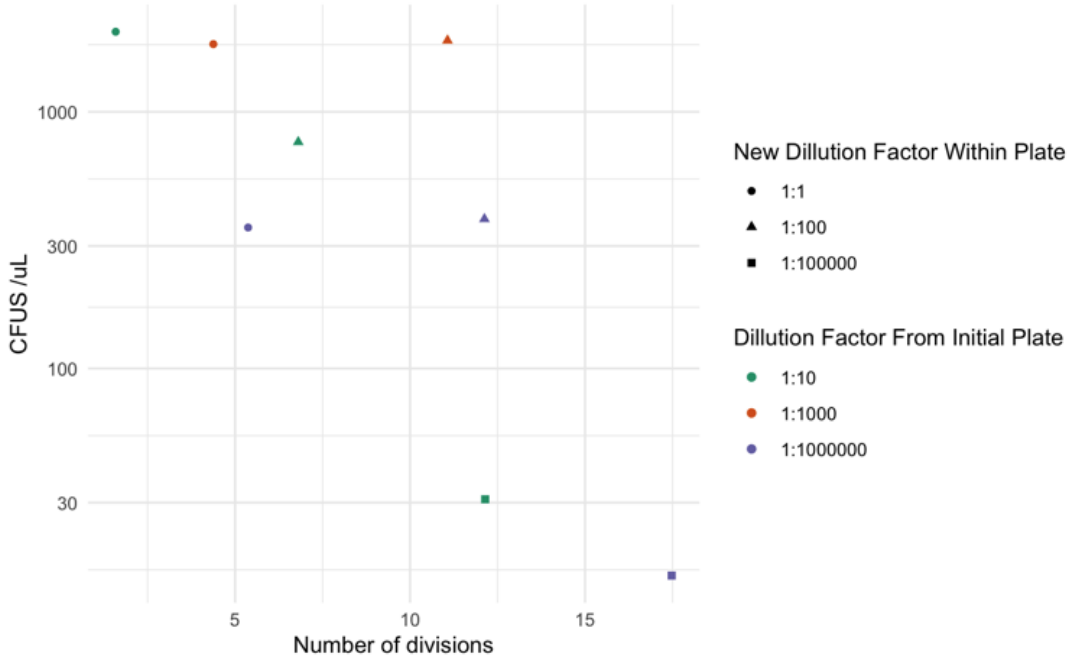

Figure 2-5: Initial number of bacteria counted in colony forming units as a function of number of bacterial divisions after the bacteria have been incubated for 24 hours in the original media without carbon and nitrogen sources.

The first potential source of carbon and nitrogen is polyvinylpyrrolidone , abbreviated PVP40 thereafter. This polymer has been added to the nutrient-limited media as it prevents cells from attaching to walls. This anti-adhesive function is necessary to measure bacterial motility, as described later in this chapter. PVP40 also is composed of heterocyclic compounds made of 4 carbon atoms and one nitrogen atom) linked through a chain consisting mainly of carbon. It has been shown that microbial consortia can degrade this chemical in particular conditions [75]. On top of that, the physical properties of PVP40 could impact bacterial growth by avoiding cell attachment to the bottom of the well. To check if PVP40 influenced bacterial growth, I compared the number of viable bacteria after one day of starvation in a milieu with or without PVP40. Both of these cultures were pre-grown in environments reflecting the presence or absence of PVP40. Both of these conditions yield a similar variation in cell numbers after one day of nutrient limitation. Because of that, I can conclude

that PVP40 does not impact the nutrient limitation, at least in the short term, when cell reductive division happens.

Another potential carbon and nitrogen source is the vitamin mix (defined in table B.3) present in the defined media. Collectively, all the vitamins could contribute up to 44.8 µM of carbon and 8.5 µM of nitrogen. Those concentrations could elucidate some of the observed bacterial divisions. It has also been shown that the strain of interest here doesn't need vitamins to grow on the minimal media (soon-to-be published data gathered by Rachel Gregor). Because of the facultative presence of vitamins for bacterial growth, the vitamin mix has totally been removed from the final media recipes. Contrary to vitamins, the trace minerals solution (presented in table B.2, stored at low pH) does not contain any carbon or nitrogen source and is included in the final media recipe without danger.

Last but not least, I need to look into a ubiquitous element in all media recipes: water. Water is the main solvent where chemicals get dissolved and diluted. The usual processing pipeline for the water includes purification and filtration steps. In the case of our lab, purification is achieved through reverse osmosis deionization. However, even when these steps are successful, some spurious concentration of organic matter remains. These purifying and filtrating systems also need to be updated regularly and monitored to avoid spikes of organic matter in water concentration. Notably, the CoVID19 pandemic impacted most of the routine checks of this equipment. At the beginning of September 2021, water that the purification system had already processed exhibited up to 2000 parts per billion of total organic carbon. This value is more than four times the amount expected in usual non-purified seawater. An update of the purification, filtration, and transport system allowed to bring back the total organic carbon value to what is expected post-processing. Nevertheless, these measurements display that water can be an unexpected source of organic matter. How much does this organic matter impact nutrient limitation in the short term? To answer this question, cells were incubated for 24 hours in media made with water before the water processing pipeline update or with water after the water processing pipeline update. As a control, I used water which was graded with high-performance

liquid chromatography to ensure the absence of contamination (that method is abbreviated HPLC). The media prepared with HPLC water didn't have any other source of carbon and nitrogen. Viable cells are counted both at time zero and after one day to quantify the number of cell divisions. With a starting cell concentration of 10^6 cells/mL, the purest milieu, made with HPLC-grade water, could sustain two cell divisions. In contrast, the milieu with the most organic matter could sustain up to four cell divisions. The media made with the optimized water pipeline could sustain three cell divisions. As the starting cell concentration of this experiment is on the higher end of the used cell concentration, this number of cell divisions is the lowest the different media can sustain.

In this section, I explored potential carbon and nitrogen sources present in the media. The goal of this thesis is to explore nutrient limitation in the short and long term. Success in this objective corresponds to minimizing the growth in the incubation media. In other words, the number of cell divisions due to spurious carbon and nitrogen sources needs to be minimal. In any case, this design constraint informs the choice to study nutrient limitation at the highest starting cell concentration to mitigate the media's carbon and nitrogen contamination. The more concentrated cells are at the beginning of the incubation, the faster they exhaust carbon and nitrogen supplies, and the shorter the effects of the presence of spurious carbon and nitrogen are.

2.1.3 Physical settings

This section tackles other challenges linked to the physical experimental set-up. Because the experiment happens on a time scale of weeks, phenomena, such as the evaporation rate, need to be addressed proactively. Evaporation could cause the media to change properties, as the liquid evaporating would make the chemicals remaining in the media, such as salts, more concentrated. This property change in salinity could, in turn, impact bacterial viability. Another element to balance with evaporation is the need for the media to be aerated for the duration of the experiment. This need for a constant oxygen supply throughout this experiment eliminates

the possibility of having a completely sealed-off system. The bacteria also need to be in the most homogeneous milieu possible throughout the experiment while being incubated in a sufficient volume for destructive sample harvesting. *Vibrio coralliilyticus*, the strain chosen for this experiment, is also highly temperature-sensitive [84]. Thus, the samples need to be incubated in a temperature-regulated environment. All of these constraints are explored in more detail in this section.

Vibrio coralliilyticus is in the research spotlight of coral scientists because its contribution to coral bleaching increases significantly with temperature changes [15, 84]. As past trends and upcoming predictions indicate that the surface levels of the oceans are warming up on a global scale [102], this coral pathogen can become more lethal to corals. It is known that the behaviors of *Vibrio coralliilyticus* are highly temperature-dependent and that a difference in 2°C can switch molecular regulatory mechanisms [84]. This has implications for the experimental set-up of long-term nutrient limitation. The temperature needs to be controlled precisely for the experiment to be reproducible. Leaving samples to the odds of room-temperature variations becomes infeasible in this case. This justifies the incubation of cells in a temperature-controlled incubator. The temperature of this incubator is set to 25°C that is optimal for *Vibrio coralliilyticus*. In the context of coral health, 26°C is the temperature at which this pathogenic bacteria becomes highly virulent [84]. In this experimental set-up, the temperature is a constant value throughout the limitation in nutrients.

Here the nutrient limitation experiment is designed to last multiple weeks. The experimental system needs to retain constant chemical concentrations and homogeneous properties for that time. The bacterial cultures are placed on an orbital shaker such that each sample mixes. A key chemical element is oxygen, as the bacteria of interest *Vibrio coralliilyticus* exhibits changes in motility depending on oxygen concentration [184]. This leads to favor a container whose largest dimension is not depth, so that oxygen can be exchanged more uniformly at the interface between the air and the media.

There is also a trade-off between the number of replicates and the range of bacterial concentration that can be explored. Bacteria can indeed exhibit density-dependent

properties [142, 133, 43], notably due to their widespread quorum sensing abilities. Thus, I need to either demonstrate that the experimental results seen are not affected by bacterial density within a certain range or to quantify how much these experimental results vary with density variations. From an experimental design point of view, a high volume of culture enables the observation of lower bacterial densities in a more reproducible manner. However, higher volumes require more space and lower the experimental throughput. Here, I settle on a system that can attain 1 bacterium per mL at its minimum by fixing the experimental volume to 5 mL. It is also the maximum volume a 6-well plate on an orbital shaker can sustain without splashing. These stackable plates allow for technical replicates while fulfilling the necessary technical requirements.

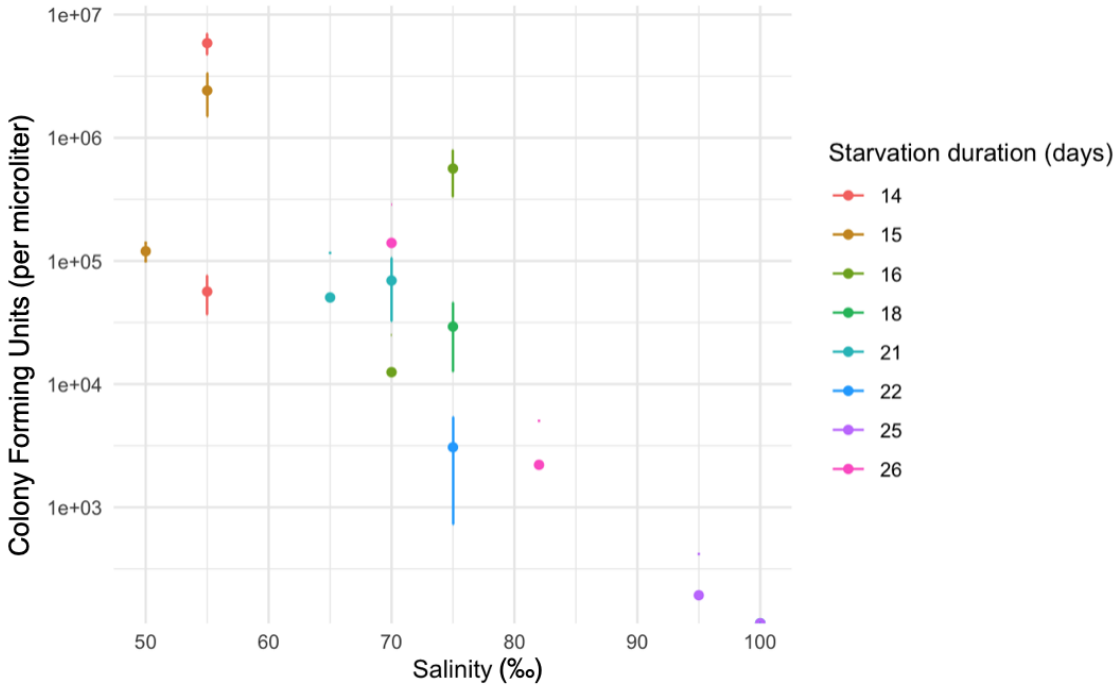

Figure 2-6: Colony Forming Units as a function of number of measured salinity in ‰. The colors present the different starvation durations of each sample. Each point is the mean of a technical triplicate, measured with a refractometer. The lines are error bars around that value.

When using 5 mL of culture in a 6-well plate with a semi-permeable plate seal,

evaporation happens at a rate of 200 µL per day. This fast evaporation rate leads to an increase in salinity. A way to mitigate evaporation is to increase the humidity in the temperature-controlled incubator by putting a reservoir of liquid within that space. Even though the implementation of this method leads to a decrease in the evaporation rate in the wells, it also increases the humidity in the whole incubator. This change induces a critical error in the temperature regulation system of the incubator. Efforts to mitigate the evaporation rate need to be more localized by the samples. It is also notable that not all plates evaporate at the same rate within a stack of plates. Wells that are the most surrounded by other wells filled with liquid evaporate at a lesser rate. Another remarkable fact is that in a stack of multiple plates, plates at the bottom of the stack evaporate faster. Therefore, the final implemented method in the experimental set-up consists of stacking the plates containing the samples above the plates containing water and sampling the middle well of each plate last. After implementing this method, the salinity in samples is tracked with a refractometer. As the freshly made media mimics seawater, the baseline salinity is 35 ‰. Figure 2-6 shows that salinity in the samples increases over time and reaches 50 ‰after 15 days of incubation. Because of that, I decided to remove from analysis any sample that is past that duration. Notably, salinity stays stable for the first two weeks, which indicates that the solutions for mediating evaporations are effective.

2.2 Observing starvation

In this section, I described the experimental methods for observing the impact of nutrient limitation on bacterial phenotypes. These readouts focus on the four bacterial behaviors that can be tied back to the ecological persistence of a bacterial population: cell viability, cell size, cell motility, and cell stickiness. Bacterial viability and motility both support successful bacterial foraging for particles. These foraging efforts lead to effective bacterial colonization if bacteria maintain their abilities to attach and re-grow on complex nutrient sources. This work aims at capturing the alterations to these phenotypic properties due to nutrient limitation. These parameters are quanti-

fied at both a population and single-cell level. The aggregated measurements give a comparison point to existing works [125, 91]. The individual-level characterizations explore the impact of nutrient limitation on population heterogeneity. They also provide precious information for modeling, be it for their conceptualization or their parameterization, especially in the case of stochastic processes such as foraging. This dual experimental approach is highlighted in each of the following sections.

2.2.1 Cell viability

The number of viable bacteria within a space determines the odds of successful bacterial foraging at a population level. The more bacteria there are, the more likely it is for some bacteria to find a particle. A first factor to take into account is that cell size can change due to nutrient limitation in order to maximize their surface-to-volume ratio [65, 128]. As optical density measurements rely on the light scattered by cells and thus depend on cell size and shape, they do not provide an accurate measurement of cell concentration. Also, after the onset of nutrient limitation, the number of viable cells is expected to drop dramatically because of cell death [144]. Optical density does not capture the difference between viable and dead bacteria. To measure cell viability, other techniques need to be deployed. Here, I present four methods which were used in my project to quantify on the number of viable cells after inoculation in a nutrient-free medium.

Colony Forming Units

This method, which has been optimized for decades, consists in counting the number of colonies formed on an agar plate made up of rich media after plating bacteria. The assumption is that each circular colony stems from one single ancestral cell. The number of cells in a sample can then be backtracked by equating the number of colonies to the number of cells in the amount of volume dispensed to make the plate. A key step of this protocol is to plate the right amount of bacteria. When there are only a few colonies, the bacterial counts are not statistically significant. Conversely, too

many bacteria can make it challenging to distinguish different colonies. High bacterial density can also lead to growth inhibition because of resource limitation. The target bacterial number on a plate is between 20 and 250 [166]. This can be achieved by plating different 20-fold dilutions from the initial bacterial sample. To increase the reproducibility in bacterial numbers, it is also notable that the way bacteria are plated needs to be consistent. In our experimental set-up, I used between 4 and 6 glass beads that are shaken on the agar surfaces with a $10\mu L$ drop of bacterial culture to plate bacteria on agar plates brought to room temperature at least 2 hours in advance and at most two days. These two decisions were meant to decrease the uncertainty due to the number of bacteria attaching to the surface of glass beads and the influence of the water content of the agar plates on the rolling of the beads.

On top of all these technical considerations, this method relies on the regrowth of each bacterium. It doesn't only estimate the number of bacteria that are in a sample. It also quantifies the number of bacteria that are able to grow again on an agar plate made of rich media. This number of bacteria is the closest approximation to the number of bacteria that will be able to resume their normal growth once they attain a particle. Even though growth on a Petri dish requires a specific set of properties that can lead to an underestimation of the number of viable bacteria [185], it is the only method for bacterial counting that relies on growth. This is the primary reason why I chose this method over others to estimate bacterial viability for starving cells.

Flow Cytometry

Another possible route to quantify viability is to use flow cytometry combined with a live/dead stain. Contrary to counting colonies, this method can provide more information, such as the count of dead cells, live cells, and potentially cell size distributions. It comes with a cost of optimization. In this section, I will present some of the data collected using flow cytometry and the reason why I decided not to use the data for precise quantification.

Flow cytometry can be used as a tool to count the absolute number of cells. As I chose not to use fluorescently labeled bacteria for the nutrient limitation experiments

2.1.1, dyeing the bacteria provides positive control of what can be considered a cell. With the aim to achieve the most precise measurement possible, I used SYBR green stain, whose signal is the most powerful. That stain is highly sensitive to both light and temperature. It is recommended to prepare a fresh stock of it every week and to thaw that stock only right before sample preparation while mixing it thoroughly with the samples. All these steps minimize potential noise in the readout on the flow cytometer. After an incubation period with the dye, the cells can be passed through a flow cytometer, here the InCyte Guava. A sample of the data collected within that assay can be seen in figure 3-2.

This data qualitatively presents similar results to the ones described in section 3.1.2 and will be reviewed in more detail in that same section. Here I focus on the technical challenges that come with analyzing the scatterplots generated with the flow cytometer. Analysis of this type of data can be conducted using licensed software like FlowJo™ Software or R packages such as CytoExploreR [64] or FlowCore from the Bioconductor suite [63]. These different options need to be evaluated given availability and compatibility with the data files and processing systems. For example, the flow cytometer InCyte Guava saves one condensed multi-run file that cannot be read by FlowJo™ Software, which then requires some data reformatting. The major technical challenge stems from the cell size reduction along with starvation duration. The main process associated with flow cytometry data analysis consists in designating a multi-dimensional shape that will select particles with a certain set of properties. This process is referred to as gating. As cells change their size over time, the gates need to either be dynamically updated at each time point or cover a large enough area to be relevant. The first method reduces the ability to compare each time point, while the second one is doomed to capture more noise. This data was analyzed through the first method.

It is notable that flow cytometry data can also reveal the changes in cell sizes. Forward scatter depends on the light diffraction from each cell, which is a function of cell size [93]. It can be used to approximate cell size. However, it is limited by how broad the angle collection for that scattering is[25]. The intensity of DNA binding

fluorescent dyes can also be seen as a proxy for cell size. The bigger the cell, the more DNA there is for the dye to bind to. The caveat of this last size estimate is that this can also be linked to cell permeability and thus does not reflect a change in cell size but in cell membrane porosity, as explored in section 2.2.4.

Live/dead staining relies on the dual staining of cells by two chemicals. In the case of the BacLight™ kit offered by Sigma, all cells are labeled by the green fluorescent die SYTO9, which binds to DNA. Propidium iodine only permeates dead cells and becomes fluorescently red when bound to DNA. This dual staining captures the proportion of dead cells in a sample. As both the dyes bind to DNA, I determined the relative concentration of those stains by running samples with known concentrations of dead and alive cells. This data was used to define gates for those two populations. However, the same challenge of quantifying bacterial concentrations for cells with a wide size range remains. This staining provides another information piece that is not available through any other method: the timeline at which dead cells appear in the media. Determining the presence or the absence of a certain population type indeed requires less precision than quantifying their abundance. It is notable that a stable bacterial concentration counted by colony-forming units could be due to cell recycling. The recycling hypothesis postulated that some dead cells support the division of cells by releasing nutrients to the media. If there are no dead cells in the media, this nutrient cycling based on necrosis cannot happen. All in all, flow cytometry coupled with live/dead staining can be used to better describe the starving sample at any time, even though cell size variation impacts the comparability between samples.

2.2.2 Cell size

The reduction in bacterial size under nutrient limitation influences the ability to quantify cell numbers. Optical density is a good approximation for cell concentrations only when cell size is constant. In figure 2-2, optical density measurements decrease right after the maximum value has been attained. This could be the result of either cell death or cell size reduction. When it comes to flow cytometry, the dynamics of cell size reduction lead to an increase in noise levels and a drop in cell count accuracy,

as shown by the raw data in figure 2-7. There are incentives to quantify the individual sizes of bacteria because of technical limitations and also because of its potential for uncovering some population heterogeneity. The variation in cell sizes also happens at a single-cell level. I investigated two methods to do this quantification. A Coulter counter estimates cell volume, whereas suspended microchannel resonators read cell buoyant mass as an approximation for cell biomass. In this section, I provide an overview of both these techniques.

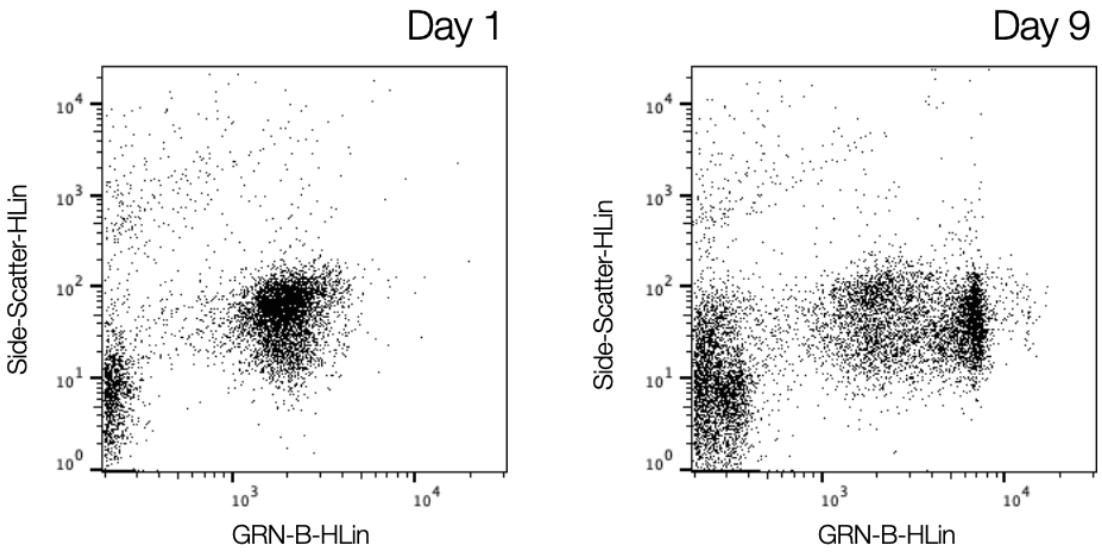

Figure 2-7: Raw flow cytometry data after 1 and 9 days of starvation. This graph presents green fluorescence on the x-axis and side scatter on the y axis. Each point is a particle detected by the flow cytometer

Coulter Counter

These instruments are based on the Coulter principle, successfully patented in 1953 for the first time [31]. The size of the bacteria are derived from the difference in conductivity between a cell and the electrolyte solution in which it is suspended. If a single cell goes through a small channel, then the impedance of this channel changes. The measured electric current going through the channel can be linked to the cell volume from a standard curve, as this current drop is proportional to the cellular volume. This method is high-throughput, as it only requires making cells

pass through a channel and tracking the drop in electrical current. Although mostly used for blood cell counts, this can be applied to bacteria in salty water too, as long as the Coulter counter is blanked with the media in which cells are suspended.

Coulter counters were first developed and are still primarily used for mammalian cells, which are significantly bigger than our bacteria of interest. Transposing this method to shrinking bacteria necessitates a higher size resolution. The precision in volume measurement depends on the size of the channel bacteria flow through. The smaller the channel is, the more significant the change in impedance is. To conduct our experiment, I selected the smallest aperture size ($20\mu m$) available at the FlowCore Operations in Harvard. Even with this aperture size, the distribution of cell volumes is truncated on the lower end (see figure 3-3). The resolution of this apparatus does not allow for the detection of smaller bacteria, as the signal-to-noise ratio would then be too low. Some spurious particles, such as crystals, could then be picked up as a bacterial signal. The Coulter counter performs better at giving a size estimate than flow cytometry. These two machines have been used consecutively before to sort cells by size first and then analyze the dyeing signatures.

Suspended Microchannel Resonator

Another way to measure cell mass is by flowing cells through a suspended microchannel resonator (abbreviated SMR throughout this thesis), a technology first developed by the Manalis lab in 2007 [54]. This device weighs single cells in real-time as they pass through a hollow channel in a cantilever while still suspended in their growth media. The change in the cantilever's weight transposes into a change in its oscillating movement. This frequency change is then measured and quantified. It can be backtracked to the volume of fluid that was displaced while the cell was in the channel. While this method requires a more complex set-up than a Coulter counter for a similar throughput [164], it exhibits a striking precision within the order of magnitude of femtograms for marine bacteria [26].

With this device, we consider that buoyant mass is a good proxy for the biomass in the cell. Buoyant mass corresponds to measuring the relative weight of the cell

with respect to the weight of the solvent surrounding the cell. That variation in the mass within the cantilever causes it to change its oscillatory pattern transiently. As the device is first calibrated with particles of known mass and buoyancy, the second mode of the frequency distribution can then be used to access the buoyant mass. One caveat in this method is that bacterial biomass has to stay at a similar density. The amount of liquid within a cell doesn't matter, as this liquid is at equilibrium with the solvent in terms of mass because of the osmolarity forces. However, the packing of molecules does. Here I consider that bacterial biomass density doesn't change with time.

The suspended microchannel resonator was first used for mammalian cells and then developed for bacteria. The device resolution needed to be adapted to smaller particles. The limit of detection for some devices is above the expected bacterial size after starvation. Cermak et al. show that the size of *Vibrio cyclotrophicus* decreases more than five-fold from exponential growth to a late steady state [26]. That device parameter is controlled by the dimensions of the channel cross-section. A smaller cross-section comes at the cost of lower throughput, as less fluid flows through the channel at identical flow rates. As the volume displaced within the channel is part of the readout, the dimensions of the device need to be consistent across samples, so the measurements for exponential and starved cells need to cover the variability in cell size over the course of the incubation in nutrient-depleted conditions. Here, the dimensions of the device of choice are $5\mu m$ x $5\mu m$. There is also now a commercially available version of this instrument, called the Life Scale developed by Affinity Biosensors.

2.2.3 Cell motility

Microbes move within their environment. This movement can be passively driven by diffusion [193] or actively motored by flagella and other cellular processes [98]. An integral component of discussing bacterial foraging consists in quantifying these cellular trajectories at both a population and a single-cell level. Advances in computational data analysis, microscopy technology, and lab techniques, such as microfluidics have

greatly contributed to a more precise characterization of these stochastic behaviors.

Lab techniques

At a population level, bacterial motility can be assayed using soft-agar plates. The principle is to inoculate a bacterial population at a localized point in the plate and look at how much the bacteria have diffused through the soft agar after a certain time using a dye that can track bacterial activity [34]. While this assay is worthwhile to screen different strains for motile properties, it does not provide quantitative information about motility. Soft-agar plates are a porous media and not a liquid media, which impacts the ability of cells and particles to move through it. It is also a binary visual assay that provides a population-level measurement. Thus, it does not fit the requirement for the data that this study aims to gather to look into variability.

Qualitative studies about the presence or absence of active motility at a single-cell level [105, 91] have typically used flat glass capillaries. Glass capillaries are very narrow tubes that can be filled through capillary action that is driven by both surface tension and adhesive force. Once loaded in a flat glass capillary, a sample with motile bacteria can then be observed by microscopy. The capillary provides the bacteria with space that is both large enough to allow them to swim and constrained enough such that the bacteria don't go out of the field of view. This motility assay can be extended to measure chemotaxis by immersing one extremity of the capillary in a drop of media full of chemo-attractants. This method provides a first approximation of the absence or presence of motility in a sample. One caveat of this method is that bacteria become deprived of oxygen once the ends of the capillary are sealed because glass does not allow for the transfer of oxygen. This starvation in oxygen impacts the ability of bacteria to move, as the flagellar forces are sensitive to oxygen concentration [3]. Figure 3-5 presents examples of trajectories recorded more than ten minutes after capillary loading. The expectation is that *Vibrio coralliilyticus* displays straight runs, while the observed trajectories here are curved, which is an indication of oxygen deprivation [184]. The observation of a bacterial sample within a capillary is thus very time-sensitive and needs to happen before oxygen concentration is depleted.

Another caveat of this method is that the channel's narrowness increases the chances of bacterial motility being skewed by either adhesion or collision with the walls. Even though these edge effects are alleviated by the addition of PVP40 in the media as explained in section 2.1.2, they impact the ability to quantify bacterial motility by potentially underestimating the proportion of motile cells. It also influences the type of motility observed.

Advancements in microfluidics make it possible to put bacteria in a chamber of the desired size that is permeable to oxygen. Channels are commercially available through ibidi (here, I use the 6-channel microscopic slide called $\mu - SlideVI0.1$). The design of these chambers is also very flexible. I chose a capillary-like chamber that is high enough to avoid vertical edge effects while small enough to be able to image the bacteria in bright field microscopy. The same considerations about edge effects were applied to choose the width of the chamber. This channel can be loaded with a pipette. The extremities of these chambers are made of liquid reservoirs that avoid the drying out of the channels. To further avoid liquid from moving around in the chamber during the imaging, these reservoirs are filled up to an equal amount of media while being sealed by Parafilm. The throughput is also increased by using these channels, as they are manufactured to fit six of them onto a standard microscopy glass slide. This set-up also decreases the time spent looking for focus. This is the device that was chosen to make all the motility measurements in this paper.

Imaging set-up and computational analysis

Another noticeable improvement to study bacterial motility comes from the evolution of imaging technology. Microscopes can now be mounted with high-speed cameras, be it directly from the provider or in a more artisanal fashion with a 3D printed support for smartphones. The increase in frame rate makes it possible to assign each cell in every frame to a particular trajectory, especially for bacteria exhibiting as high a speed as *Vibrio coralliilyticus* [184]. During its straight runs, this bacteria can move up to $56\mu m/s$. A high frame rate decreases artifacts in trajectory assignment for each bacteria, as the distance that one bacteria goes through between two frames is

smaller. In an ideal case, the time between two frames is shorter than the time it takes for a bacteria to move less than half its diameter. This way, when these two frames are superposed, the bacteria from both the first and the second frames overlap. There is then less uncertainty on how to label bacteria through time. The speed of acquisition associated with the ability to detect individual bacteria generates a large dataset of movies that then need to be analyzed.

Quantification of such images relies on the more widespread accessibility of the newest computer vision technology. That change stemmed from the release in 2000 of the OpenCV library [22], an open-source resource to make computer vision tools usable by most. This library, whose performance is still regularly upgraded and maintained, provides an efficient base for many other applications and circumvents the need to reinvent the wheel with every new image processing pipeline. The videos gathered for motility analysis present a computer vision challenge as small objects like bacteria need to be detected and distinguishable for noise, while their run length needs to be covered. This trade-off already appears when capturing images. The chosen objective, here the 20x objective on the ImageXpress® Micro Confocal automatic imaging system from Molecular Devices, needs to zoom in enough for bacteria to be detectable. The bacteria I consider are less than $1\mu m$ in size. However, it also needs to zoom out enough to enable a large field of view. That last property is key to follow a bacteria for the longest distance possible and also to enhance the number of observed trajectories, as many more bacterias are tracked. Here, I use the Python package trackpy to detect bacteria [6]. For each frame, the features, here the microbes, are located by entering parameters such as the approximate size of the considered objects. Given the small bacterial size, it is important to note that the microscope settings of image digitalization such as the binning size matter. The binning size configures the real size in micrometers of a pixel. The higher the binning, the bigger the pixel, the smaller the recorded bacteria. This leads each movie to be approximately 4 gigabytes as each image is 2048 pixels wide and large with a frame rate of 40 images per second. Considering the size of this dataset, the parallelization tool of object detection offered by trackpy is necessary for efficient image processing.

Once bacteria have been detected, another computational challenge stems from extracting information from the position of the bacteria, which corresponds to assigning each bacteria to its own trajectory. The trackpy package implements the Crocker-Grier blob detection algorithm in a scalable and testable manner [32].

2.2.4 Cell Stickiness

Once cells find a nutrient-rich patch, they need to attach to it in order to take advantage of all the resources available there. This transition from a free-living foraging state to a growing state is influenced by how long the cells have spent in their foraging environment. The attachment rate depends on the duration of bacterial foraging. In the particle system from a bead-centric approach, detachment rate is the parameter being measured and simulated [42]. Here, I focus the study on the free-living environment, and thus measure attachment. The dependency on the initial state then makes attachment to particles the focal point.

Attachment by a cell to a particle is the fruit of an interaction between the cellular membrane and the physicochemical properties of the particle. The surfaces of the two encountering elements need to be compatible with respect to their hydrophobicity and their electronegativity [92]. Quantifying attachment is then specific to a particle type. On a larger scale, colonization of the bacterial community is indeed dictated by the available particle types [44]. Here, I only focus on the first step of particle colonization: cell stickiness to the particle material of choice. Bacteria can also mediate attachment to surfaces with active molecular machinery such as type IV pili [183]. In this study, I am interested in the emergent property of attachment and not necessarily which mechanism renders it feasible. This is why I focus on the attachment to chitin by *Vibrio coralliilyticus* before and after starvation.

The physical properties of chitin make it a very challenging carbon source to study. Chitin is indeed insoluble in water. Previous studies have used a system of pre-manufactured chitin beads [34, 44, 45] to look at bacterial colonization. Those chitin beads can be filled with magnetic cores, which allow for easier manipulation by facilitating the washing step. To maintain their integrity, they are indeed stored

at 4°C in an alcoholic solvent that is absorbed inside of the beads at equilibrium because chitin is a biogel [1]. As those beads were indeed originally conceived for protein purification and not bacterial growth assay, preparing these chitin particles effectively requires washing them thoroughly. It is also notable that outsourcing the fabrication of such a key element calls for chemical lot tracking and lot consistency, as the manufacturer can choose to change their process, which may in turn alter the structure of the chitin, which influences adhesion to chitin [117]. There must also be consistency in the number and size of the beads present in each incubation. This requires filtration steps of the original bead stock and a working knowledge of the bead concentration in the lot.

Bacteria can be inoculated with magnetic chitin beads. This inoculation happens within a solvent, artificial seawater. This experimental system needs to be controlled for fluid dynamics. Recent studies have underlined the importance of flow when looking into the ability of cells to colonize a particle [5]. The water movement in the media changes the encounter rate, as bacteria can then be transported by the ebbs and flows. As seen in a later chapter 3, the impact of turbulent flow can outweigh the contribution of bacterial motile abilities. A first iteration of this inoculation consists in incubating bacteria with chitin particles in a 96-well plate to allow for time-lapse microscopy. Even though these wells are sealed with MicroAmp optical adhesive film (ThermoFischer), the stage movements of the microscope and the natural condensation that happens lead to a non-static liquid environment. This first set-up was used to uncover the dynamics of long-term bacterial colonization on particles, as further explored in Appendix D. When it comes to quantifying attachment though, it lacks reproducibility. The unconstrained fluid movement is an emergent property of this system that is difficult to control. A second iteration of this encountering dance between chitin beads and bacteria embraces this idea that the milieu is dynamic [43]. In that case, the incubation happens in a 15 mL Eppendorf tube put on an overhead rotating wheel. This enables reproducible turbulence patterns within the media. The number of beads is also known and reproducible (250 beads per mL). The drawback of this assay is that building a time course then cannot be automated on a micro-

scope. The inoculation needs to manually be transferred to wells for observation. This lowers the throughput of that experiment significantly. However, in the comparison between the different physiological states of *Vibrio coralliilyticus*, time-lapses are not necessary. This is why I choose this second method for the sake of heightened reproducibility.

One disadvantage of using the chitin bead system is that imaging on a sphere is tricky. It requires either confocal microscopy or a way to consistently determine focal planes. As chitin is a biogel that can theoretically take many forms, it would be ideal to image a flat chitin surface. The diverse shapes chitin takes in the exoskeletons of animals vouches for the feasibility of such an endeavor. I explored two avenues to forming chitin flats.

The first one consists in using chitosan, a deacetylated version of chitin, that is soluble in acetic acid and thus can be shaped into a flat surface. It is for example possible to etch a glass slide using Piranha solution then drop-cast the liquid chitosan to then spin coat that chemical. As spin coating forms a very thin layer of chitosan (of the order of one molecule high), it can then be dried up and functionalized with an acetyl group. Even though the height of the chemical that needs to be functionalized is short, this protocol would still require a careful quantification of the success of the reaction from chitosan to chitin. The low thickness of the obtained surface is also a drawback when considering bacterial growth, as the supply of resources would then be very limited and could create spatial artifacts. On top of these technical and conceptual limitations, this protocol also contains a very hazardous step. I did not follow through with this method.

The second technique aimed at dissolving chitin itself and then casting it in the desired shape. Hexafluoro-2-propanol (later abbreviated HFIP) is the solvent that can dissolve purified chitin. For this dissolution to work, it is notable that chitin flakes need to be thoroughly purified, as most chitin purchased through industrial vendors is isolated from natural samples and thus mixed with other molecules such as proteins. After the purification step is done, chitin flakes are incubated with HFIP in a stirring flask for at least 48 hours. It can then be drop-casted on a 96-well

plate, then left to dry off. As HFIP is highly volatile and the casting happens in small volumes, the speed of the drying off needs to be mitigated by covering the surfaces. Otherwise, it impacts the structural integrity of the chitin film. The surface on which the dissolved chitin is cast also needs to be functionalized so that chitin stays attached to the bottom of the wells in the case of a 96-well plate when surrounded with media. Some surfaces come ready for such a use, like the delta-treated Nunclon Thermo plate (catalog number: 168055). If this is not available, plasma treatment offers an option to make the chitin sheet stick more to the bottom of the plate for an easier imaging process. A drawback of this method used in a 96 well-plate is again that flow around the chitin and within the media is not controlled. I used these flat chitin sheets to measure bacterial growth on chitin with an optical density readout. However, quantifying cell attachment to chitin requires spatial definition and hence microscopy.

Chitin is also an auto-fluorescent chemical. Its biogel properties also make it more likely to absorb and trap whatever is in the solvent. Even though chitin is theoretically transparent, it is still a material whose structure impacts visibility when imaging. For example, quantification of attached bacteria on chitin beads or on chitin sheets can not be obtained by phase-contrast microscopy, as the surface of chitin is irregular and creates imaging artifacts. That is why I use a stain that binds to bacterial DNA to distinguish the bacteria from the beads. The signal of the dye needs to be triggered by a binding and needs to be powerful enough to overcome the noise created by the chitin auto-fluorescence. The dye of choice is SYTO-9, which is notably used within the BacLight staining kit presented in section 2.2.1. High concentration of this dye changes bacterial behaviors, such as growth. This is not an issue when considering single-time sampling, such as the chitin bead assay with controlled dynamic flow. The dye can then be added right before the imaging. All of the attachment data presented in section 3.3 has been taken using this assay.

The output of the microscopy data is a projection of the maximum intensity on the Z-axis from a confocal Z-stack for each bead. This image is then analyzed using a pipeline developed on Matlab, which first identifies the localization of the bead using

its auto-fluorescence and then distinguishes the bacteria on the beads. Both of these features are detected after denoising the image through a Gaussian filter and then thresholding the image using either a global threshold or a local one.

2.2.5 Cell Regrowth

Successful bacterial colonization doesn't only rely on finding and attaching to a particle. It also requires the attached bacteria to revert their starved state to a growth state. That's why I aim to quantify the growth of bacteria after starvation on different carbon sources. These carbon sources range from simple soluble sugars such as N-acetyl-D-glucosamine to insoluble chitin. I measure the optical density with a time-resolved 96-well plate assay on a plate reader in the case of simple, soluble carbohydrates. The bacterial inoculum is then composed of cells starved for a range of durations at different initial concentrations. This extensive set-up casts light upon potential cooperative behaviors that bacteria could exhibit once starved. The shape of dependency of lag time with respect to the initial bacterial concentration gives information on the population's cooperation [8]. Growth curves build a wealth of parameters such as the growth yield and rate.

However, these assays are challenging when it comes to the insoluble carbon and nitrogen source: chitin. In the previous section, I explored the different structures that chitin can be shaped into to study attachment. Here, I will focus on using colloidal chitin with an assay that was first developed by Pollak, Grakla et al. [137]. This particular physical form corresponds to suspended microparticles of that insoluble chemical within an artificial saltwater media. After inoculating the bacteria with these colloids, these clumps make it impossible to directly measure the optical density of bacteria, as they interfere with the readout. One step of the protocol consists in separating the colloids from the bacteria. As they have a bigger mass, centrifugation helps sediment those particles in the bottom layer. The top layer is then sampled and dyed with the DNA stain SYBR™ Gold, developed by Invitrogen. The measured fluorescence after incubation is a proxy for the DNA concentration. That amount is not strictly equivalent to the number of cells, especially when considering that starved

cells are way smaller and potentially have less DNA than exponentially growing cells. Counting colonies is a way to avoid that caveat. Nevertheless, more DNA means that cells are definitely growing, but not necessarily in numbers. As this assay requires centrifugation and bacterial extraction, it is destructive and significantly lower throughput than a typical optical density growth assay. This method provides some important information on the bacterial ability to re-grow on chitin. This protocol notably gives a rough timeline on chitin growth that can be used as a sanity check for attachment measurements on chitin beads.

2.3 Protocols

This section sums up all the methods implemented within the lab to obtain the experimental results presented in chapter 3.

Bacterial culturing

Wild-type *Vibrio coralliilyticus*, YB2, was streaked from a glycerol stock onto a Marine Broth (Difco 2216) plate with a 7% agar concentration. After 24 hours of growth at 25°C, a single colony was used to inoculate 2mL of rich media, whose recipe is described in table B.9; incubations at 25°C lasted for 4 hours, shaking at 200 rpm. Subsequently, that culture was diluted by factors of 10^3, 10^4 and 10^5 in base media (see table B.7). After 20 hours of incubation at 25°C, based on optical density (abbreviated OD), the cell concentration was diluted down to an OD of 0.005 in a final volume of 5mL of media depleted in carbon and nitrogen (see table B.8). This inoculum was put in a 6-well plate sealed with breathable culture film at 25°C, lodged between four other 6-well plates filled with water (to mitigate evaporation). This assemblage of plate was then shaken for the desired duration of starvation at 200 rpm.

Bacterial staining

For flow cytometry purposes, cells were stained either with the LIVE/DEAD™ BacLight™ Bacterial Viability Kit (Catalog Number: L7007) or with fresh 0.3% SYBR™ -Green stock (Catalog number: S7563) diluted in mPBS.

To measure attachment with the ImageXpresss® Micro Confocal system, a $195\mu L$ cell sample was stained with $5\mu L$ of 1:20 stock of SYTO™ 9 Green Fluorescent Nucleic Acid Stain (Catalog number: S34854).

Viability

Colony Forming Units were counted by plating different 1:20 dilutions of the initial sample onto Marine broth agar plates. Spreading on this plate was done using 4-6 sterilized glass beads. The colonies were then manually enumerated after 20 hours at 25°C.

Cell size measurements were done with Guava® easyCyte for flow cytometry (gated using FlowJo), with a Coulter Counter of $20\mu m$ aperture and with a $5\mu m$ x $5\mu m$ Suspended Microchannel Resonator. The data on that last device was collected by Yanqi Wu.

Motility

$20\mu L$ samples were incubated in the 6-channel microscopic slide called $\mu - SlideVI0.1$ (Catalog number: 80666). The chambers at both end were filled with up to $40\mu L$ of the same media to balance out the potential capillary pressure. These chambers were then sealed with Parafilm and imaged using ImageXpresss® Micro Confocal system via stream acquisition in Phase-contrast with a 20X objective at a fixed frame rate of 40 frames per second. The images were quantified using the trackpy package on Python [6] and the resulting trajectories were analyzed with R.

Attachment to Chitin Beads

The bead stock was made of $500\mu L$ of magnetic chitin particles (Catalog number: E8036S, Lot number: 10034184). After adding 1mL of starvation media, that stock was washed three times with the help of a magnet. For size selection, that stock was first poured on a $40\mu m$ strainer. Particles on the strainer were then transferred onto a $100\mu m$ strainer, filtered through with 40 mL of media for the final bead stock.

The inoculum for an attachment assay consisted in 4 mL of starvation media, 4 mL of the chitin bead stock and 4 mL of the bacterial inoculum at the desired concentration. This mix was incubated in a 12 mL Falcon tube in an overhead rotating wheel undergoing 1 full rotation in 20 seconds, at room temperature. After usually 20 hours, $195\mu L$ of the mix was transferred to a 96-well plate with $5\mu L$ of SYTO™ 9 for imaging a Z-stack on the ImageXpresss® Micro Confocal system.

Rescue on chitin

To prepare flat chitin sheets, 50 mg of purified chitin powder was put in a 6 mL glass vial with a cap and a stir bar. Once in a fume hood, HFIP is added to make a 10 mg/mL chitin solution. This solution is stirred for at least 3 days. To coat the bottom of a 96-well plate, we added $32\mu L$ of chitin solution on the bottom of each well and seal the plate with plastic wrap to avoid fast dry-up. This should sit for one day in the fume hood. Then, bacteria (pre-stained with SYTO™ 9) can be inoculated in the well. After removing the air bubbles trapped under the chitin sheet (by pushing the tip of a pipette on top of it), the plate can be placed in a plate reader for optical density measurements.

To measure growth on colloidal chitin, $50\mu L$ of bacterial inoculum can be incubated in $150\mu L$ of a 4-fold dilution of the colloidal chitin stock in starvation media. The bacterial concentration at different time points is measured by centrifugating the plate for 30 seconds in a repurposed salad spinner and by transferring $50\mu L$ of top layer into $150\mu L$ of SYBR™ Gold After waiting 15 minutes, the fluorescence can be measured on a plate reader.

Image Analysis

The code for image analysis of attachment on chitin particles and of motility movies is available at https://github.com/eledieu/lostinstarvation

Chapter 3

Experimental evidence of phenotypic plasticity under nutrient limitation

This chapter gathers the results of our experimental measurements pertaining to the dynamic changes of bacterial behaviors under nutrient limitation. The aim is to characterize bacterial phenotypes relevant to microbial foraging at both a single-cell and population levels. This dual quantification could highlight the emergence of heterogeneities within one bacterial population and validate the hypothesis for bet-hedging. Here, I rely on the experimental set-up presented in chapter 2 that focuses on the incubation of *Vibrio coralliilyticus* in a media free of both carbon and nitrogen. Qualitative and quantitative observations are then leveraged in the next chapter to evaluate the constraints on successful foraging for a bacterial population in a patchy landscape.

3.1 Viability & Reductive Division

For bacteria, time scales of foraging and of other processes such as growth and death overlap. The quantification of bacterial foraging requires the tracking of abundance changes in the population during nutrient deprivation. I first measure the amount of bacteria in a nutrient depleted environment, and then I look into individual cell biomass to unravel potential heterogeneities in cell sizes and morphologies.

3.1.1 Cell abundance

The null hypothesis for bacteria in a nutrient-limited environment is that they die with a constant death rate fixed for each population [144]. Figure 3-1 presents the change in the absolute number of viable bacteria in function of starvation duration. Viability is here defined as the ability of a bacterium to grow on a rich media plate. This property is quantified by counting colony forming units on agar plates, as explained in section **??**. Here, the null hypothesis doesn't hold. Bacteria don't start dying until the seventh day of starvation. After that time during which the bacterial population persists, they die with a constant death rate of 0.01 per hour, which corresponds to the order of magnitude of the death rate observed in *Escherichia coli* [144]. This decrease in persistence is also not correlated with general media measurements such as salinity or pH, as seen in section 2.1.3.

As a comparison to this data, I can use the dataset collected by Holmquist et al. which tracks the changes in viability and respiratory activity in *Vibrio sp. 14* [67]. While cells in a carbon-depleted environment persist for up to five days, they also observe a delay to death for cells starved for nitrogen on the order of two days followed by dynamics governed by decay. When cells were incubated in a media free of carbon, nitrogen and phosphorus, they followed the trend of carbon limitation. Even though the time scale of their experiment is shorter than the one presented here, it brings additional evidence for the first phase of observed persistence in our case. It is notable that it is unclear how long *Vibrio spp.* can survive in a nutrient-depleted environment, when studies have shown that 80% of bacteria remained viable after 40 days in a nutrient-depleted media [139].

Another noticeable fact in this graph is that the number of bacteria doesn't only stay constant at the beginning but also goes up by an order of magnitude. This comes as a surprise as bacteria are inoculated in a new media without any carbon or nitrogen, as explored in detail in section 2.1.2 and 2.1.2. The carry-over from GlcNAc from the previous medium and potential contaminations cannot explain all the 3 divisions that cells undergo. Another hypothesis is that these bacteria can store

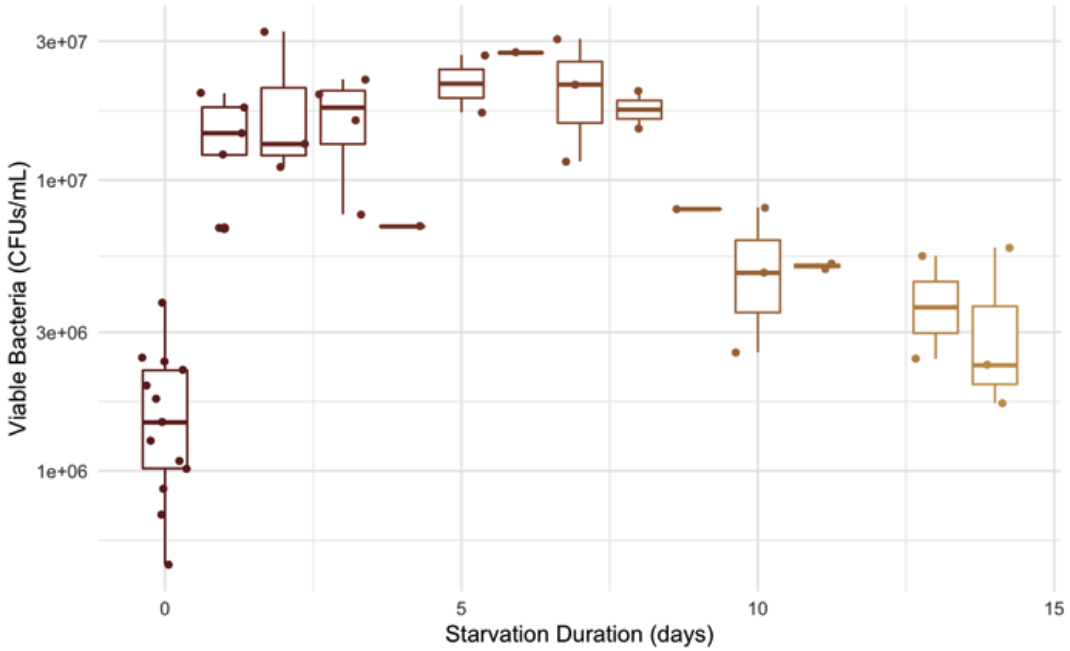

Figure 3-1: Abundance of viable bacteria as a function of starvation duration. The abundance is counted by colony forming units per mL. Each point is the average measurement of three technical replicates. Boxplots represent the 10 %, 25%, 50 %, 75 % and 90 % quantiles of the data for one day.

and utilize compounds, such as PHB, at the early stage of nutrient limitation. This is highly unlikely as the bacteria here are pre-grown in a controlled artificial seawater that provides them with everything they need but with nothing in excess [see table], contrary to marine broth. This difference in culturing conditions translates into a difference from more than 100 femtograms in the average cellular mass. This divergence hints towards a lack of nutrient storage in the bacteria used in this experiment.

Another potential explanation for the early increase in cell numbers is that cells are able to divide by reducing their total biomass. Here, I define reductive division as the process through which a daughter cell never reaches the maximal biomass of the mother cell. This hypothesis is motivated by the observation that *Vibrio spp.* can form ultramicrocells under nutrient limitation [129]. These smaller bacteria are believed to be more persistent. Validating this hypothesis requires precisely measuring cell sizes, which is the focus of the next section 3.1.2.

3.1.2 Cell size

Bacterial size corresponds to a single-cell property that can now be measured with a high-throughput. Here I present the results of three different methods, accessing three definitions of cell size. There is a dual aim to these measurements: the validation that cell size reduction occurs at the beginning of nutrient limitation and the exploration of heterogeneities between cells from a similar population.

The first cell size measurement is an indirect measurement, collected as a by-product to a flow cytometry run. In figure 3-2, I show that the mean of the forward scatter decreases ten times more from day 0 to day 1 of nutrient deprivation than between the next two days. Forward scatter is a proxy for cell diameter. This drop fits the time scale of the increase in bacterial abundance that primarily happens at the very beginning of nutrient limitation. As mentioned in section 2.2.1, the interpretability of forward scatter data is limited and is a good first hint that cell size reduction happens.

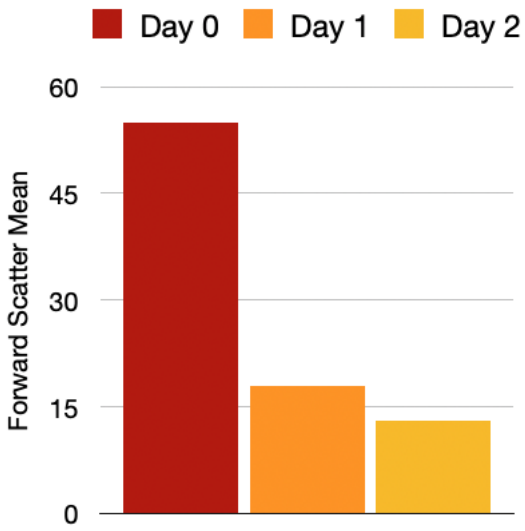

Figure 3-2: Forward Scatter Mean of bacteria in function of starvation duration. These average values was calculated for samples of more than 10^4 bacteria from a sub-population gated by a threshold for minimal dye concentration of SYBR-Green.

The second cell size measurement is yet another quantification of cell diameter done with a Coulter counter. This method presented in section 2.2.2 assesses the diameter of single cells within a certain range. In this case, the minimal cell diameter

detected is 0.7 µmeter. Within the first 12 hours of starvation, there is a shift in the cell diameter measured towards lower values, as shown in figure 3-3. In this lapse of time, big bacteria dwarf down, as the tail with the higher values of size gets slimmer. The distribution is also skewed from 1.0 µmeter towards the detection limit. These distributions are bell shaped and appear to have one mode within the observed values. The lack of range of the Coulter counter does not allow to have a full picture of cell size reduction in bacteria, as the distribution of starved cells' diameter is truncated at the lower end of the spectrum.

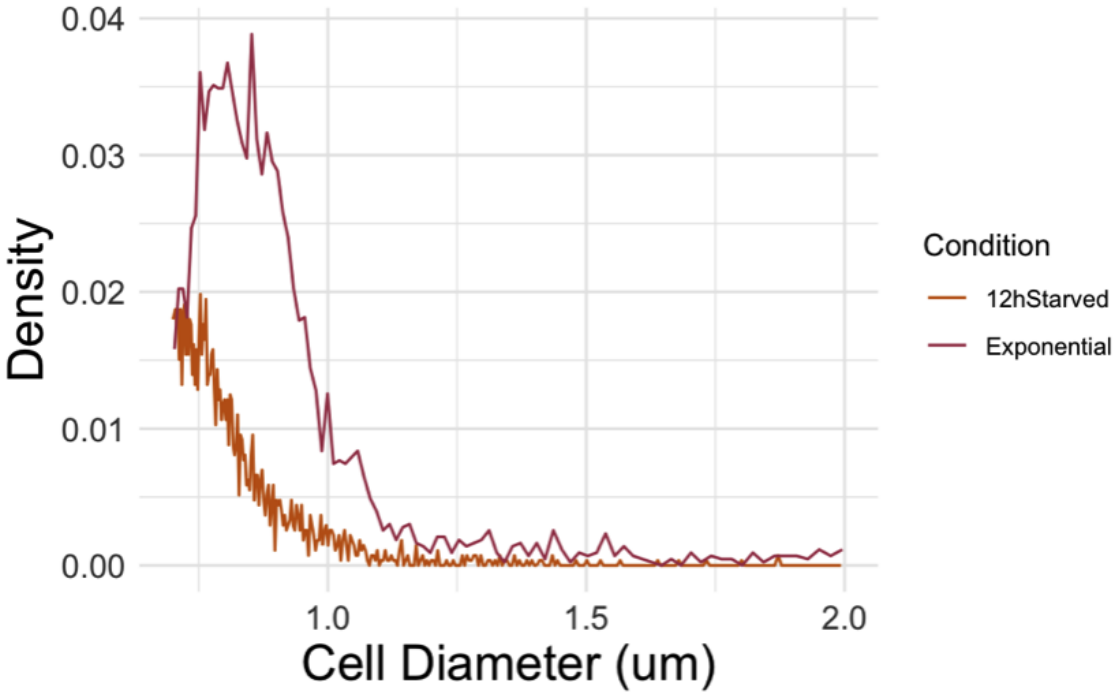

Figure 3-3: Distributions of bacterial size as measured by a Coulter Counter of aperture $20\mu m$ for around 2000 bacteria per sample.

The last cell size measurement leverages the technology of suspended microchannel resonators to output values of the cell buoyant mass. This state-of-the-art technique exposed in section 2.2.2 determines to a precision of one femtogram the mass of individual cells. In figure 3-4, each density distribution aggregates three independent biological replicates. The biomass of cells diminishes at a rate of 0.45 femtograms per hour over the first two days and continues to decrease at a rate of 0.09 femtograms

per hour throughout the whole starvation duration.

The early drop in biomass mimics the data collected for the cell diameter through flow cytometry and Coulter counter. This vouches for the hypothesis of reductive cell division. Compared to other mentions of the formation of ultramicrocells in *Vibrio spp.* [129], the phenomenon of reductive cell division happens earlier here. One potential explanation for this is the pre-culture of cells on a minimally rich seawater before their incubation in a nutrient depleted medium. This step could eliminate the apparition of storage compounds. Nile red staining that highlights the presence of PHB conferred negative results within our cells. The lack of significant storage compounds then skips the first step [129] from the exponentially-growing cell to the dwarfed cell.

The continuous decrease in the mean of the cell buoyant mass is driven by both the homogenization in cell size over time and the decline in the mode. That late-stage drop could be linked to protein degradation. The calculated rate corresponds, for example, to the degradation of one ribosomal protein per hour. As bacteria reallocate their resources in nutrient-limited environment [149, 190], protein synthesis is paused while protein degradation continues to occur spontaneously. The cost of maintenance of proteins is high enough that some bacteria could shed some weight due to that [177]. This phenomenon is notably what leads to nutrient recycling in the late stationary phase in *Escherichia coli* [135]. However, the context in which the cells are cultured and the observation of death after the sixth day of starvation indicate that nutrient recycling is not enough to sustain bacterial growth. When considering this late stage decrease, it could be argued that this constant decay rate is already happening at the beginning of starvation.

These distributions in cell biomass exhibit multiple modes towards the start of starvation, while there is only one mode left at the tenth day of nutrient limitation. The variability within each sample deccreases with starvation duration. Contrary to the expectations of the bet hedging hypothesis that would predict the apparition of distinct populations, here, the environmental stress leads to the homogeneization of the bacteria. When considering the main modes at the start of starvation, it could be

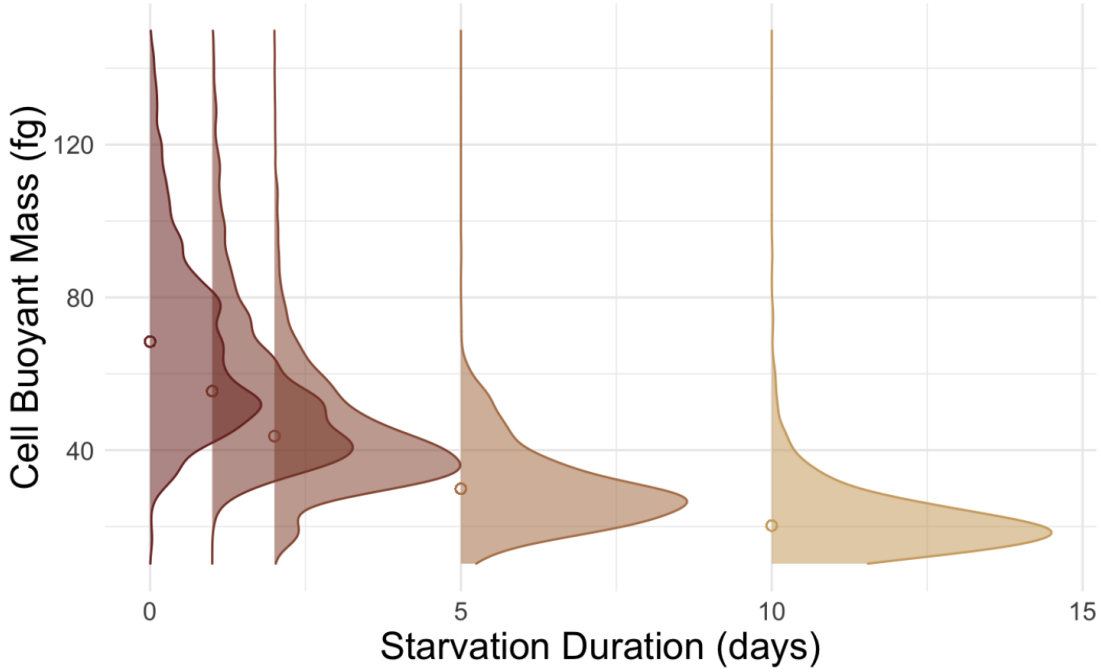

Figure 3-4: Distributions of cell buoyant mass in femtograms as a function of starvation duration. For each distribution, the dot corresponds to the mean value of the cell buoyant mass. Each distribution aggregates the measurements for three biological and technical replicates. Each distribution was created from at least 1500 bacterial measurements.

interpreted that there are two main states in bacterial biomass. There could indeed be a transfer between the main mode (around 60 femtograms) at day 0 and the main mode at day 2 (around 40 femtograms) during day 1, which exhibits a high density abundances in these two modes. It is also clear from this data that there are less modes at day 5 and at day 10 than during the first day of starvation.

All in all, these morphological datasets don't support the hypothesis of bacterial differentiation. However, it does underline the ability of bacteria to adapt to a new nutrient-limited environment.

3.2 Motility

Motility is a costly cell function [121]. On top of the large amount of resources needed to build the flagellar machinery [179], propulsion requires 10^{4-6} ATPs per second.

However, motility is also key to successful foraging as the diffusivity of motile cells is three orders of magnitude higher than the one of their non-motile counterparts [98]. Bacteria need to make a choice when it comes to using the limited pool of resources at their disposal in a nutrient-deprived media. They could for example repurpose the molecular material used in the flagella to maintain other cellular functions [195]. Previous research has shown that motility can decrease within 24 hours for *Vibrio spp.* [186]. Here I investigate the retention of cells' motile abilities over time, given the protocol made explicit in section 2.2.3.

I collected movies at a rate of 40 frames per second for up to 5 days of starvation in brightfield microscopy. The results can be seen in figure 3-5. Each image is a projection of the 40 frames gathered over one second after one and five days of incubation in a nutrient-limited environment. The colors were inverted such that bacteria are white dots here. A bacterial trajectory consists of multiple bacterial impressions nearby each other, which form lines. The more spaced out the bacteria are, the faster a bacterium is scavenging the nutrient-limited landscape. After one day in a nutrient-deprived environment, bacteria are still moving, as the left image attests with a mixture of lines (motile bacteria) and dots. That motile fraction is rendered almost nil at day 5. The few bacteria that exhibit motility have way shorter trajectories - so they are slower than on day 1. These projections provide the qualitative insight that motility can be lost within five days as a result of nutrient limitation.

I then quantify the diffusivity of a bacterial population over time, as explained in section 2.2.3. The measurement of diffusivity is a population level measurement that leverages the mean square displacement of the bacterial population. This variable is a proxy for speed, as it presents the average distance traveled after the start of the observation of a trajectory, as seen in figure 3-6. The diffusivity of a bacterial population is obtained by fitting a power-law function to the start of this curve, here performed with the nlsfit function in R. The exponent at day 1 (1.34) is greater than one which means that the process is super-diffusive. This drops down to 1.04 at day 5. On top of that, the normalizing parameter, which corresponds to the diffusivity of

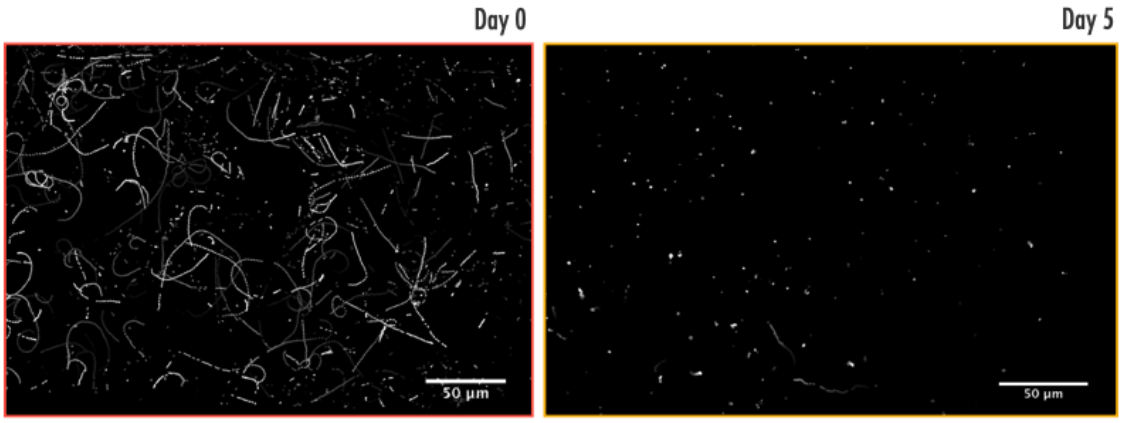

Figure 3-5: Projections over one second of bacterial trajectories (here in light colors) for non-starved phenotypes (day 0) and starved phenotypes (day5). The colors from the original images obtained with the ImageXpress have been inverted for better contrast. The frame rate of each video is 40 frames per second.

the population, decreases from $10^2 \mu m^2 s^{-1}$ to $3.1 \mu m^2 s^{-1}$. This lowering of bacterial diffusivity linearly impacts the encounter rate by a factor of 50, as considered in further details in section 4.1.1.

The data I gathered also provides a way to quantify bacterial motility on a finer scale by looking into the square displacement of individual trajectories. Once a bacterium is detected by the image processing, I add the distance traveled between each frame to the square. Figure 3-7 shows the distribution of this output for day one and day five of starvation one second after the first observation of each bacteria. There, the long tail corresponding to motile cells after the first day disappears at the fifth day. The shift in distributions between day 1 and day 5 exemplifies the motility loss identified through the global measurement of diffusivity in figure 3-6.

When it comes to motile bacteria, the few bacteria that are still motile after the fifth day of nutrient limitation exhibit a similar speed (over $10 \mu m$ displacement in one second) to the ones which are motile after the first day of starvation. The added granularity, offered by the logarithmic scaling of figure 3-8 also allows to determine the motile fraction of the bacterial population, which drops from 80% at day 1 to 8% at day 5. Differences in the bacterial displacement would have required further investigation. An increase in the ratio of time spent tumbling and a drop in the

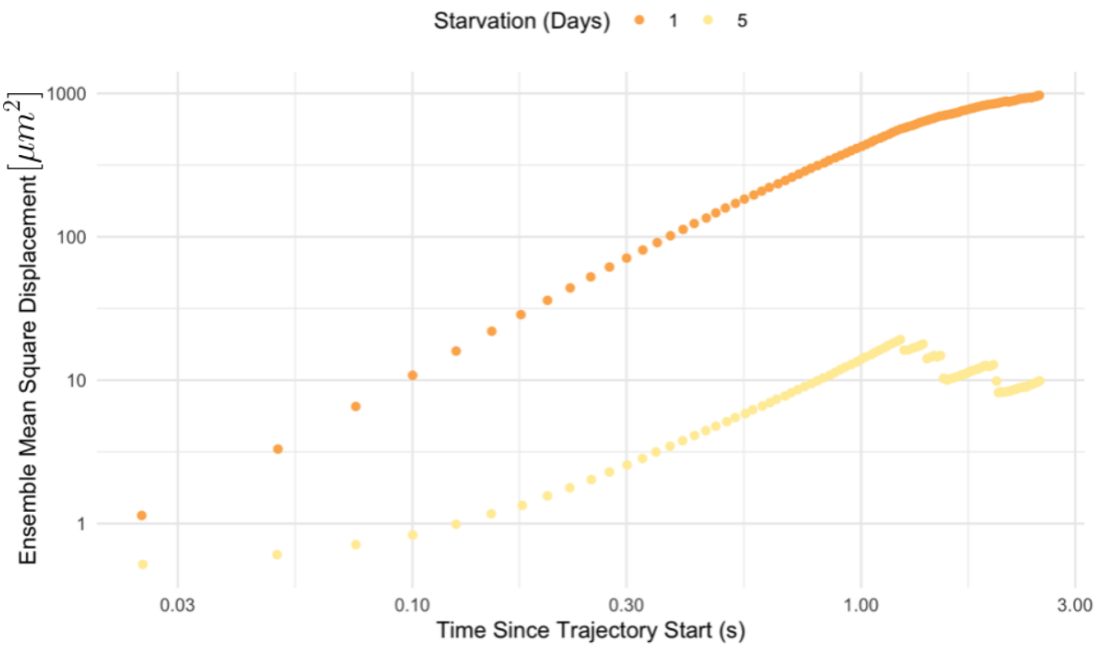

Figure 3-6: Ensemble Mean Square Displacement in function of the time since trajectory start for cells starved respectively 1 and 5 days. These values were obtained through a *trackpy* pipeline on Python for 4539 trajectories at day 1 and 193 trajectories at day 5.

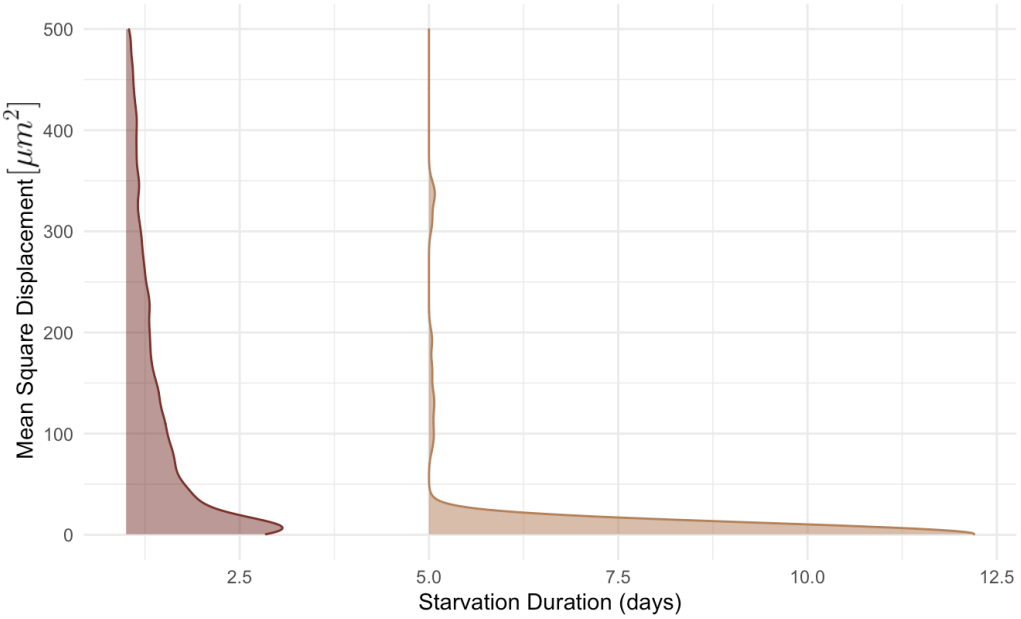

Figure 3-7: Distributions of individual square displacement during one second as a function of starvation duration. These values were obtained through a *trackpy* pipeline on Python for 4539 trajectories at day 1 and 193 trajectories at day 5.

run speed could both lower the value of traveled distance for bacteria within the same duration [130]. The decrease in run speeds is a rarer occurrence which has only been observed in *Vibrio spp.* so far and implies that bacteria are able to fine tune the energetic cost of the motility machinery [195]. However, here, I did not observe a difference in the square displacement of the motile cells, which hints towards constant run speeds and tumbling ratio.

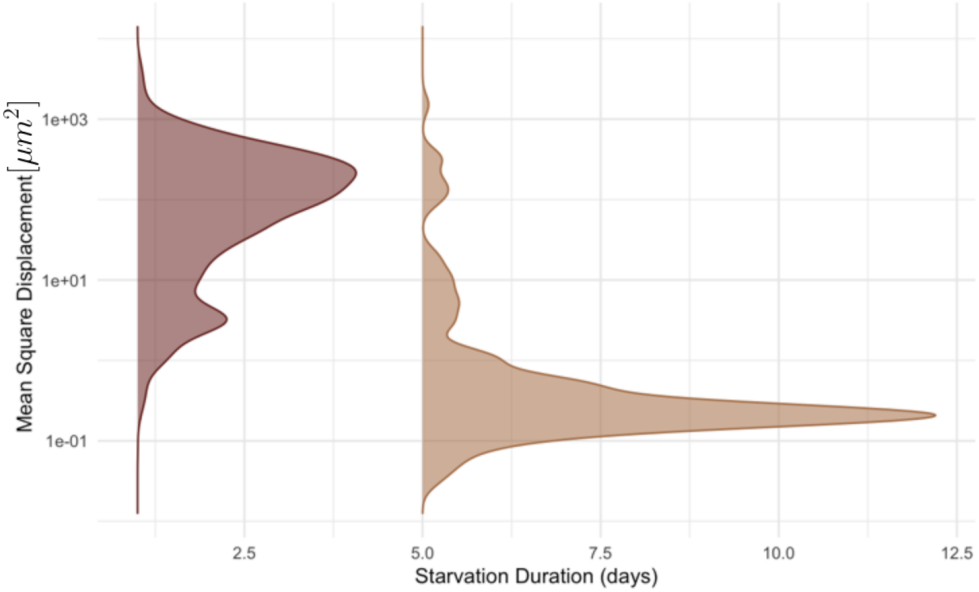

Figure 3-8: Distributions of individual square displacement during one second in function of starvation duration with a logarithmic axis. These values were obtained through a *trackpy* pipeline on Python for 4539 trajectories at day 1 and 193 trajectories at day 5.

Figure 3-8 reveals the presence of a total of three modes for the bacterial displacement. The highest peak at $230\mu m^2$ per second and the lowest one at $0.2\mu m^2$ respectively correspond to motile and non-motile cells. The intermediary mode that reaches its maximum density with an individual square displacement of $3\mu m^2$ per second at day 1 and $8\mu m^2$ at day 5 has the potential to be another class of cells away from the parsimonious dichotomy between motile and non-motile bacteria. Further inspection of that mode reveals that it contains the bacteria that rotate during the first second of the trajectory observation for a significant amount of time.

In section 5.2.1, I review the hypothesis that the flagella here is not lost, as motility

can be revived by the addition of a chemoattractant.

In a nutshell, most spontaneous motility is lost within five days in nutrient limitation for *Vibrio coralliilyticus*, as the motile fraction drops from 80% at day 1 to 8% at day 5. Compared to the other studies [186], the percentage of motile cells after 24 hours in a nutrient-depleted environment for *Vibrio coralliilyticus* vouches for its high resilience to nutrient limitation. Thus, the calculated motility loss rate can be considered minimal. Further surveys of other motile bacterial types could verify this statement. I estimate this minimal motility loss rate is $0.75h^{-1}$, assuming a linear motility loss between day 1 and day 5.

3.3 Attachment

So far, I measured cell viability and motility which are bacterial properties that impact the encounter rate between bacteria and particles. However, this reductionist approach does not capture the full scope of what a successful encounter requires. Even when a bacterium finds a particle, it needs to attach to the particle [**?**] despite the flow around the particle and thanks to its membrane properties. As attachment quantifies the interaction between particles and cells, it becomes specific to the environment the cell is in. That is why measuring physical properties of individual bacterial membranes only builds a first intuition on what attachment can be like [92].

Here, I seek to measure the attachment properties of cells within a defined chitin bead landscape. The specificity of the experimental set-up presented in section 2.2.4 makes an environmentally relevant argument while presenting a quantitative way to compare the starved and non-starved phenotypes when it comes to attachment. More precisely, I want to know if cells under nutrient limitation attach more or less than cells in the exponential phase in a comparable set-up with a predetermined flow and resource conditions.

Figure 3-9 shows original images gathered through confocal microscopy where the scale bar is thirty microns wide. The image analysis relies on Z-projection of half a chitin bead. The spherical shape of the chitin particles allows for this data compression without losing resolution, except around the equator of the bead. In these pictures obtained with SYTO9 staining in fluorescent light, colors were inverted for higher contrast: bacteria are here in black and chitin beads in light gray. Chitin beads are visible thanks to their autofluorescence. There is a qualitative decrease between the colonization patterns after 16 days in nutrient limitation and right after the exponential phase. It is also notable that even non-starved cells don't form microcolonies within the 20 hours of incubation with chitin beads, meaning that the process of attachment is uncoupled from the process of growth on chitin. Growth on chitin is quantified in more detail in section 3.4.2.

From these images, I quantified the attachment of bacteria in this particular set-up

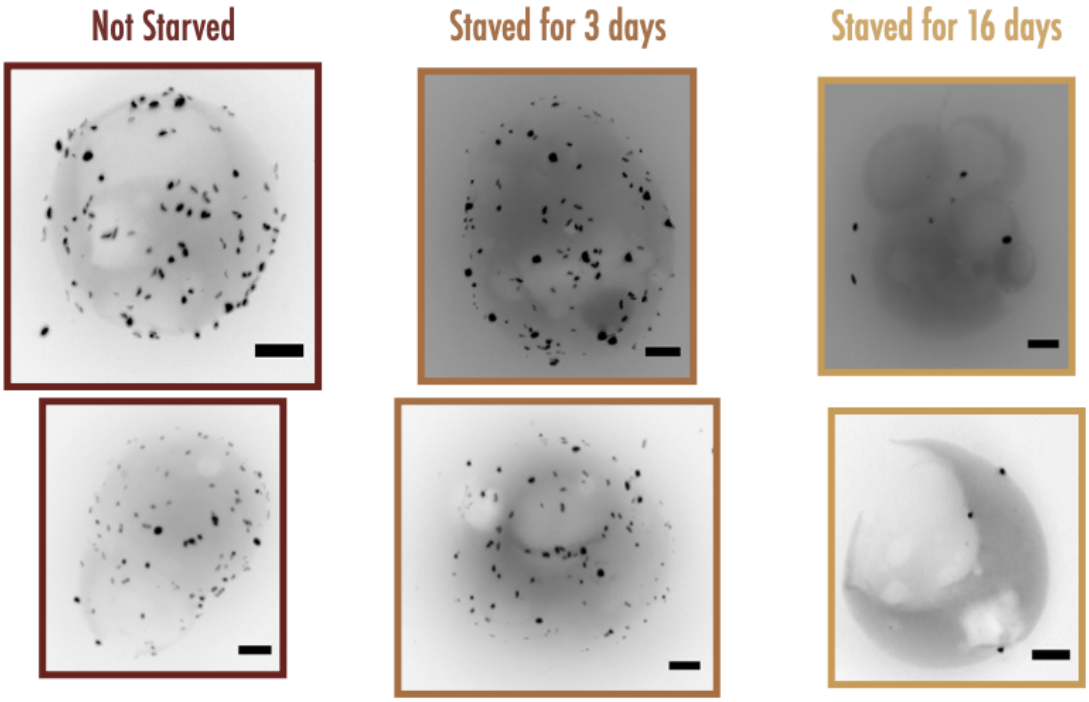

Figure 3-9: Projections over the Z-axis of bacterial chitin bead colonization for different duration of starvation. Here the bacteria are in black and the chitin beads are in light gray. The scale bars are $30\mu m$ long.

with an automated image analysis, written in Matlab. In figure 3-10, chitin particles were incubated with a set initial concentration of viable cells measured via colony forming units for 20 hours. These cells were starved beforehand for diverse durations ranging from 0 days to 16 days. The output here corresponds to the number of attached cells to chitin beads normalized to the area of the chitin particle surface. Every detected blob of cells is quantified as one attachment event. Any saturated area of the bead was removed from this calculation. These areas are found at the edge of the Z-projection, which equates the equator of the beads, where anomalies appear due to the spherical nature of the bead and the superimposed signal of different bacteria. The colonized area on the bead was also quantified but then discarded for consistency's purposes. Starved bacteria were indeed less fluorescent than their exponentially growing counterparts. Thus, different thresholds were required for different starvation durations which impacts the comparability of the results. I settled on the quantification of the number of cellular blobs per bead. As the size distribution of

beads is fairly narrow (the diameter of the beads is $85\mu m \pm 24\mu m$, it does not impact the quantification. At very high cell concentrations, when many cells attach, our quantification method of single attachment events breaks because cells are so close that they become indistinguishable from each other (data not shown).

Figure 3-10 shows that at similar initial cell concentrations, the number of attachment events consistently drops with starvation duration, which defies the expectation that cell stickiness increases after nutrient limitation [92]. However, these colonization patterns present a holistic view of attachment to beads, where both foraging and stickiness are main players. As the particles are physically mixed with an overhead rotation, mixing and active motility contribute more to the encounter kernel than thermal diffusion. In equation 3.1, the number of cells on a single bead is described as the product of the encounter kernel γ, the initial concentration cells $[C_{initial}]$, the concentration of beads $[N_{bead}]$ and the time of the experiment t. Three factors add up to build the encounter kernel: thermal diffusion of cells $\gamma_{thermal}$, mixing of the system γ_{mixing}, and active motility of cells $\gamma_{motility}$.

$$N(t) = (\gamma_{thermal} + \gamma_{mixing} + \gamma_{motility}) \times [C_{initial}] \times [N_{bead}] \times t \tag{3.1}$$

These three encounter functions can all be estimated within the context of the experiment, as expressed in table 3.1. Here, the mixing kernel corresponds to a turbulence kernel, as the incubation tubes undergo an overhead rotation. The rotative speed multiplied by 2 is then a first-order approximation of the shear force experienced by bacteria. The multiplicative factor of 2 comes from the observation that the tube is not filled with liquid, which causes two back-and-forth movements of the liquid in the tube. The estimation of the motility kernel can be done with two methods that assume that the encounter between a bacterium and a bead is either ballistic when the run length is smaller than the size of the bead or diffusive when the run length is significantly smaller than the particle size. Ballistic kernels tend to be an overestimation, whereas diffusive kernels tend to be underestimations. Thanks to the motility measurements in section 3.2, I can deduce both these parameters. All

in all, theoretically, in our setup, mixing and motility contribute equally when cells are motile. When cells are not motile, the baseline attachment can be explained by mixing.

Table 3.1: Encounter kernels for our experimental design, all units are in SI

Notation	Kernel Name	Expression	Variables	Estimate
$\gamma_{thermal}$	Thermal	$\frac{k_B \times T}{6 \times \pi \times r_{bact} \times \eta}$	k_B Boltzman constant T Temperature r_{bact} Radius of a bacterium η Fluid viscosity	3×10^{-16}
γ_{mixing}	Mixing	$1.3 \times (r_{bact} + R_{bead})^3 \times sh$	r_{bact} Radius of a bacterium R_{bead} Radius of a bead sh shear force	2.1×10^{-13}
$\gamma_{motility}$	Motility (diffusion)	$4\pi D_{mot} \times R_{bead}$	R_{bead} Radius of a bead $D_{motility}$ Diffusivity of motile cells	1.5×10^{-13}
$\gamma_{motility}$	Motility (ballistic)	$\frac{16}{3}\pi U_{swim} \times R_{bead}\hat{}2$	R_{bead} Radius of a bead U_{Swim} Swimming speed of motile cells	6.7×10^{-12}

A caveat of these approximations is that computing equation 3.1 with these values leads to a two order of magnitude divergence between these theoretical expectations in the ballistic setting and the experimental observations for both motile cells at day 0 ($N_{theory}(20) \simeq 12$ and $N_{experimental}(20) \simeq 250$) and non-motile cells at day 7 ($N_{theory}(20) \simeq 0.4$ and $N_{experimental}(20) \simeq 40$). Negative controls for bacterial quantification on beads yield to the detection of zero cells, which enhances the confidence for $N_{experimental}(20)$ at day 7. This last value is also a conservative estimate as the mode of the lowest distribution peak and not to the mean of the distribution (in the off-chance that the secondary mode is due to bacterial motility, even though the expected motile fraction at day 7 is nil). These differences between theory and experiments hint towards a theoretical underestimate of the mixing kernel, which is only loosely based on experimental data. The updated γ_{mixing} by a factor of 100 would then be of the order of 2.3×10^{-11}, which is a contribution slightly higher to the potential overestimate of the encounter kernel due to motility. The mixing kernel definitely leads to the attachment dynamics of the bacterial-particle encounter

of non-motile cells. The observed decrease in attachment after day 5 would then be due to a drop in stickiness σ, a parameter whose upper bound is 1 in this case, as described in equation 3.2.The stickiness parameter sigma here would then drop to 0.25 by day 16, assuming that the bacteria still have full attachment potential at day 7. These modelling efforts support the qualitative insight that stickiness decreases for *Vibrio coralliilyticus* over the duration of starvation.

$$N(t) \simeq \sigma \times (\gamma_{mixing} + \gamma_{motility}) \times [C_{initial}] \times [N_{bead}] \times t \tag{3.2}$$

The variability in particle colonization also decreases with starvation duration, which hints towards a more uniform population of cells. This observation is consistent with the conclusions made about cell size in section 3.1.2 and motility in section 3.2. If exponentially-growing cells can exhibit very high attachment (above 300 cells per bead surface area) for a few beads, this jackpot attachment does not happen after one day of starvation. Our quantification method rules out the possibility that this high attachment is due to cellular growth. However, bacteria could be releasing chemotactic signals to guide other free-living cells towards the bead. This potential for cell cooperation can be observed with different starting concentrations of viable cells, as done in figure 3-11.

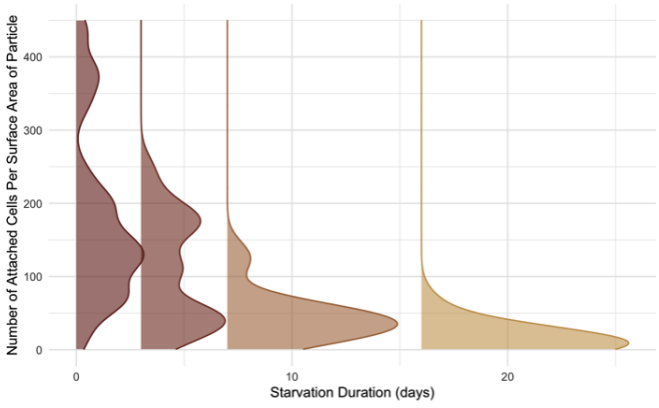

Figure 3-10: Distributions of number of attached cells to chitin beads in function of different starvation durations for one initial cell density. Each represented distribution aggregates the results of, at least, 20 particles.

The expectation is that attachment to particles is linear with the initial cell concentration as expressed in equation 3.2. If bacteria were synergizing in the attachment process, a higher cell concentration would lead to an non-linear increase in cell colonization. This phenomenon has been observed with *Psychromonas sp.* in a similar setup [43]. In figure 3-11, the linear behavior holds for low starvation durations, which supports the hypothesis of absence of cooperation. However, after 16 days of incubation in a nutrient-limited media, there is a jump in cell attachment for the highest initial cell concentration. This unexpected non-linearity could be interpreted as the need for a critical concentration of bacteria in order to colonize particles after starvation. Earlier starvation durations (day 7) do not exhibit such a threshold.

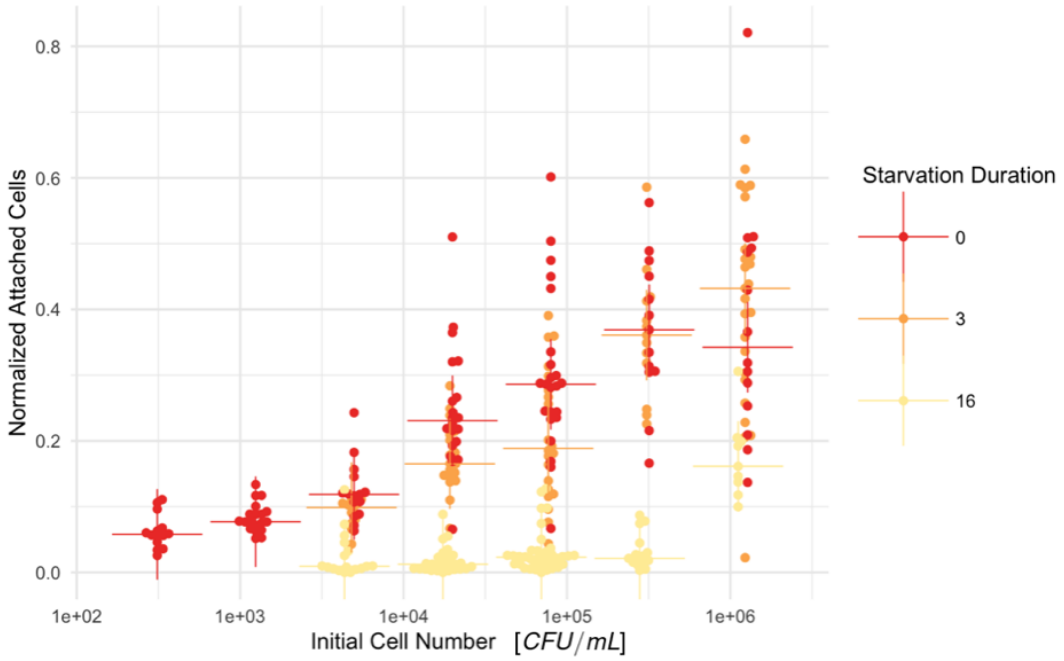

Figure 3-11: Number of attached cells to chitin beads for different starvation durations in function of the initial cell density, normalized per particle area. The cross represents the median number of normalized attached cells for each initial cell distribution.

Another way to present the data appears in figure 3-12. I establish an arbitrary threshold distinguishing colonized from uncolonized particles at 100 cells that need to be attached per particle. This threshold is experimentally motivated by the distribu-

tion data in figure 3-10. This parsimonious measurement leads to the quantification of the percentage of colonized beads and gives a clearer picture of colonization patterns. It shows that particle colonization depends on both initial cell concentration and starvation duration. This figure also casts light on the possibility that colonization happens for a critical threshold of bacterial concentration and that this threshold increases with starvation duration.

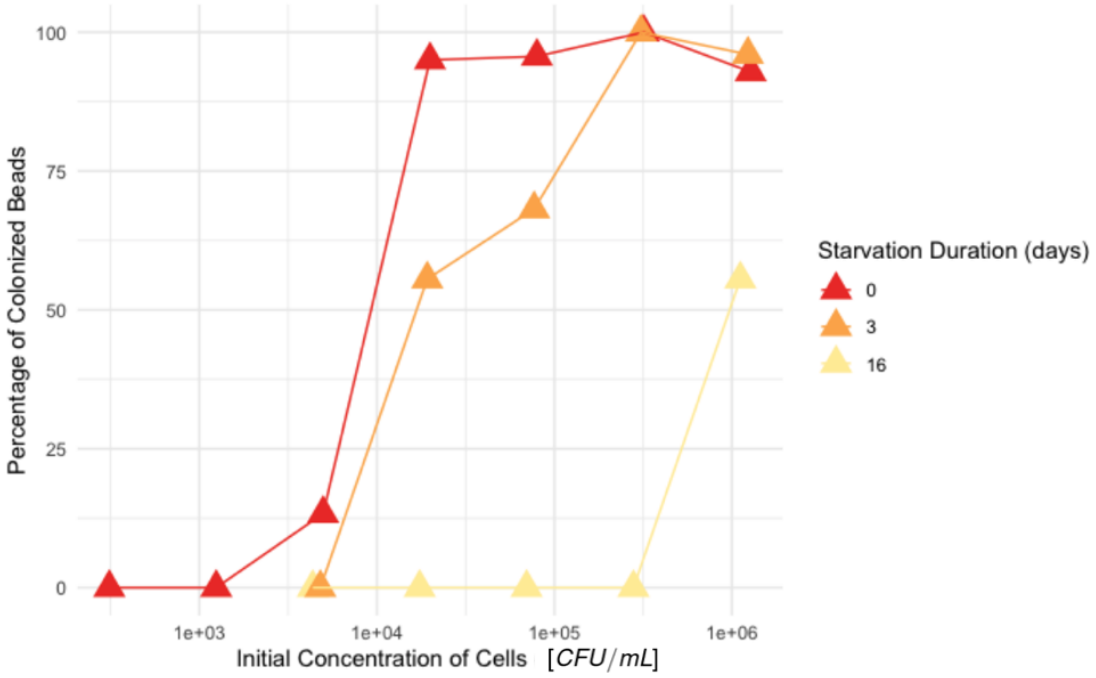

Figure 3-12: Percentage of colonized beads for different starvation durations as a function of the initial cell density. Here, the colonization threshold for normalized attached cells is 0.18.

To sum up, bacterial attachment on chitin beads decreases with their exposure to nutrient limitation. This phenomenon depends both on the loss of motility experienced by cells but also on the decline in cell stickiness. The initial concentration of cells also impacts successful bacteria-particle interactions. The data hints towards the emergence of cooperative behaviors after long starvation periods.

3.4 Regrowth

Bacteria stressed by nutrient limitation change their behaviors such as viability, motility and stickiness which impacts their propensity to successfully attach to a particle. Once a bacterium has found a particle and its wealth of resources, it needs to be able to leverage these resources to grow again. In this section, I investigate how fast bacteria can resume growth and change its state from starved to an exponentially-growing cell. I first rescue the cells with GlcNAc, the chitin monomer, which allows for high-throughput data, and with chitin for ecological relevance.

3.4.1 Rescue on GlcNAc

Unlike chitin, GlcNAc is soluble, which enables the use of a plate reader assay over up to 40 hours. Figure 3-13 shows an example of an optical density measurement, whose initial inoculum consists of 100 cells starved during 3 days. Time points are gathered every 20 minutes. I build a dataset comprising different initial cell dilutions for different starvation durations. To compare the effect of the nutrient limited pre-treatment, I focus on three variables that describe bacterial growth curves: the threshold time to visible growth, the growth rate and the yield. The first one describes the time bacteria take to reach a threshold value, which is equivalent to the lag time to growth. I expect this measurement to be the most impacted by nutrient limitation, as it can be interpreted as the time needed for cells to return to their full-growth potential in their exponential state. The growth rate corresponds to the slope of the exponential phase. A change in the growth rate would highlight some memory of the stress of nutrient limitation for cells that were once starved, even after they are back to a nutrient-rich environment. The yield symbolizes the asymptotic value of optical density that cells are able to reach in the stationary phase for the given concentration of GlcNAc. Differences would support that starved cells use resources more or less efficiently than their non-starved counterparts.

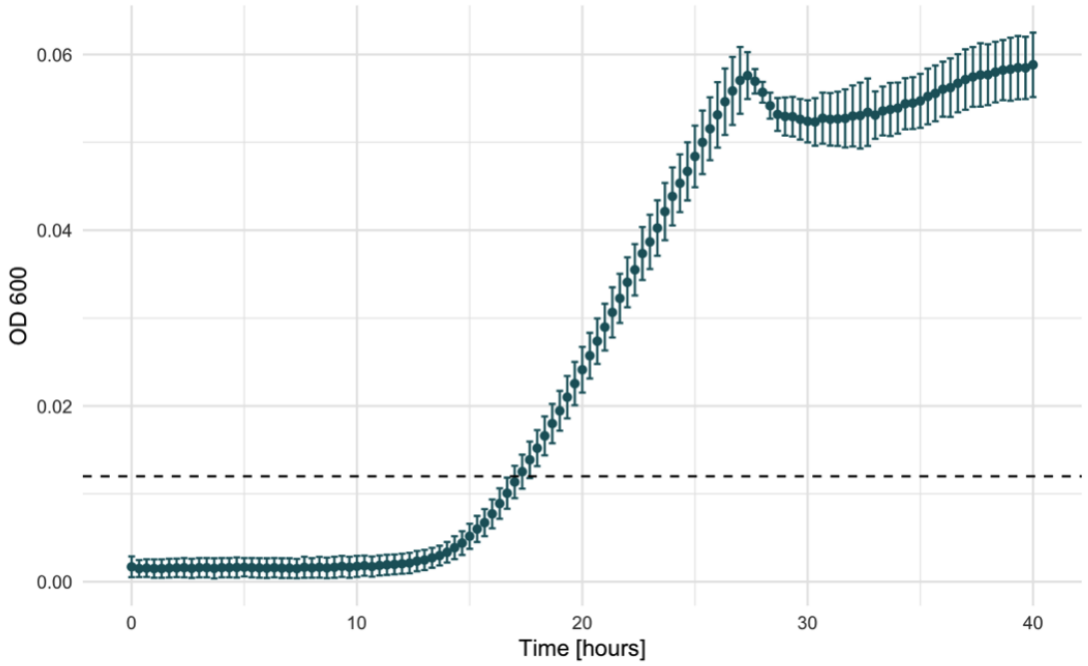

Figure 3-13: Optical Density measurement to assess growth on $20\mu M$ GlcNAc for 100 cells starved 3 days. This trajectory aggregates three technical replicates, as hinted by the error bars.

First, starvation duration affects the time to visible growth, as observed in figure 3-14. For similar initial viable cell concentrations, it takes three more hours for starved cells to start growing than for cells coming from the exponential phase. Starved and non-starved cells exhibit a linear dependency between initial cell concentration and lag time. This means that within the GlcNAc concentration they are immersed in, there is no apparent cooperation between bacteria to escape the lag phase. This dataset has several blindspots, as both the resource and the initial cell concentrations are fairly high, compared to other studies on cooperation to the exit of the lag phase [8]. Another possible interpretation of this three-hour delay to growth is that within the pool of viable cells measured by colony forming units on marine broth agar plates, there is a consistent subset of founder cells that supports an early growth start. As none of the data gathered within this experimental set-up supports such a population heterogeneity, this hypothesis seems likely to be false. Nevertheless, this three-hour

lag time could impact the ability of cells to successfully colonize a new particle, as competition with other cells relies on fast resource utilization. This is further explored in section 5.3.

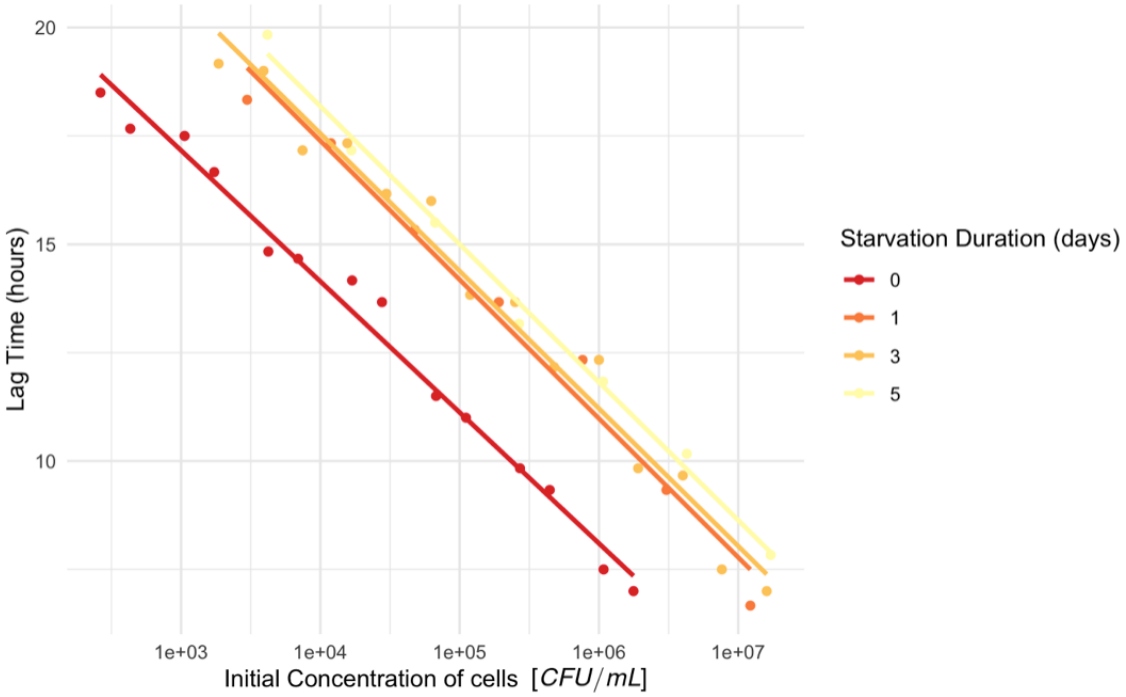

Figure 3-14: Time for the growth on-set on GlcNAc after various starvation durations in function of initial cell concentrations. Each experimental point was calculated as the lag time of the mean of three technical replicates The lines correspond to a linear regression of the data for each starvation duration.

The starvation duration (here up to five days) does not influence the delay in lag time to the same extent that early nutrient limitation does. When considering the viability data presented in section 3.1, this phenomenon of lag time delay is synchronized with the process of reductive division. This hints towards a potential effect of reductive division on the bacterial rescue after starvation. As ribosomes take up a lot of the cellular volume (up to one third for fast growing cells), a mechanism that could support the hypothesis that reductive division creates a delay in growth is the reduction of translating ribosomes under nutrient limitation, which has been observed in *Escherichia coli* before [33].

Contrary to lag time, growth rate is not correlated with starvation duration for different initial cell concentrations, as shown in figure 3-15. This means that after switching back to the exponential phase, starved bacteria do not have a disadvantage anymore. This equal footing between starved and non-starved bacteria is also supported by similar yields after nutrient limitation (data not shown).

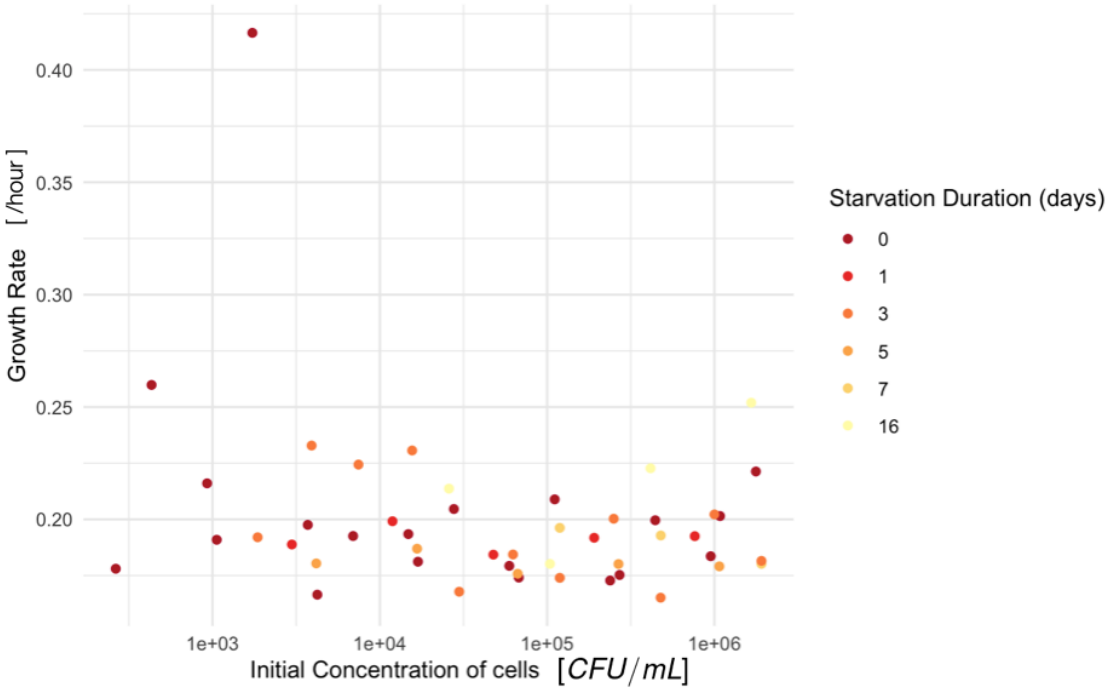

Figure 3-15: Growth rate on GlcNAc after different starvation durations in function of initial cell concentrations. Each point was calculated as the growth rate of the mean of three technical replicates.

When growing back on a monomeric substrate, starved bacteria only exhibit a three-hour delay to the start of growth. The bacterial nutrient-limited state stops influencing growth dynamics when cells reach their exponential phase.

3.4.2 Rescue on chitin

As chitin is a less labile resource than GlcNAc is, rescue on chitin requires more experimental development, explained in section 2.2.5. Figure 3-16 measures the yield of starved vs non-starved bacteria on colloidal chitin and on marine broth. The fold-growth is similar for both resources and both initial cell states after 48 hours. This further supports that starved bacteria can use resources as efficiently as the non-starved bacteria, even when these resources are more complex.

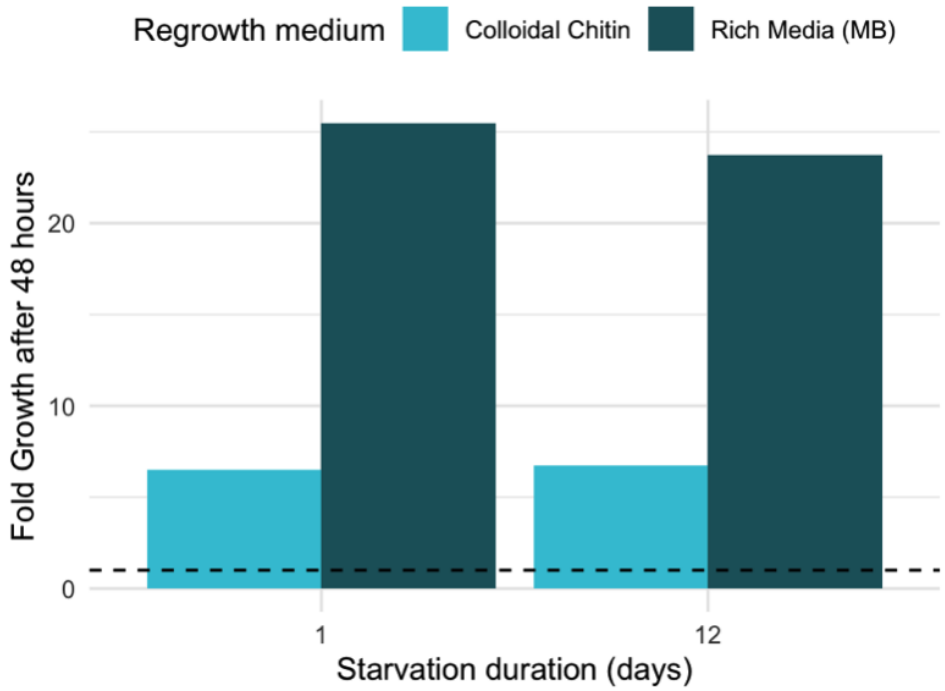

Figure 3-16: Bacterial yield after 48 hours for starved and non-starved phenotypes on chitin and marine broth (n=1)

In figure 3-17, bacterial growth is observed on flat chitin sheets using optical density measurements. These measurements exhibit similar dynamics to rescue on GlcNAc when it comes to growth rate and growth yield. After 15 days of starvation, the yield on chitin decreases for the first time.

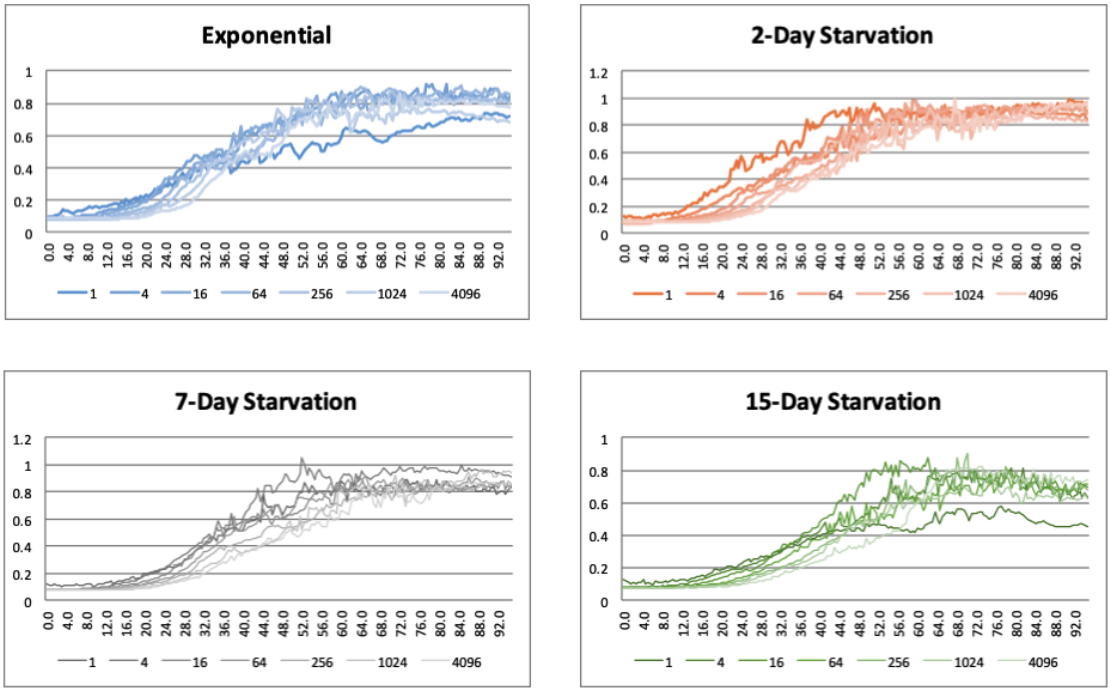

Figure 3-17: Optical Density measurements to assess growth on flat chitin sheets after different starvation durations for different initial cell concentrations (the dilution factor is indicated in the legend). Each of these trajectories is a single replicate.

In figure 3-18, I then consider the time to growth for bacteria. In this case, the lag time increases with starvation durations at similar cell concentrations. That delay is on the order of magnitude of the one measured for rescue on GlcNAc, even though chitin requires more enzymes to be degraded. This could be interpreted by the fact that the growth machinery is the potential bottleneck of re-growth for starved bacteria and not necessarily nutrient acquisition and breakdown. It is notable that these experiments on chitin sheets have only been done once and would require replicates for stronger conclusions. For example, the fact that the lag time for the highest concentration of non-starved bacteria is higher than the one for the concentration of bacteria limited in nutrients for 2 days. This could be due to an experimental error, such as the offset in the initial number of exponential cells that was not recorded.

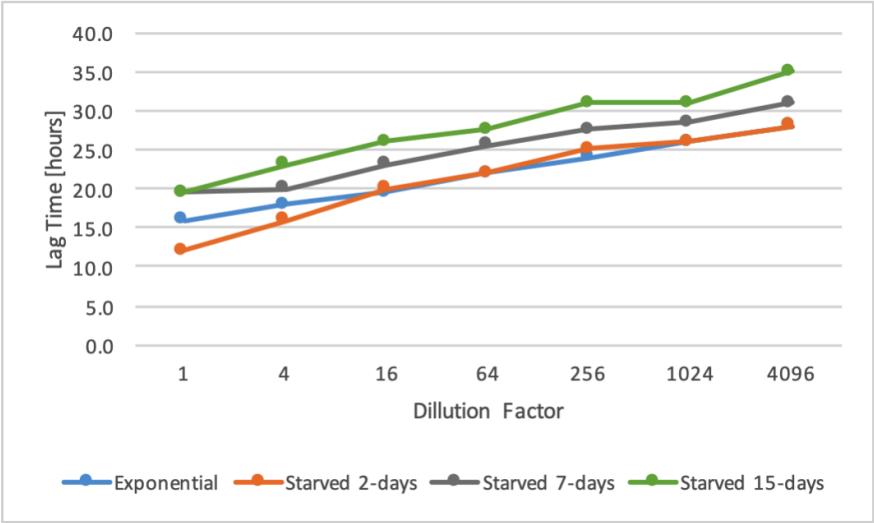

Figure 3-18: Time for the growth on-set on flat chitin sheets after different starvation durations in function of initial cell concentrations. Each point was calculated from the optical density measurements presented in figure 3-17

Rescue on a complex nutrient source yields similar results than rescue on a simpler sugar: starved bacteria experience a delay to start growing but once growth resumes, any difference with their non-starved counterparts is erased. This leads to the fact that once cells are attached to a particle, they can use the resources to replenish their population's cell number, except if they are faced by other competitive strains. In other words, I can hypothesize that nutrient limitation during foraging mostly impacts the process of particle foraging and not the following process of growth. As this experimental set-up deprives cells from both carbon and nitrogen, it could also be interesting to further investigate rescue on uncoupled inputs of these resources in carbon and in nitrogen.

3.5 Conclusion

In this chapter, I establish the phenotypic changes of *Vibrio coralliilyticus* due to nutrient limitation. Furthermore, I show that the behavioral responses of the bacteria to the lack of nutrients is a dynamic process that requires quantification over time.

Nutrient limitation affects population size in a non-linear way, as the microbial abundance counted by colony-forming units increases before plateauing and then dropping down. Bacteria undergo reductive division within the first day in the starvation media and then postpone the onset of death for up to seven days. Additional data gathered with flow cytometry, Coulter counter, and suspended microchannel resonator display the decrease in cell size at the single cell level. The absence of nutrients also causes the motile bacterial fraction to go from 80 % to 8 % within four days of starvation, as hinted by measurements at the population and individual scales. Population size and motility influence the encounter rate between bacteria and particles. In the next chapter, I estimate the impact of these dynamic changes on bacterial foraging.

Once a particle is found, the physiological state of a bacterium can determine if this encounter is successful. Here, I show that starvation duration governs the attachment propensity of a bacterial population to magnetic chitin beads. The longer cells are exposed to nutrient limitation, the less likely they attach to the particular substrate. This decrease is the product of both the decline in motility and stickiness. I also investigate the ability of starved bacteria to regrow on GlcNAc and chitin. The initial bacterial physiological state affects only the lag time to growth.

This chapter draws a complete picture of the behavioral state of a free-living bacterium in an environment deprived of nutrients. These physiological insights feedback into the ecology of the bacterial population, as explored in the next chapter.

Chapter 4

Quantitative predictions of nutrient limitation on ecological processes

Chapter 3 presents experimental evidence of phenotypic changes triggered by nutrient limitation. My experimental findings suggest that bacteria undergo rapid reductive cell division and lose motility within two days. They also attach less successfully than exponential cells. Starved cells retain a similar growth yield in nutrient-rich media after a delayed start. However, questions about the impact of these these behavioral changes on the foraging time scales and the persistence of a population within a patchy landscape remain. These estimates are hard to answer experimentally. Thus, I turn to modelling in this chapter that describes three different modeling approaches based on stochastic processes. They qualitatively and quantitatively integrate the experimental knowledge gained in chapter 3 to produce estimates of the foraging time scales.

Every model presents a simplified world view with different biases. As this work focuses on the fate of free-living cells, most of the simplifying assumptions concern life on particles. The dynamics of microbial assembly on particles stem from a complex interdependence between resource availability [44], inter-strain competition [45], and metabolic abilities [137]. Ideally, a model of foraging would take all these phenomena into account or even better be agnostic to them. I introduce four models of increasing complexities to capture the intricacies of the foraging process. I first present a clas-

sic framework for bacteria-particle encounter [87, 98]. Then, I develop a variation to this classic model by incorporating a motility loss event. The population-based model adds complexity to that first variation on the classic model by also taking into account changes in viability. Where the population-based model aggregate the fate of whole populations using a stochastic framework, the individual-based model presented in the last section simulates individual microbial foraging trajectories. That last framework helps to determine the minimal concentration of nutrient patches needed for a bacterial population to survive.

4.1 Classic encounter rate model

Encounter rates between resources and bacteria govern the foraging dynamics in patchy resource landscapes [87]. The ocean's surface layer is indeed an heterogeneous environment for heterotrophic bacteria. Marine snow particles become hotspots of bacterial activity that microbes strive to find when they are in a free-living state [161]. The quantification of this bacteria-particle encounter provides better estimates for sinking particle degradation and bacterial population dynamics. Here, we present a variation on a classic model that takes into account motility loss when bacteria forage in a nutrient-deprived environment.

4.1.1 Mathematical definition of bacteria-particle encounter rate

Encounter Rate

In the simplest case, encounter can be thought of as a memoryless stochastic process between two types of objects. It can be described as a Poisson process, whose rate is linearly controlled by the concentration of particles N_{part} and bacteria N_{bact}. The more objects to encounter, the easier the encounter is. This linear dependence comes from the superposition of $N_{part} \times N_{bact}$ Poisson processes describing the encounter of one bacteria with one particle. The per-capita and per-particle rate λ for that

encounter rate depends on bacterial diffusivity and size, as well as particle movement and size [87].

From here on, for this section, N_{bact} is set to 1, as the focus is put on the Poisson process describing the encounter of a single cell with particles. I note E the per-capita encounter rate, which is $E = \lambda \times N_{part}$, where λ_{part} is the per-particle per-capita encounter rate.

Time for the 10% luckiest bacteria to find a particle

To get a better intuition of the time scales of foraging, we consider here the time T_{10} it would take for the first 10 % of bacteria to attain a particle. This threshold, appearing in [98], is based on the assumption that if 10% of a population finds a particle, then the population can persist. It would indeed only require less than 4 divisions per bacteria on particles to replenish a population to its original headcount. As encounter is a Poisson process with a per-capita rate of E, T_{10} can be derived from the cumulative probability function $P(t < T) = 1 - exp^{-t \times E}$. This leads to $0.1 = P(T_{10} < T) = 1 - exp^{-T_{10} \times E}$. Equation 4.1 expresses T_{10} in hours from an encounter rate given per second.

$$T_{10} = -\frac{ln(0.9)}{3600 \times E} \tag{4.1}$$

This critical value for foraging is the main output of this model. Using this equation, Lambert et al. estimate that it takes up to 3.6 days for 10% of a motile bacterial population to find a particle in highly oligotrophic environments [98]. This approximation depends on properties of both the bacteria and the patchy landscape.

4.1.2 Parameters for the encounter rate

Bacterial diffusivity

In theory, bacteria influence the encounter rate through their size and their ability to move. As particle sizes are typically defined to be at least 20 times larger than the average size of a bacteria, the geometrical constraints of size are determined by

particles only. In this case, the only contribution of bacterial behavior to the encounter rate is through the diffusivity of bacteria, that can range from $D_{nonmot} = 10^{-12} m^2 s^{-1}$ for non-motile bacteria to $D_{mot} = 10^{-8} m^2 s^{-1}$ for the fastest motile bacteria [98, 86]. The diffusivity of non-motile bacteria is indeed non-zero because they are still undergoing Brownian motion, as described by the Stokes-Einstein equation described as the thermal encounter kernel in table 3.1 [83, 98]. Active motility in the form of a random walk results in a higher diffusivity that can be approximated by the swimming speed ν and the run time τ to $D_{mot} = \nu^2 \tau / 3$ [16]. The updated encounter rate expression is presented in equation 4.2, where $\lambda_{part} \times N_{part}$ establish the contribution of particle dynamics to the encounter rate. It is notable that the dimension of λ_{part} is per particle.

$$E = 4\pi \times D_{bact} \times \lambda_{part} \times N_{part} \tag{4.2}$$

For a given particle distribution, encounter depends linearly on bacterial diffusivity. Figure 4-1 presents the time for the 10% luckiest bacteria to find a particle as a function of that population's diffusivity. It ranges from more than 40 days for non-motile bacteria to 5 hours for the most active ones. In our experimental set-up, the highest measured diffusivity for a population of cells is $10^{-10} m^2 s^{-1}$. According to these equations, for set particle parameters [158] whose influence is explained in the next subsection, the matching T_{10} is around 100 hours, which is more than four days. However, the experimental results presented in section 3.2 highlight a significant decrease in motility by the fifth day of starvation or 120 hours. This dynamic change in bacterial diffusivity occurs in the range which can impact the foraging time scales, at least for this particle distribution.

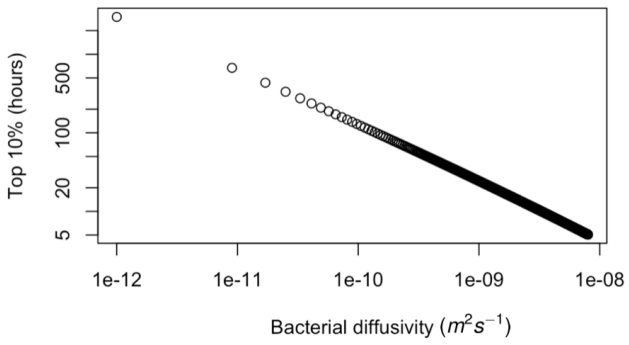

Figure 4-1: Time taken for the 10% luckiest bacteria to find a particle in hours as a function of bacterial diffusivity in $m^2 s^{-1}$. Note that both axes are in logarithmic scale. The set particle size distribution is from [158].

Particle size distribution

When a bacteria navigates a landscape of particles, its encounter rate depends on the size and the concentration of those particles. In the natural environment, particles come in a wide variety of different sizes, whose radii range from the micrometer scale $r_{min} = 20 \times 10^{-6} m$ to the millimeter scale $r_{max} = 2.5 \times 10^{-6} m$ [98]. The number of particles for each size follows a Junge distribution [76]. The parameters of this distribution $N_{part}(r) = N_0 \times (\frac{r}{r_0})^{\beta}$ has been measured at different oceanic locations, notably via video plankton recorder [134], satellite observations [95], and via *in situ* underwater vision profiler [158]. All these methods agree that the value of the exponent of this distribution β is around 4. Thus, the factor N_0 is the one that controls how concentrated particles are in different places because the radius of reference r_0 is fixed to $1 \mu m$. As bacteria can encounter particles of all sizes in the landscape it navigates, the encounter rate contains the integral of this particle size distribution $N_{part}(r)$ (abbreviated PSD) over the range of particle sizes, as indicated in equation 4.3.

Equation 4.3 also takes into account the fact that particles are sinking by factoring in the Sherwood number $Sh(r, D)$. This function describes the contribution of convective forces due to the downward particle movement relative to the one of the

bacterial diffusivity. Its complete expression that depends on the seawater's kinematic viscosity and other experimentally measured parameters can be found in the work of Lambert et al. [98]. It scales in the following way $Sh(r, D) \sim r^{0.519} \times D^{-0.333}$.

$$E = 4\pi D \times \int_{r_{min}}^{r_{max}} N_{part}(r) Sh(r, D)\, \mathrm{d}r \tag{4.3}$$

Table 4.1: Influence of the particle size distribution on the encounter rate for motile and non-motile bacteria

Bacterial Type	Diffusivity	Source of PSD	Per-capita Encounter Rate	Time for 10% to find a particle
	D	N_0,β	E	T_{10}
	$m^2 s^{-1}$		s^{-1}	h
Motile Bacteria	$D_{mot} = 8 \times 10^{-9}$	[95]	6×10^{-6}	5
		[158]	2×10^{-7}	200
Non-Motile Bacteria	$D_{nonmot} = 1 \times 10^{-12}$	[95]	1×10^{-10}	3×10^3
		[158]	3×10^{-11}	9×10^4

Table 4.1 quantifies the influence of the PSD on foraging timescales for motile and non-motile cells. It shows that the three order-of-magnitude difference in diffusivity between motile and non-motile bacteria causes a similar gap in encounter rate. That discrepancy, in turn, translates into a difference of about 1000 days to find a particle. These estimates exemplify that motility loss could dramatically impact the time scales of particle foraging. They also confirm that depending on the particle distribution, cells could spend up to 200 hours looking for a particle. That time scale far exceeds the time scales over which we can expect phenotypic changes due to starvation.

Chemotaxis

Another factor to take into account is that in the oceans, nutrient hotspots do not only consist of the particles, but also of their surrounding chemical cloud. The substances

released by the metabolic activity on particles can act as attractors to bacteria. It means that microbes can be absorbed by a particle at a distance due to the process of chemotaxis, explored in more detail in section 5.2. This phenomenon leads to bacteria finding a particle once they enter the surrounding chemical cloud, which can be up to 10 times the size of the radius of the particle [155]. The experienced particle radius by the bacteria is then ten times the one of the initial particle. Figure 4-2 presents the revised time scales of T_{10} when bacteria undergo chemotaxis. The non-linear dependency of the encounter rate to the particle radius makes chemotaxis a potential game changer in the foraging dynamics. Even when bacteria are not inherently motile but can activate motility on the cue of chemicals, the number of hours it takes for the top 10 % of bacteria to arrive at a particle drops to less than 5 hours.

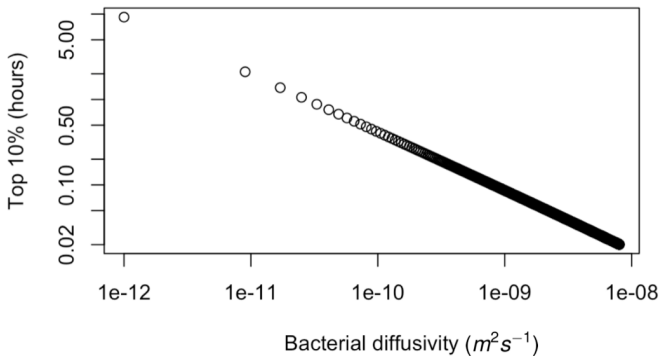

Figure 4-2: Time taken for the 10% luckiest bacteria to find a particle in hours as a function of bacterial diffusivity in m^2s^{-1} when bacteria are chemotactic, which corresponds to an increase of the particle effective radius by a factor of 10. Note that both axes are in logarithmic scale. The set particle size distribution is from [158]

The dynamics of bacterial chemotactic abilities under nutrient limitation are outside the scope of this thesis but propose interesting future directions to explore as explained in section 5.2.

4.2 Classic model with discrete motility loss

4.2.1 Rationale

The time scales presented in the preceding section does not account for the interdependence between the bacterial environment and their physiological state, impacting viability, motility, and attachment, as seen in chapter 3. State-of-the-art foraging time scales consider bacteria with a constant physiological state as if bacterial properties like bacterial diffusivity were independent of the nutrient concentrations around. However, as shown in chapter 3, when bacteria are foraging for resources, their immediate environment is nutrient-poor, which can lead to loss of motility.

4.2.2 Mathematical definition of a motility loss event

The initial Poisson process can be expanded to include this motility loss in various ways, from gradual decay of motility to a discrete motility loss event after a certain time. Here, we choose a discrete motility loss event because in section 3.2, I showed that if the bacterial diffusivity of the motile fraction does not decrease with time, the percentage of motile cells drops over time. This experimental results justifies the fact that motility loss is a discrete event at the scale of each bacterium. Equation 4.4 spells out that the motility loss event at time t_{loss} triggers the bacterial diffusivity in the encounter rate kernel to switch from the motile value D_{mot} to the non-motile one D_{nonmot}. This way, the encounter rate depends on a new variable: the time to motility loss.

$$E = E(D_{mot}) \text{ if t } < t_{loss} \text{ and } E = E(D_{nonmot}) \text{ if t } \geq t_{loss} \tag{4.4}$$

4.2.3 Impact on foraging time scales

Figure 4-3 uncovers the relationship between time of motility loss and the ensuing variation in foraging time scales. Here, the change in foraging time scales is compared and normalized to a baseline value. That comparison point stems from the constant

case, as seen in Table 4.1, where bacteria are not affected by nutrient limitation and thus stay motile at all times. As this baseline value is calculated in reference to each particle size distribution, the output on the vertical axis of this graph becomes independent of the particle size distribution.

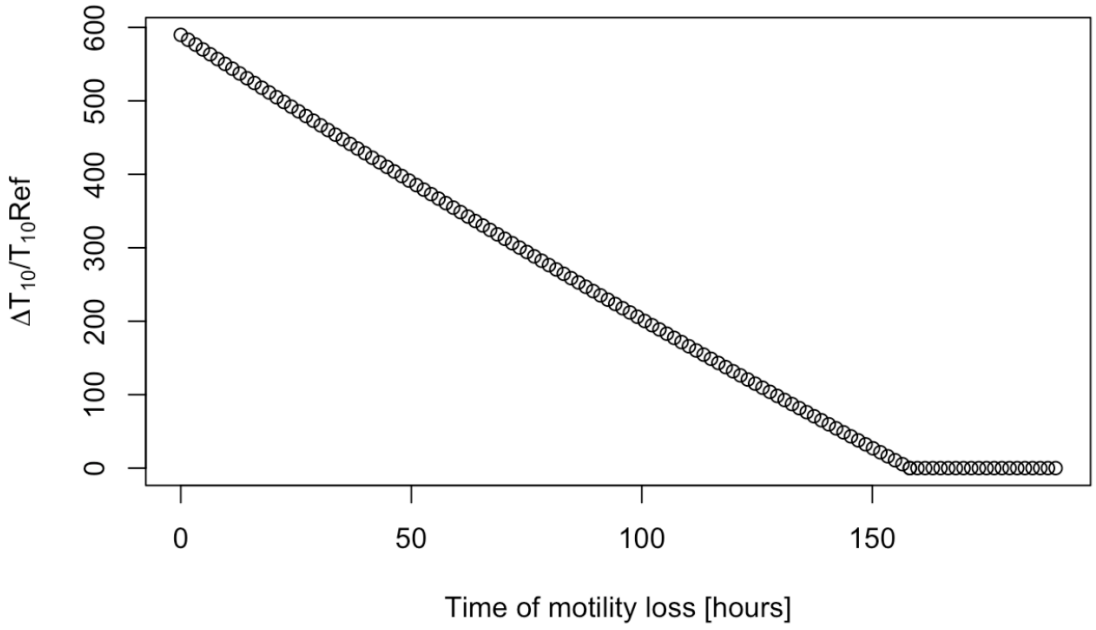

Figure 4-3: Percentage of variation in T_{10} in function of the time of motility loss

The earlier the motility loss happens, the more dramatic the impact of that loss is. Motility loss leads to a two order-of-magnitude increase of the search time for the first 10% of the bacteria to arrive at a particle. This simplistic model captures the influence motility loss can have on the time scales of particle foraging.

4.3 Population-based model

Nutrient limitation causes microbes to lose their motility but also alters their viability, as quantified in section 3.1. This change directly impacts the number of cells foraging: Cell death decreases the number of available cells able to find a particle, while cell reductive division increases foraging success by inflating the number of cells. My experimental results show that the bacteria don't start dying before seven days and that reductive division happens early on in nutrient limitation. The time scales of reductive division and even death fall in the range of the time needed for bacteria to scavenge for particles. These two changes in cell concentrations hence interfere with the encounter process at the population level. Equation **??** which describes the encounter rate for a bacterial population within a patchy landscape is parameterized by a constant number of bacteria N_{bact}, which is not true.

Here, I propose a bypass to re-write the encounter process as an absorbing Markov chain model. This corresponds to an inhomogeneous Poisson process with discrete time increments. This is a generalization of the discrete motility loss presented in section 4.2. This model consists in creating different subpopulations for the free-living contingent, with different abilities to attach given their cell numbers. After describing the assumptions underlying this model, I will present the model while considering the different possible outputs. In the end, I address the limitations of such a model, which leads to the development of the last model presented in this work.

4.3.1 Assumptions

Encounter means persistence

Once a population encounters a particle, it resets its life history to a similar starting foraging population. This means that when bacteria find a particle, they can establish themselves to grow up to a similar population density, no matter the particle type and history. This assumption is justified within the context of an experimental system of chitin beads. In section 3.4, I showed that the initial physiological state of microbes

did not impact their ability to re-grow either on GlcNAc or even on a less labile carbon and nitrogen source chitin. Bacterial cell densities reached the same final yield independently of their starvation history. These datasets ground the equivalence between encounter and persistence in the context of chitin particles.

Detachment as a discrete event on the population scale

The foraging for resources by a bacterial population is synchronized, which means that all bacteria detach from a particle at the same time. The dynamics of particle detachment depend on many parameters influencing the dynamics of the attached bacterial life style, such as a potential phage infection [42]. This could be taken into account by using a full-scale agent-based model, as presented by the individual-based model in section 4.4. However, this population-based model aims at looking at the persistence of an entire bacterial population. The simplifying hypothesis of detachment being a single event is also supported by the data presented in the last appendix of this thesis in figure D-3, where *Vibrio coralliilyticus* reliably exhibits a sudden wave of synchronized detachment from chitin beads. Such a discrete phenomenon can be triggered by the switch between the nature of the carbohydrates, from a complex polymer to monomers [41]. This assumption leads to the free-living population having the same physiological age.

4.3.2 Formalization of the model: Markov Chain

This section presents the null model deriving a population-scaled stochastic process of foraging. Here, we rely on the mathematical model presented in section 4.1.1. The particle-microbe encounter can be described by a rate, which takes into account properties of the particle landscape and the bacterial population. However, the experimental parameters such as bacterial diffusivity, bacterial concentration and bacterial stickiness that govern this equation are time-dependent. Thus, we describe a Markov chain that discretizes the physiological state of bacteria, by different time durations. A Markov chain is a stochastic model that describes the transition between possible

states with respect to the last current state. The application of this model to the life cycle of the free-living population is inspired by models describing the life cycle of animals, such as turtles or gulls [175, 80].

Mathematical Definition

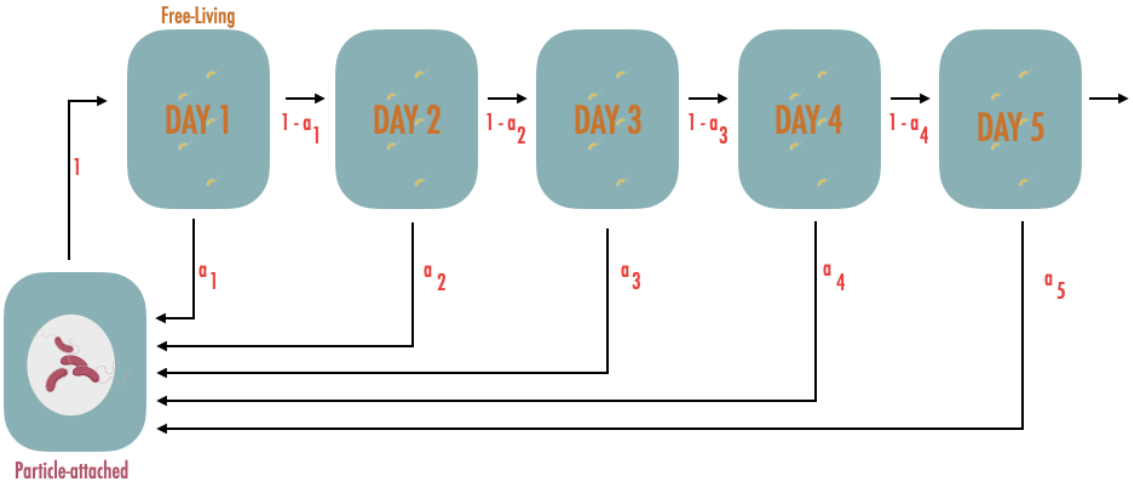

Figure 4-4: Absorbing Markov Chain describing the model

Figure 4-4 presents the schematics of the Markov chain which has two different types of states: the particle-attached state and the free-living states. The properties of a bacterial population are coarse-grained to be constant over the duration of one Markov chain state which lasts 24 hours in the example below. Each state N_i corresponds to a subpopulation that has been planktonic in a nutrient-depleted environment for i days. The transition from the particle-attached state to the first free-living state is 1 by virtue of the two assumptions presented in section 4.3.1. Each free-living state can switch to two different states: the next free-living state or the particle-attached state. As expressed in equation 4.5, the transition probability a_n between the free-living state aged n and the particle state is the probability that an encounter happens within the time frame T_{box}, which I here take to be 24 h. As we consider that the free-living population maintains the same set of properties in terms of motility, viability and stickiness, while in a state, that probability is then the cumulative probability

distribution of the Poisson process of encounter with a parameter e_n, whereas the probability of not encountering a particle, and thus starving for another day and transitioning to state $n+1$ is $1-a_n$.

$$a_n = 1 - exp^{-T_{box} \times e_n} \tag{4.5}$$

Equation 4.6 defines the encounter rate of a bacterial population of size $[B]_n$ for the n^{th} free-living state as a function of bacterial stickiness σ_n, bacterial concentration $[B]_n$, bacterial diffusivity D_n and the particle density function $PSD(D_n)$. All these parameters can be different for each free-living state , and thus can dynamically describe the properties of the bacterial population. Bacterial stickiness σ_n can vary between 0 and 1, where the maximum value means that an encounter event is always successful and the minimum value implies that bacteria have attachment issues and don't attach at all to the particles they encounter. The range of bacterial diffusivity was explored in section 4.1.2. That same section also introduces the particle size distribution, which only depends on the bacterial state through bacterial diffusivity.

$$e_n = 4\pi\sigma_n[B]_n D_n PSD(D_n) \tag{4.6}$$

This model captures the dynamics of the bacterial phenotypes scavenging for resources. The probability for a bacterial population to persist corresponds to the probability for a population to attach at any time of their free-living journey before they die. Here, we can assume that $lim_{n\to\infty} a_n = 0$, as a bacterial population in a nutrient-limited population that does not attach is fated to die off at a rate r [144], whose value is expressed in table 4.2. This causes the bacterial concentration $[B]_n$ to reach 0 within a finite amount of time. Equation 4.7 expresses this analytical output. As this expression is agnostic to potential simulation parameters, it provides a better output than simulation-based measurements, such as the mixing time and the percentage of attachment events.

$$P_{persistence} = \sum_{i=1}^{\infty} a_i \prod_{j=0}^{i-1} (1 - a_j) \tag{4.7}$$

Mixing time is the number of transitions required for the system to settle in an asymptotic distribution. As $lim_{n\to\infty} a_n = 0$, there exists a N_{death} where for all $n > N_{death}$, $a_n = 0$. In this case, the Markov chain model can be truncated to a finite amount of attainable states $N_{death} + 1$. That latest free-living state is an absorbing state, which bacteria cannot escape. This property makes the Markov Chain absorbing, which leads to the existence of an asymptotic distribution and thus to the one of a finite mixing time. The mixing time can also be calculated as the number of times a population goes through the particle-attached state before going extinct to ensure the independence of that value with the number of states. The Matlab function *asymptotics* provides the mixing time of a Markov chain through its second argument. Figure 4-5 shows that the mixing time for a population of motile bacteria increases with the bacterial concentration over time more than the mixing time for a non-motile bacterial population. It means that a motile population takes more time to attain the state of total death. As properties of the simulation of an absorbing Markov chain, mixing times are rooted in the mathematical world, which makes a quantitative transposition into the notion of bacterial persistence challenging, contrary to the probability of persistence from equation 4.7.

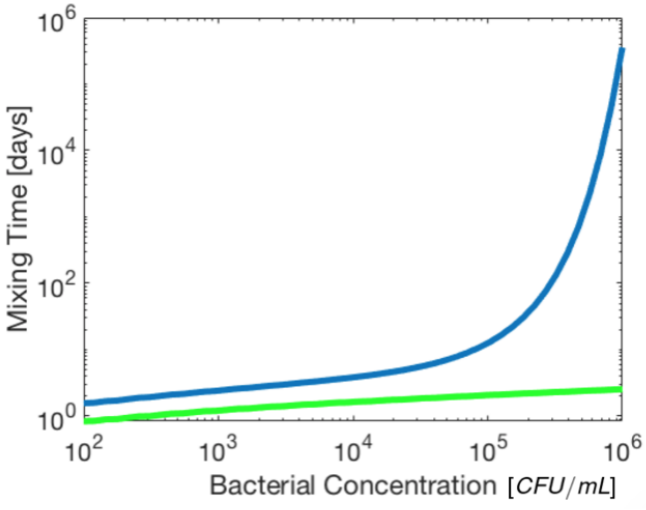

Figure 4-5: Mixing time (days) as a function of the initial bacterial concentration for the null model of an absorbing Markov chain. The blue line corresponds to a simulation for motile bacteria, whereas the green line is for non-motile bacteria.

Parameters

This population-based model here is based on the assumption that when in a nutrient-limited environment, bacteria die at a rate r [144], whose value is expressed in table 4.2. This model also considers that bacterial diffusivity and stickiness are constant properties over time. There is no change in the bacterial phenotype due to nutrient limitation. This means that the output for this model can be calculated for motile and non-motile bacteria alike, as illustrated in figure 4-5. Below, I will introduce a dynamic switch between the two phenotypes between these two physiological states, motile and non-motile, as a function of time since detachment.

Table 4.2: Parameters for the encounter rate function of the Markov Chain model

Parameter Name	Notation	Unit	Value	Source
Stickiness	σ_n	N/A	1	
Concentration of cells after detachment	$[B]_0$	N/A	10^5	
Death rate	r	h^{-1}	0.25	3.1
Diffusivity (Motile cells)	D_{mot}	$m^2 s^{-1}$	8×10^{-9}	[98]
Diffusivity (Non-motile cells)	D_{nonmot}	$m^2 s^{-1}$	10^{-12}	[98]
Particle Size Distribution	PSD	N/A	1	

4.3.3 Limitations

This population-based model offers a first way to consider a bacterial population and its dynamics under nutrient limitation. However, it discretizes the processes such as motility loss and changes in viability to constants for slices of time. The modeling parameter that determines the duration of the free-living population is T_{box}. There is a trade-off between tractability (for a very small T_{box}) and accuracy (for a high T_{box}). This parameter also needs to be biologically relevant. Any use of this model needs to precisely check the influence of this parameter.

It is also important to note that this model quantifies the probability of bacterial persistence within a patchy landscape and not the time scales of a foraging population. The mixing time and the probability of persistence are highly biased by the set of simplifying assumptions, presented in section 4.3.1. As mentioned, the dynamics of microbial ecology on a particle depend on a plethora of other factors this model turns a blind eye to.

Nevertheless, the main drawback of this model is that so far, the attachment probabilities correspond to the attachment of one bacteria. The expression of a_n given in equation 4.5 is the probability of one encounter between the sets of bacteria and particles. Thus, in the current description of the model, if one bacteria attaches, the whole population is salvaged. In an earlier section 4.1.1, the critical foraging time scale was determined by the threshold of 10 % of the initial population. Changing this threshold would require changing the expression of a_n, which adds complications in the form of desynchronization of the processes of attachment and detachment. Indeed, when bacteria attach in an early stage, they do not contribute to attachment in later days so the bacterial concentrations of these later days need to be updated. This new concentration leads to a change of a_n, which increases the complexity of this model. It would indeed require updating all the parameters for each iteration of the model. This pitfall also renders the outputs of the model less interpretable.

4.4 Individual-based model of a foraging bacterial population

The following iteration of a foraging encounter model is based on simulating individual bacterial trajectories in an independent manner. This gets around the caveats of the previous models by including all phenotypic changes (contrary to the model presented in section 4.2) and by removing the liability of aggregating the behaviors of individual stochastic process (unlike the model presented in section 4.3).

4.4.1 Model without dynamic phenotypic changes

The principle behind this model is that foraging is a realization of two simultaneous phenomena, as seen in the schematics 4-6. When in a nutrient-limited environment, a bacteria is fated to either find a particle or to eventually die. These two outcomes can be modeled by Poisson processes. As seen in section 4.1.1, encounter for one bacteria within a particle landscape is a Poisson process whose rate λ depends on bacterial diffusivity. Meanwhile, birth and death are stochastic processes that can be counted via Poisson processes. For example, an application for such modeling is the counting of the residual number of bacteria in food packaging after desiccation [97]. Here, death is considered to be a Poisson process with a rate δ. Both these values can be estimated with the data presented in chapter 3.

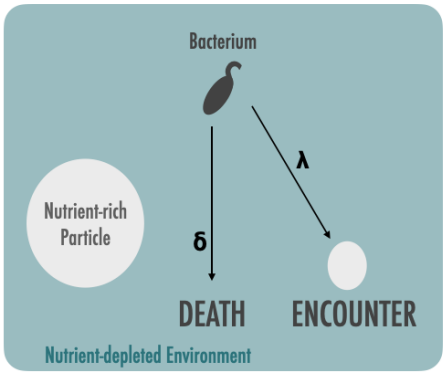

Figure 4-6: Principles of stochastic modeling for one foraging bacterial in a nutrient-depleted environment

As a bacteria is subject to both these processes at the same time, these two processes can be superposed into a new Poisson process whose rate is $\lambda + \delta$. In the Matlab code implementing this model, the time of the first instance of this superposed process is calculated given properties of the cumulative density function of a Poisson distribution. First, I generate a random number p between 0 and 1, which is then used in the inverse of the cumulative density function $-ln(1-p)(\lambda+\delta)^{-1}$. That value corresponds to the time at which either death or find arrives. The probability that this event is death is $\frac{\delta}{\delta+\lambda}$, whereas the probability that this event is finding a particle is $\frac{\lambda}{\delta+\lambda}$. All in all, success in foraging depends on the balance between the death rate and the encounter rate.

4.4.2 Output: Nutritional Requirement for a bacterial population to survive

This process can be simulated for many bacterial trajectories in an independent manner. This leads to data on both the time of the event (death or attachment) and the type of event ending the free-living lifestyle of bacteria.

One output of such simulations is the percentage of bacteria encountering a particle. For the null model, the expected value of that variable is $100\frac{\lambda}{\delta+\lambda}$. As seen in section 4.1.1, the encounter rate λ depends on the particle concentration, notably through the parameter N_0. That parameter is a proxy for the number of particles available in different spots. For example, N_0 in the South Pacific gyre is $5 \times 10^{14} m^{-3}$ [158], while N_0 in the North Atlantic can go up to $1.25 \times 10^{17} m^{-3}$. Figure 4-7 presents the percentage of bacteria finding a particle in function of that value N_0, which impacts λ, for two different values of the death rate δ. The number of encounters increases with the number of available particles.

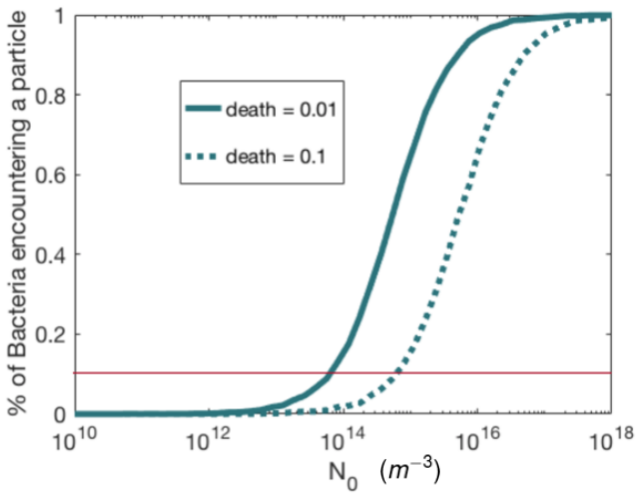

Figure 4-7: Percentage of bacteria encountering a particle with respect to N_0, a proxy of the number of particles, as simulated for 10^4 bacteria. Each blue line corresponds to the data for different death rates. The red line corresponds to the threshold cut-off for bacterial viability.

As the percentage of encounters for a bacterial population is monotonous with the number of particles, the foraging success of bacteria can be backtracked to the number of available particles. Here, I define foraging success when 10 % of a bacterial population finds a particle, as suggested by Lambert et al. [98] and described in section 4.1.1. This threshold on the attachment of the bacterial population provides the minimal amount of particles needed for this population to survive and persist. This value can serve as a proxy to estimate the viability of a bacterial population within a certain patchy environment given some phenotypic information. Conversely, when considering a bacterial population living in a patchy landscape, this minimal N_0 value also constrains the phenotypic space a bacteria needs to belong to. To be able to persist within that environment, the bacteria needs to be able to exhibit a minimal trade-off in terms of persistence and diffusivity. This model enables to determine the feasible behavioral space of bacterial behaviors within a patchy landscape, which is especially precious when foraging success is more critical at low particle concentrations.

4.4.3 Implementation of the phenotypic changes

After establishing a null model and the output from the model, I introduce dynamical changes in bacterial behaviors that were suggested by the experimental data presented in chapter 3: motility loss, death delay, and reductive division. This section discusses the implementation choices of these three phenomena.

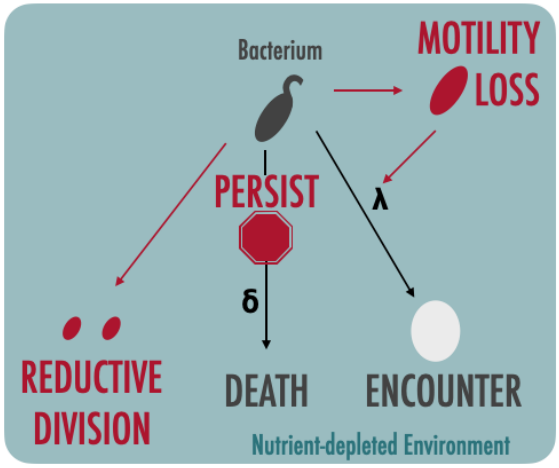

Figure 4-8: Modifications to the baseline stochastic modeling are noted in red.

Motility Loss

The loss of motility mainly impacts bacterial diffusivity, which appears in the expression of the encounter rate, as seen in Equation 4.2. So far, the loss of motility has been considered to be a discrete event, as bacteria don't slow down their speed but stop exhibiting active movement, as illustrated in section 3.2. To mimic the process, I make the choice to consider yet another Poisson process with a rate ρ simulating the time of motility loss for one bacteria. This rate is notably estimated to be $0.75h^{-1}$ for a nutrient deprived *Vibrio coralliilyticus* in section 3.2. This modification implies the simulation of the superposed Poisson process of rate $\delta + \lambda(D_{mot}) + \rho$. If the event of loss of motility is chosen, then the rate of the encounter rate is updated to $\lambda(D_{nonmot})$. The next event is simulated with the rate $\delta + \lambda(D_{nonmot})$, as loss of motility can only happen once. The dependence between the rate of encounter and the event of motility loss follows the properties of a Compound Poisson process. If changes in motility

were to be considered continuous in time, the chosen implementation would entail simulating a non-homogeneous Poisson process, as the rate of encounter $\lambda(t)$ would then be a function of time.

Death Delay

As seen in section 3.1, bacteria do not start dying right away. It means that the death process experienced by bacteria only starts after a certain time delay. For *Vibrio coralliilyticus* in our experimental conditions, this duration is seven days on a population level. This persistence mostly influences the Poisson process for death governed by the rate δ. To formalize this, I keep the Poisson processes the same. However, when a death event is drawn, the waiting time of the event is compared to the duration of the death delay t_{dd}. If it is below that threshold value, the event is discarded and a new waiting time is redrawn from the superposed Poisson process. In the case that another event (such as motility loss) happens after waiting time t_{w0} before the drawing of death event, the duration of the death delay is updated such that the newest accepted waiting time t_{w1} is $t_{dd} - t_{w0}$. As the waiting times of a Poisson process are exponentially distributed, the expected mean arrival time for death with a death rate set at $0.01h^{-1}$ (as calculated in section 3.1 is 4 days, which is on the same order of magnitude as the death delay observed experimentally. This notably means that, with this set of values, this method does not lead to an infinite loop of redraws. This implementation breaks down if the rate of the death process δ is very high compared to the rate of the encounter process λ and the duration of the death delay is significantly longer than the expected mean arrival time. However, within the context of this model, I consider the death rate δ as a point of reference to all the other rates considered.

Reductive Division

Another phenomenon observed in section 3.1 is reductive division. The number of cells within a bacterial population indeed continues to grow even when they are immersed in a nutrient desert. In this implementation of an individual-based model, it means

that individual bacteria need to be able to multiple. Here, I choose to add yet another Poisson process with a rate β which corresponds to the reductive division rate. This Poisson process is superposed with the processes of death, encounter, and, if relevant, motility loss. Then, waiting times are drawn given the procedure explained in section 4.4.1. When the reductive division event is chosen, one new bacterium is added to the pool. This new bacterium has the same properties as the microbe it is replicating. In this implementation, it is also possible to add a parameter Rd describing the state of the bacteria in terms of reductive division power. This variable counts the number of times a bacterium that detached from a particle can undergo reductive division. When one reductive division event happens, that counter decreases by one. This parameter is also transferred to the microbe stemming from the reductive division event.

This choice of implementation might come as a surprise because it does not describe the usual birth-death process used to describe the abundance of a bacterial population [170]. In this Markov chain description, each state corresponds to a different number of cells within a population and the transitions can lead to either the addition or the subtraction of one individual from the pool. Here, a decrease in the free-living bacterial population would be mediated by both the death and the encounter processes, while an increase would be caused by the reductive division process. The drawback of this method is that some of the Poisson processes depend on time, notably via the changes in motile properties for the encounter rate and the delay to death for the death rate. This means that the transitions to remove an individual from the population are time-dependent in the case of the death delay. These transitions even need to be governed by another Markov chain when it comes to tracking stochastic motility loss. That parallel Markov chain could for example track the motile fraction of the population. Compounding the birth-death model with another Markov chain is the definition of a quasi birth-death model. The birth-death model variations present the advantage of looking at a whole population and of having a bigger toolset supporting analytical insights. However, the main drawback of this model is the lack of flexibility when it comes to modeling the interdependence

between two events. For example, similarly to motility loss, the number of events of reductive divisions needs to be tracked, as there is only a limited amount of those which can happen. On top of that, there is experimental evidence that a bacteria that underwent reductive division could be more likely to persist longer [12]. This dependency could be added easily in the individual-based model described in this section. Another inconvenience of the birth-death model is that it is not easily parallelizable.

4.4.4 Results

This stochastic individual-based model for bacterial foraging quantifies the influence of all three phenotypic changes due to nutrient limitation on the ability of a bacterial population to persist within a patchy landscape. Reductive division and death delay are expected to be advantageous for the bacterial population, while motility loss has a deleterious impact on finding particles. Here, I analyze the balance of this trade-off between phenotypic changes during nutrient limitation.

The null model of motile bacteria that start dying right away at a rate of $0.01h^{-1}$ without experiencing reductive division requires a concentration of particles whose N_0 is around $10^{14}m^{-3}$ to survive, as shown in figure 4-7. To put that in perspective with the natural environment, this type of cells would survive even in the South Pacific gyre which is poor in particles. Even though this is a minimal amount of particles needed, it is noteworthy that the death rate δ controls the order of magnitude of the needed particles for a population to persist. Here, δ is set to the experimentally-determined value measured in section 3.1 which is comparable to the mortality rate measured for *Escherichia coli* [144].

When adding the effect of one allowed reductive division per cell, the minimal number of particles needed to survive does not change. The minimal number of particles required to survive N_0 stays similar to the null model. That's due to the fact that reductive division affects neither the rate of death δ nor the rate of encounter λ. When considering 10 % of the initial cell population attaching, that phenomenon doubles the chances of attaining that threshold. Even when modifying the number of times a cell can divide within the limits presented in the experimental data, the impact

of reductive division does not match the influence of motility loss which changes the encounter rate λ by three orders of magnitude. However, the rate of reductive division can significantly change the time needed for the first 10 % of a bacterial population to arrive at a particle, as illustrated in figure 4-9. The 10 % of bacteria to first arrive on particles require 21 hours less to find particles when reductive division is fast. That combines the advantage of both the doubling of the number of cells and also the speed of that multiplication. This could mean that a population that undergoes rapid reductive division may have a significant advantage at colonizing new particles relative to other populations, as discussed in more detail in section 5.3.

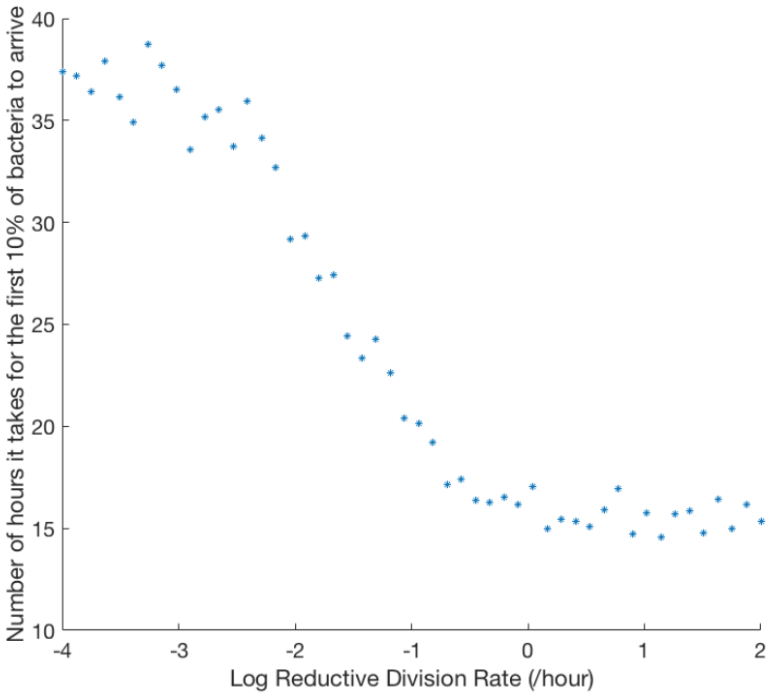

Figure 4-9: Number of hours it takes for 10% of the initial bacterial population to find a particle in function of the rate of reductive division. The x axis is in logarithmic scale. This data was generated with 10^4 replicates

When considering all the ecological mechanisms improving bacterial survival such as death delay and reductive division, Figure 4-10 offers a summary of the decrease of the minimum number of particles required for bacterial persistence. The bottom left corner of that graph corresponds to the null model when there is no death delay

and bacteria are unable to undergo reductive division. The minimal particle concentration required for bacterial persistence spans three orders of magnitude. The death delay confers the most resilience to a bacterial population and is therefore selected to compare the influence of the deleterious motility loss.

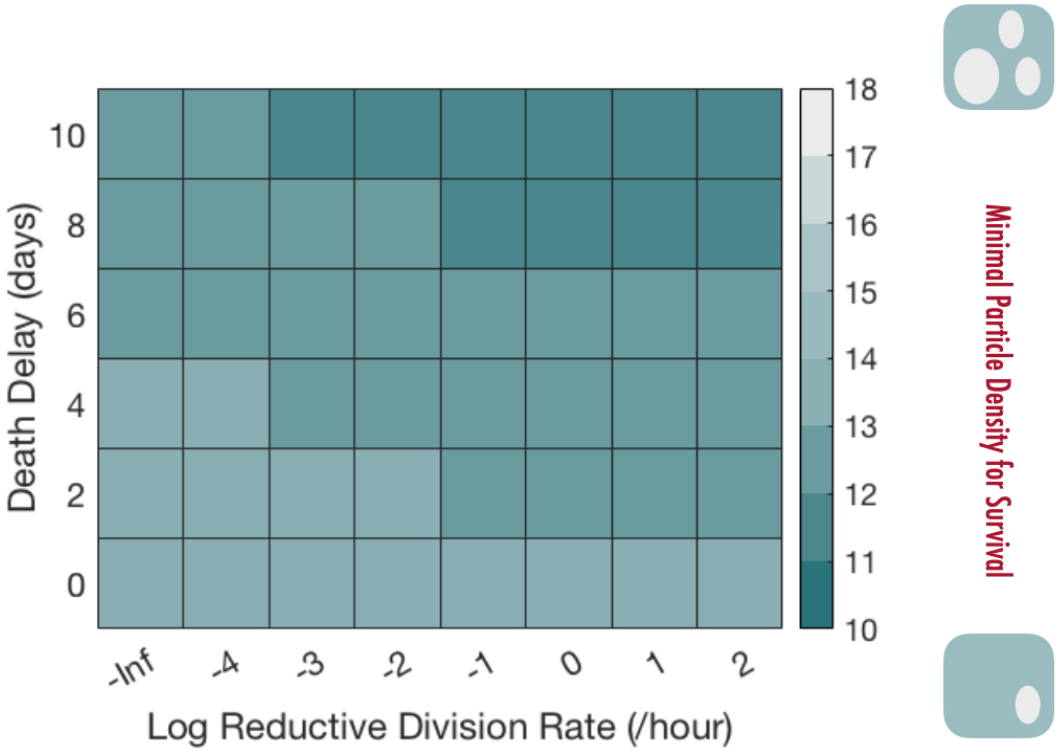

Figure 4-10: Heatmap of the minimum nutritional requirement for a bacterial population to survive with respect to the number of days bacteria can persist (death delay) and the rate of reductive division. The colors represent the minimal N_0 for which 10% of the bacterial population can survive. This heatmap was generated with 10^4 bacterial trajectories.

Figure 4-11 explores how the minimal particle concentration changes as a function of these two opposing factors, motility loss which reduces persistence and death delay which enhances it. As expected, the changes in the rate of motility loss influence the bacterial persistence the most, as the change in motility incurs a difference of three orders of magnitude in the encounter rate λ. When considering the bottom row which corresponds to the absence of death delay, the loss of bacterial motility brings

the minimal particle concentration within the range of what is observed in the North Atlantic ocean. The loss of motility then impacts where a bacterial population can survive. Bacteria that can delay the on-set of death due to nutrient limitation can offset this drawback.

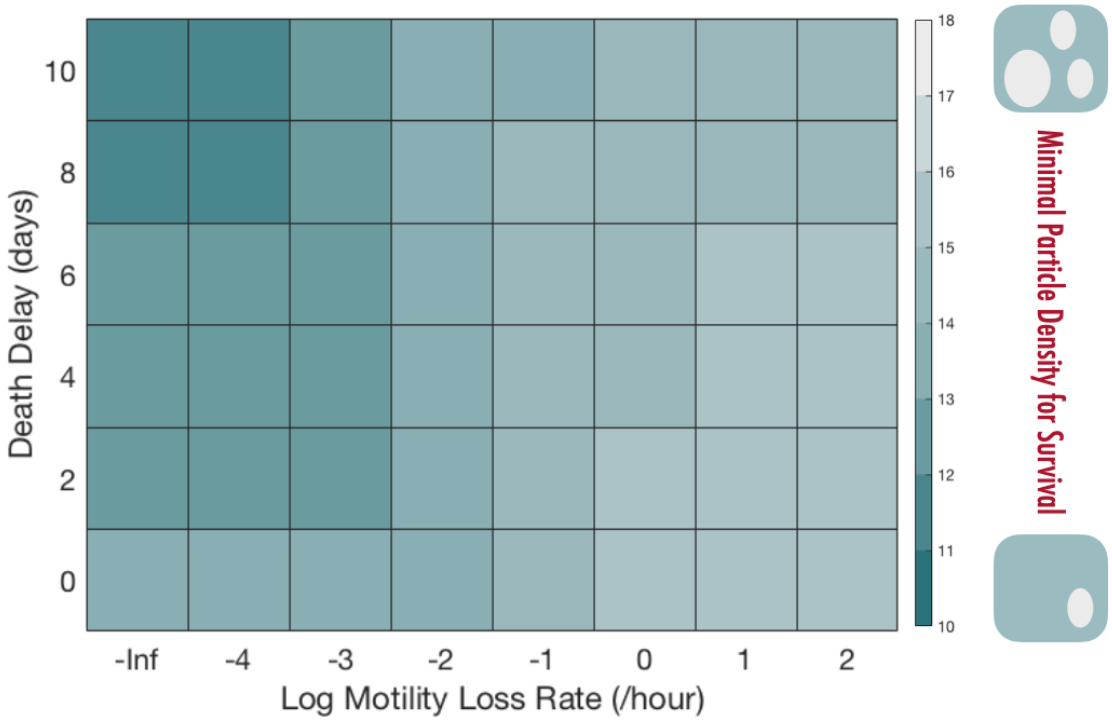

Figure 4-11: Heatmap of the minimum nutritional requirement for a bacterial population to survive with respect to the number of days bacteria can persist (death delay) and the number of days after which bacteria lose their motility. The colors represent the minimal N_0 for which 10% of the bacterial population can survive. This heatmap was generated with 10^4 bacterial trajectories.

Limitation

In this individual-based model, the realization of bacterial phenotypes is assumed not to depend on particle concentration. However, it can be argued that microbes that live in a particle-rich environment can adapt their behavior to that particle concentration, where the selective pressure stems from particle growth and not foraging. The adapted bacterial phenotype could then favor competitive traits for particle col-

onization. The reverse could also be true, where a particle-poor environment would emphasize selective pressure for advantageous foraging traits. Microbes that can regulate those behaviors tightly would then be able to colonize a wide variety of patchy environments. This individual-based model could reflect such insights if needed.

4.5 Conclusion

In this chapter, I present three models that describe the foraging dynamics of free-living bacteria in a patchy landscape. Bacterial diffusivity determines the time scales of bacterial foraging, as explained in the classic encounter rate model. When considering the loss of bacterial motility due to nutrient deprivation, the time needed for bacteria to find a particle increases. After parametrizing a population model to take into account the effect of population size variability, I develop an individual-based stochastic model for foraging that explores the effect of reductive division, death delay, and motility loss.

Reductive division mostly changes the time scales of particle finding, while death delay and motility loss impact the ability of a bacterial population to persist within certain particle landscapes. The requirement for the concentration of particulate organic matter increases with the rate of motility loss and decreases when bacteria postpone death. Given the dynamic behaviors of free-living bacteria, the individual-based model presents the lower bound of particles needed for bacterial survival. For example, the results align with the ubiquity of *SAR 11* in oceans, as its lack of motility is compensated by its ability to trump death. For a given particle concentration, bacterial foraging behaviors then also exist within a constrained feasible space. This model also provides hypotheses about the type of bacterial behaviors that can be observed at different particle concentrations.

Chapter 5

Beyond single-strain foraging on chitin particles: future directions

The preceding chapters present experimental results and modeling insights pertaining to the influence of nutrient limitation on bacterial foraging in patchy landscapes. In this chapter, I will expand the scope of the thesis by introducing new levels of complexities, presenting preliminary data that survey a number of future directions and open questions raised by this work. I first explore the implications that a foraging population is not uniform but consists of an assemblage of bacteria that have undergone nutrient limitation for different time intervals, resulting in phenotypic heterogeneity. Second, I consider that the patchy landscape bacteria navigate is not composed of discrete particles but rather of a sea of gradients [161], which suggests that the effect of starvation on chemotaxis may be a key factor in the estimation of successful foraging. Thirdly, as particles are hotspots of activity for many different bacterial strains that compete for nutrients and sometimes share public good resources [45, 137], I ponder the role of starved phenotypes in the establishment of particulate microbial communities. Finally, I investigate the potential impact of this bacterial state heterogeneity in the modeling of nutrient fluxes within the oceans.

5.1 Interaction between starved and non-starved cells

As bacteria roam through a patchy landscape, they build a complex population whose starvation age is heterogeneous. While some bacteria might have just detached from a particle, others might have been scavenging for different durations causing their phenotypes to change. This heterogeneity can lead to the emergence of new population level properties.

5.1.1 Starved bacteria as a seed bank for non-starved cells

Particle-attached bacteria are more metabolically active than their free-living counterparts [59]. In order for free-living bacteria to access the abundant resources available on a particle, bacteria need to forage for a particle, attach and resume their growth. The success of this transition depends on a population-wide trait, as there is a minimal critical bacterial density threshold for bacteria to colonize a particle successfully [43], even when bacteria seeding the particle all stem from exponentially growing cultures. However, a particle is surrounded not only by exponential cells but also by cells that have undergone nutrient limitation, as the process of foraging for a particle is highly stochastic. Considering that nutrient limitation affects bacterial attachment [92], the role of a sub-population of starved cells has been ignored. They could potentially strengthen the population headcount to attain the crucial density dependence that attachment requires to be successful and even reduce the amount of exponential cells required for a successful transition. How much can these starved bacterial seeds facilitate particle colonization and growth of a more exponential population?

5.1.2 Evidence for cooperative behaviors between exponential and starved cells

Attachment is the process that concludes the foraging period. While the process of attachment depends on individual level properties such as motility, viability and stickiness, it also materializes the emergence of population level success at particle

colonization. As shown by Ebrahimi, Schwartzma et al. [43] and further demonstrated in section 3.3,, bacteria rely on a critical density threshold to successfully attach to particles. This is the phenomenon we focus on to investigate ecological interactions between exponential and starved cells.

Method

Two separate bacterial cultures were made from the same frozen glycerol stock at -80°C. They are both pre-grown in liquid Difco 2216 marine broth for four hours at 25°C before being transferred for an overnight culture in the base media presented in the table B.7 with different dilutions. Once they reach late exponential phase, the first batch of bacteria is passaged on in the starvation media for a duration of 12 days at 25°C, while the second batch is harvested for inoculation. The two prepared batches are then inoculated with chitin beads at different initial cell concentrations, determined *a posteriori* via the counts of colony forming units. This mix of starved cells, exponential cells and chitin particles is then incubated in an overhead rotation device at room temperature for 20 hours before being sampled, stained with SYTO9 and imaged with confocal microscopy. This protocol is a variation of the attachment method presented in section 2.2.4.

Preliminary data

Here, I quantified the attachment for the mixed population for 12-day starved and exponential cells. As controls, I also measured the attachment of the two populations independently. If there is some cooperation between the starved cells and the exponential cells, I expect the mixture of both to attach more than the sum of the mean of the homogeneous populations, as shown by the straight blue dotted line in figure 5-1. Starved cells are able to attach more than the exponential cells as their initial concentration is more than 16 times higher than the exponential cells (5×10^6 vs. 3×10^5). However, it is notable that a starved cell population attaches less than an exponential cell population at equal initial cellular concentrations. The main take-away is that the mixture of both cell types attaches more than the expected addition

of both starved and non-starved cells. The variance in the number of attached cells is also higher for the mixed population than for the homogeneous populations. This data indicates a potential positive interaction between the two phenotypes. A potential caveat is that the mixed population of cells here is the most concentrated in bacteria. This requires the quantification of higher initial cell densities.

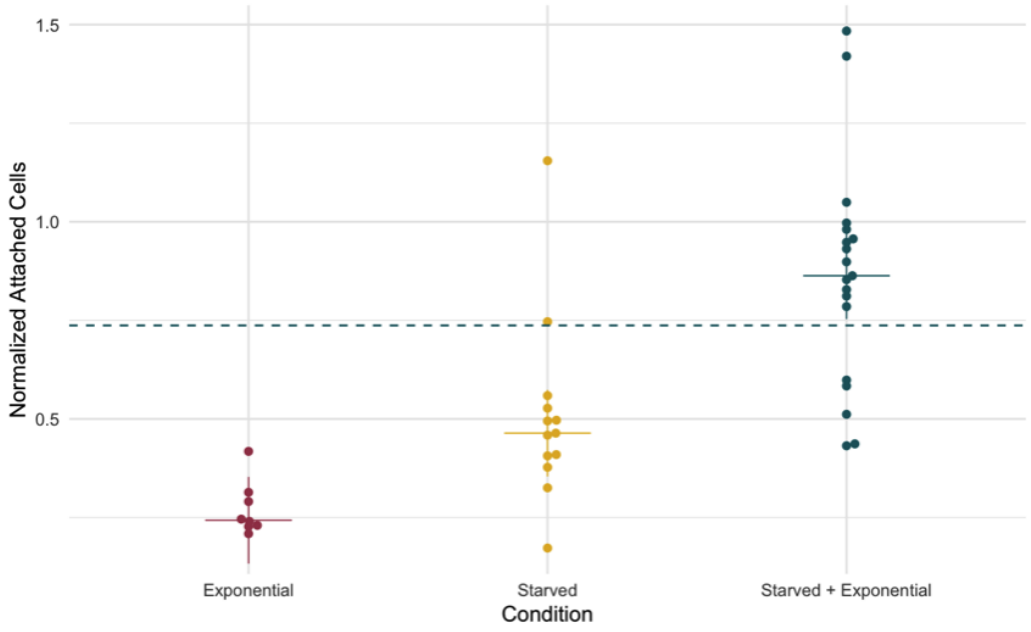

Figure 5-1: Number of attached cells normalized by bead area for 5×10^6 12-day starved cells, 3×10^5 exponential cells and the mixture of both.

To cast light on the differences in initial cell concentrations for the three populations, figure 5-2 presents similar data to figure 5-1. This experiment includes two new controls: both are higher concentrations of either exponential or starved cells than the ones in the mixed population case. As a sanity check, both concentrations of the exponential cells attach more here than the 10-day starved cell populations. This dataset also reproduces the result that the mixed population of non-starved and starved cells attaches more within 20 hours than the expected sum of the two populations inoculated separately. The controls also indicate that starved cells on their own are not able to reach the same attachment potential as when aided with a lower

concentration of exponential cells. This means that exponential cells facilitate the attachment of the starved population. As suggested by the number of cells attaching at the highest concentration of exponential cells, the more cells in an exponential state, the more likely the attachment success is.

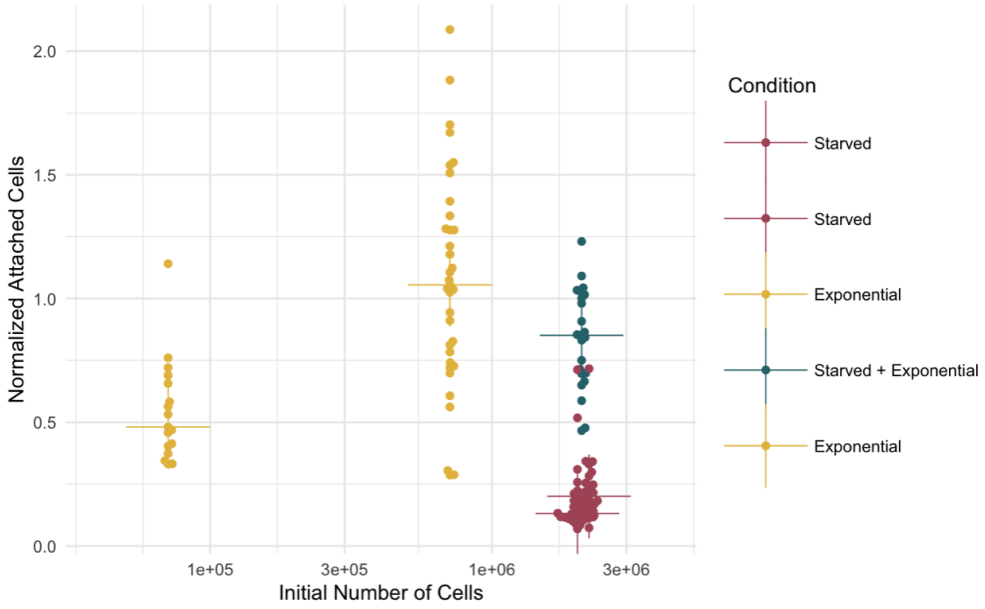

Figure 5-2: Number of attached cells normalized by bead area for 10-day starved cells (in red), exponential cells (in yellow), and the mixture of both lowest presented concentrations of each population (in blue). This mixture consists in inoculating exponential cells and starved cells together.

As seen in figure 5-3, I completed this dataset with the addition of a set concentration 2×10^6 of starved population to multiple exponential cell concentrations, notably lower ones. Here, a concentration of 10^4 exponential cells facilitates the attachment of the starved pool. It remains unclear from this data how significant this effect is because these experiments were conducted while the water used to fabricate all the media, notably the starvation media where the incubation with chitin beads takes place, was contaminated, as explained in section 2.1.2. Even though all the experiments presented were done in similar conditions, the contamination could affect the strength of the cooperation between cell types.

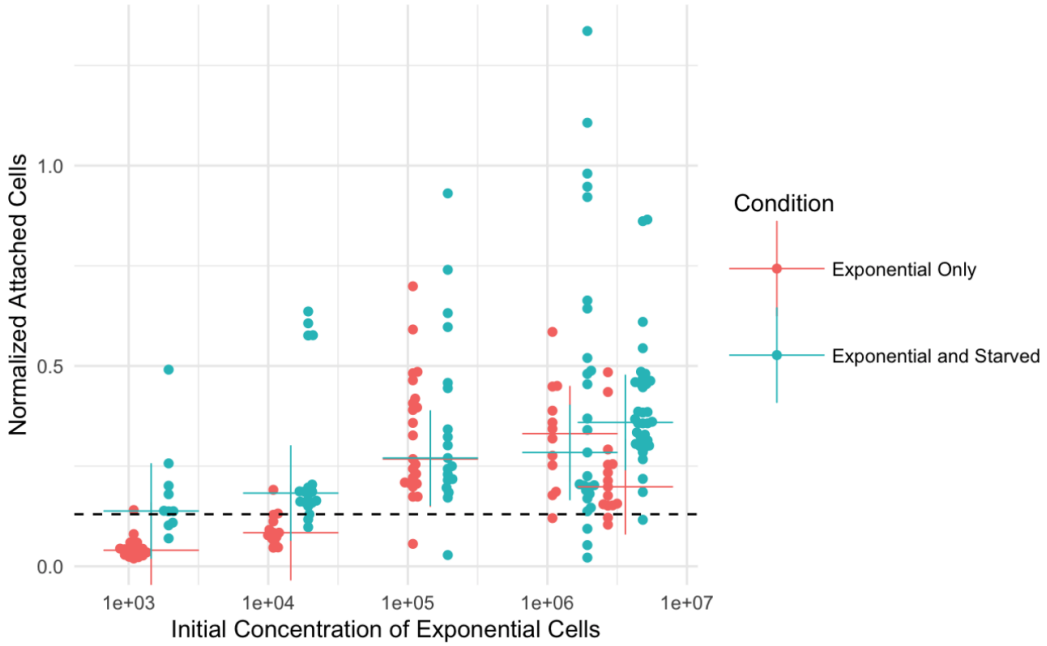

Figure 5-3: Number of attached cells normalized by bead area for different concentrations of exponential cells supplemented (or not) with 13-day starved cells. The cross represent the median of the point cloud, where each point is a different particle. The black dotted line is the median value for the pool of starved cells alone.

This data presents a holistic view of the encounter system, where both motility and stickiness are taken into account. Here, the effect of population size variation has been controlled for, as seen in figure 5-2. As the starvation durations are more than 10 days in all the data collected, section 3.2 builds the expectation that the motile fraction of the starved cells is negligible. Thus, both motility and stickiness explain difference of attachment between homogeneous populations of either starved or exponential bacteria, as investigated in section 3.3. The mechanisms for positive interaction in the mixed bacterial population of starved and non-starved cells can thus be tied to these two properties.

5.1.3 Discussion

This preliminary data suggests that the make-up of a bacterial population with cells starved for different time intervals in bulk seawater influences the colonization propensity of this population in a non-linear fashion. The contribution of the various phenotypes is not additive but relies on interactions between the subgroups of cells. Exponential cells can rely on lingering starved cells to build up the total concentration of cells above the critical density threshold for successful colonization, while the attachment of starved cells can be enhanced by the presence of not yet starved cells. In the environment, the composition of the foraging population would correspond to a balance between the detachment rate and the attachment rate. As detachment rate is highly dependent on the microbial dynamics on a particle [42], quantifying that phenomenon would be an interesting direction for future studies. Estimating the composition of the foraging population calls for the merging of the particle-centric and the free living-centric approaches, leading to better estimates of the microbial ecology around particles.

The mechanism for the interaction between starved and non-starved phenotypes remains an open question. A first approach to explore this that takes advantage of the current experimental set-up and the existence of dsRED-labeled strains of *Vibrio coralliilyticus* would be to mix a population of dsRED-labeled cells in exponential phase with one of non-labelled starved bacteria. Both subgroups would be stained with SYTO9. This differential labeling would enable the localization of the different groups of cells and could clarify if the interaction happens on the particle or in the bulk. Implementation details about the pre-incubation with antibiotics of the labeled strain and potential pre-staining of the two populations would need more experimental optimization. Another possibility for differentiating these two cell types would be to leverage the fact that membrane properties change with starvation [92] and design fluorescent quantum dots probe to attach to the exponential cell phenotype [180].

A mechanistic basis for cell cooperation for attachment could be due to the secretion of molecules that trigger a cellular behavior, such as the induction of cellular

motility (see section 5.2), or a particle property change like the coating of the particle surface with sticky exopolymeric matrix [90], which confers a foraging advantage to the free-living bacteria looking for a particle. The main hypothesis for the existence of facilitation is that exponential cells that attach first start to produce chemoattractants that then provide a roadmap for other bacteria to attach. These chemical signals could be either public goods or small molecular byproducts of chitin such as GlcNAc. If starved bacteria are able to navigate these gradients, then they could find a particle faster, as chemotaxis is theoretically equivalent to enhancing the size of particles by 10-fold [98]. This reinforces the key role of micro-gradients coming from particles in bacterial foraging [155, 23, 79].

5.2 Influence of nutrient limitation on chemotaxis

Bacteria navigate a complex landscape within oceans. One of the reductive assumptions of the experimental set-up presented in this thesis so far is that bacteria forage for resources in a nutrient desert, deprived of any other chemical cues. The real environment is composed of a combination of particles aggregating resources (marine snow) and other soluble molecules. For example, when phytoplankton undergo lysis, they locally release dissolved organic matter in their surroundings that bacteria can utilize [155]. This emission of resources becomes a hotspot of bacterial activity and is the source for diffusion of soluble molecules into the environment. This creates a gradient that bacteria can navigate using the process of chemotaxis, in which motile microbes adapt their patterns of movement to find a particle faster by for example reducing their tumbling ratio [162, 79]. Once a chemotactic bacteria enters the vicinity of a particle (up to ten times its radius), it can be captured by a particle [98]. The apparent size of the particle is then bigger. Chemotaxis is an important tool in the arsenal of bacterial foraging strategies that enhances the odds for attachment [60]. It is not a surprise that this natural process has inspired a wide array of computational methods for gradient navigation in optimization [131].

Chemotaxis has prerequisites: a bacterium needs to have tunable motile machinery

and to sense the differential concentrations of chemical signals. As seen in section 3.2, nutrient limitation triggers motility loss, which could impact the ability of bacteria to follow gradients. Below, I first discuss the implications of some preliminary data about the revival of motility by a chemoattractant. I then review the literature of nutrient limitation and chemotaxis to identify gaps that can be explored.

5.2.1 Revival of motility

Most bacteria lose their motility by the fifth day in a nutrient-limited media, as seen in section 3.2. However, it is unclear if this event is reversible. Motile behaviors can be stopped because the proton or ion motive forces powering the flagellar movement do not provide fuel to the flagella anymore [107, 94]. This would lead to a transient stop in active bacterial movement. When a bacterium loses its flagellum, the absence of machinery would require the renewed fabrication of proteins for the bacteria to exhibit active motility again. Here, I aim to observe if a spike of GlcNAc can revive motility within a timescale that would not allow for flagellar regrowth.

Figure 5-4 shows the projections of bacterial trajectories for 5-day starved cells before (on the left) and after (on the right) the addition of the chemoattractant GlcNAc at a high concentration. The images were taken five minutes after the spike. This preliminary data suggests that motility loss is only transient for *Vibrio coralliilyticus* after being immersed in a nutrient-limited media for 5 consecutive days. As the time scale to recover motility is so fast, it can be assumed that the flagellar integrity of 5-day starved bacteria remains intact. In a way, motility stays dormant until bacteria sense a signal.

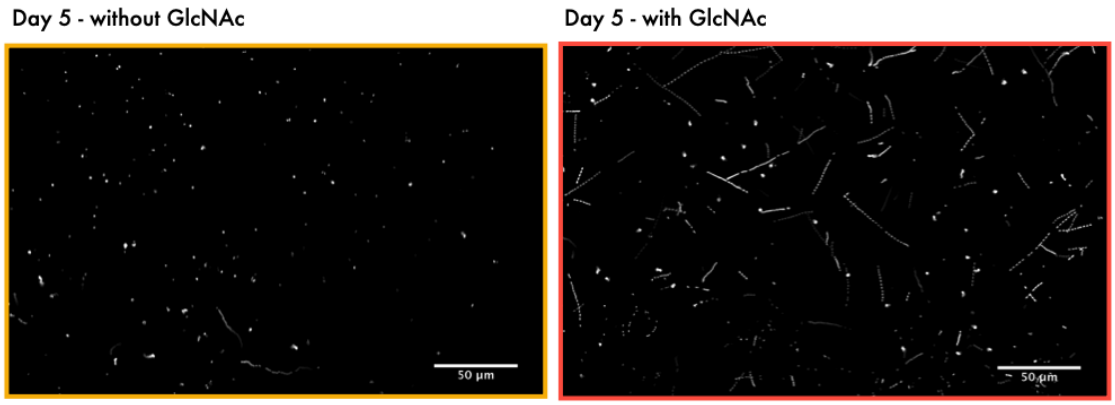

Figure 5-4: Projections over 1 second of bacterial trajectories (here in white) for 5-day starved cells before and after the addition of GlcNAc

This set-up supports the fact that bacteria conserve a functional flagella up to 5 days after the start of nutrient limitation. However, it does not quantify their chemotactic efficiency, as the concentration of GlcNAc is uniformly distributed across the wells.

5.2.2 Discussion: Chemosensitivity and chemotaxis

Chemotactic abilities were first observed using glass capillaries [2, 122]. Advances in microfluidics and computation have enabled a more precise and dynamic quantification of this process [4], as the creation of gradients has been more fine tuned and computational methods have enabled higher throughput. Applying these methods with cells in different nutritional states would give insights on the impact of nutrient deprivation for bacteria. Moving through a gradient requires resources to sense the chemoattractant and bias motility towards [79].

Chemotaxis starts with the cellular measurement of a surrounding concentration of a signal. This process relies on chemosensory pathways [178] which can count the discrete number of chemoattracting molecules a bacterium encounters [17, 23]. These sensing arrays are either soluble or located in the cell membrane [74]. As seen in section 3.1.2, nutrient limitation induces a reduction in cell volume and thus a drop in the cell surface area. This phenomenon could cause a decrease in sensory precision

for gradients, especially because bacteria such as *Vibrio ordalii* have been shown to sense chemoattractants at the detection limit of their molecular machinery [23]. This defect in sensing chemoattractants could temper the spatial range at which bacteria can detect a gradient.

At odds with this logic, there is evidence that chemotactic responsiveness in starved phenotypes can increase in *Spirochaeta aurantia* [171], in *Rhizobium meliloti* [181] and even in *Vibrio sp. 14* with some nutrients [105], as long as the duration of nutrient limitation does not exceed 24 hours. These studies imply that the control of chemotaxis is a complex regulated system that depends on cell history with nutrient limitation. There is a need for a systematic survey for longer starvation durations, coupled with proteomics and genomics, to attain an understanding of the regulation of chemotaxis under nutrient-limited conditions.

Another layer of intricacy in the quantification of chemotaxis stems from the diversity of chemoattractant molecules and the different levels of specificity exhibited by the chemoreceptors. The chemosensitivity for exponential and starved phenotypes will depend on the available signals, even for chemically close molecules [122]. In some cases, chemoattractants can serve a dual function as a metabolite and a signal, leading to a trade-off between uptake and chemotaxis [123]. When bacteria are stressed by the absence of nutrients in their environment, the incentives for both these functions get skewed, which could cause differences in the bacterial phenotype. Additionally, the plurality of chemoattractants can also cause the establishment of opposing gradients. These competing forces could both increase or decrease bacteria's ability to detect each signal [77]. As some bacteria are co-limited for multiple nutrients at the same time [13], they can coordinate their response to environments with multiple stressors [66], which could forge new preferences in their chemotactic choices. It is unclear how specific and dynamic nutrient limitation on bacteria will impact their ability to follow gradients.

On top of that, the primary criteria to be a chemoattractant is solubility, a property that chitin doesn't have. All chemotaxis around chitin particles must then come from the secretion by other cells of secondary signals, for example small metabolites

such as GlcNAc or quorum sensing molecules [79]. In the experimental system presented in this thesis, this process is collectively mediated by cells already attached to particles, which adds yet another intermediary to a complex system. Chemotaxis creates an interdependence between the life in the bulk and the life on particles. Investigating the fascinating questions around chemotaxis within the context of particle foraging requires integrating knowledge of the free-living and attached bacterial states while developing high throughput spatial assays.

5.3 Competitivity of starved phenotypes with other bacteria

So far, this thesis has focused on a single strain of *Vibrio coralliilyticus* navigating nutrient limitation and particle foraging at the same time. In the free-living state, the interactions with other strains can be assumed to be negligible, as cells are relatively far apart from each other, relatively metabolically inactive [72] and continuously moving in a non-synchronized manner, except for chemotaxis. Once a bacterium is in the vicinity of a particle, which have also been referred to as hotspots [161], the density of bacteria goes up and bacteria now have to compete for the available resources against other bacterial strains. This leads to interactions between microbes that are already on the particle and the ones that are attempting to invade that resource-rich space. These microscale ecological forces shape microbial assembly around particles [104, 45].

In section 3.4, I presented results on the rescue of the growth properties after different starvation durations for the strain of interest. Except for the lag time, *Vibrio coralliilyticus* exhibits similar growth rate and yield no matter the time spent in the nutrient-limited environment. While these results convey that these bacteria can successfully colonize particles *de novo*, they do not describe the ability of bacteria to invade a pre-colonized space by other bacterial strains. Nutrient limitation doesn't only influence metabolic and foraging abilities but also other bacterial functions,

impacting for example the propensity for host infection [53] or potentially antibiotic production. That last function is indeed boosted when *Vibrio coralliilyticus* is grown in a co-culture [24].

In the context of chitin particles, interactions between strains have so far been quantified with respect to the dynamics of particle degradation [45]. The drawbacks of this method such as the lack of control for flow and landscape map, the complexity of pre-colonization, and the focus on ecological function make the search for a more reproducible set-up necessary, especially when asking questions about free-living bacteria. Quantifying interactions on chitin requires the development of a visual non-destructive competition assay with labeled bacterial strains. This would require the usage of flat chitin surfaces (as explored in section 2.2.4), which could be coupled with microfluidics for the sake of reproducibility. Such a device renders the spatial organization of a community available, enabling precise and localized measurements of microbial interactions. For example, it could cast light on the interaction mediated by chemotactic properties between strains. Competing cells in different phenotypic states would offer a more complete picture of interactions on chitin particles.

5.4 Impact of nutrient limitation on the carbon cycle

In this thesis, the fourth chapter presents foraging on a patchy landscape from the lens of the persistence of a microbial population. As seen in figures 4-10 and 4-11, the selected output is the minimal amount of patches needed for a population to survive within such an environment. This provides information on bacterial persistence but does not tackle the influence of the phenotypic changes due to nutrient limitation on the dynamics of carbon sequestration. Microbes indeed contribute to the carbon cycle by dissolving particles that would otherwise sink to the bottom of oceans [48]. In this context, the timescales of bacterial foraging in a patchy landscape can influence the fluxes of particles. This would notably impact environments with sparse particle concentration, where the mean distance between particles is large. The question then emerges: how is the time scale of particle degradation influenced by the timescales of

bacterial foraging in a nutrient-poor environment?

This could be estimated by expanding the last individual-based model presented in the section 4.4 of chapter 4. It requires complexifying it by adding an explicit pool of particles, whose size and concentration can be drawn from a realistic particle size distribution [158, 95, 134]. During a simulation, when a bacterium encounters a particle, this microbe could then be assigned to a particle at random. This pick for a particle would only depend on particle size. Once enough microbes attach to the same particle, this patch can be considered colonized and thus dissolving. Such a model would also enable a better quantification of the effect of chemotaxis on particle colonization. This model could then output a timescale for particle colonization depending on the phenotypic changes experienced by bacteria while they are foraging. So far, the state-of-the-art for integrating microbial dynamics with particle fluxes [120] models the bacterial encounter rate with the assumption that bacteria stay motile. Modifications of this global scale model would enable the characterization of the influence of these phenomena on global particle turn-over.

Chapter 6

Conclusion

6.1 Summary

This thesis quantified the phenotypic adaptation of foraging bacteria to nutrient limitation and its implication on a population's ability to persist in a patchy landscape. In the first chapter, I reviewed the literature about the patchy landscape marine bacteria live in, where a nutrient-depleted environment surrounds nutrient-rich particulate organic matter. This nutrient heterogeneity requires microbes to forage for resources under nutrient limitation, which impacts bacterial physiology. In turn, dynamic changes to physiological properties such as motility, viability, and stickiness can affect the scavenging abilities of a bacterial population, thus creating a feedback loop that can change the timescales of foraging. Such variation can impact the timeframe of particle colonization and degradation by bacteria, which influences the carbon cycle in the oceans.

To quantify the changes in bacterial foraging traits under nutrient limitation, I designed an experimental system in chapter 2. Here, I chose to focus on the multi-day deprivation of GlcNAc, the monomer of the common marine biopolymer chitin, as a source of both carbon and nitrogen for a strain of *Vibrio coralliilyticus*, YB2. This required a careful examination of potential contamination sources, as well as the development of an evaporation-controlled system. From this incubation, I then optimized state-of-the-art methods for measurements of cell viability, size, motility,

stickiness, and regrowth at the population and individual scales. Highlights from these methods include the use of a Suspended Microchannel Resonator, developed by the Manalis lab, to quantify individual cell buoyant mass, as well as the optimization of attachment and regrowth assays involving the insoluble polymer chitin.

The findings from these experiments are described in chapter 3, in which I identified behavioral changes linked to nutrient limitation. First, I show that *Vibrio coralliilyticus* can trump death for up to seven days and sustain up to three divisions in a nutrient-free environment. This last phenomenon is akin to reductive division, as it corresponds to a decrease in individual cell size. These marine bacteria also experience discrete motility loss events over the course of starvation, resulting in a decrease of the motile fraction from 80% after one day of starvation to 8% after five days. Attachment experiments suggest that bacterial stickiness decreases as a function of starvation duration, contrary to the expectation built by literature [92]. When the time comes to be rescued in a nutrient-rich environment, *Vibrio coralliilyticus* experiences delays to regrow after starvation, with lag times on the order of magnitude of hours. However, these bacteria still maintain a similar final yield no matter the time they spent in a nutrient-depleted environment. The side-by-side comparison of population-wide measurements with the quantification of individual traits led to the conclusion that in this experimental system, nutrient limitation was a driver of population homogeneity, not heterogeneity. The results are at odds with prior expectations that nutrient limitation would lead to heterogeneity as a part of a potential bet-hedging hypothesis. All these experimental results highlight the dynamic phenotypic adaptations of *Vibrio coralliilyticus* to nutrient limitation and the effect of starvation on numerous key foraging traits.

Chapter 4 investigates the influence of the different phenotypic changes on the time scales of bacterial foraging and persistence using modeling tools. While reductive division and death delay provide more opportunities for microbes to find a particle, loss of motility and stickiness decrease the bacterial encounter rate with particles. After defining a classic model describing the stochastic process of encounter between particles and bacteria, I explored the increase in foraging time by adding a discrete

motility loss to that model. On top of that, to include the changes in bacterial viability such as death delay and reductive division, I contrasted a population-based model with an individual-based model that simulates bacterial trajectories. This last individual-based model cast light on the minimal amount of particles required for a bacterial population to persist given these dynamic phenotypic changes.

Chapter 5 expanded the scope of the experimental and modeling chapters by adding layers of complexity in order to make it more relevant to the natural environments. An additional source of heterogeneity in a foraging bacterial population is the amount of time individual cells have spent in the nutrient-limited environment. Here, I present preliminary data on this phenomenon by examining the facilitation dynamics in the attachment to particles between exponentially-growing and starved cells. As these interactions between two different physiological states could be mediated by chemotaxis, I then explored how chemotactic abilities in bacteria are affected by nutrient limitation, and found that motility loss can be reversible at day 5 by the addition of a chemo-attractant. This underscores the importance of chemotaxis on the time scales of bacterial foraging, adding another layer of complexity to explore in future work on this topic. I additionally consider how interactions with other strains in a complex, natural community may affect the phenotypes described here. Lastly, I discuss how the results presented in this thesis can be included in the modeling of carbon cycling in oceans to have better estimates.

6.2 Discussion

To estimate bacterial foraging, it is important to consider the impact of nutrient scarcity on bacterial phenotypes. Here, I show that motility loss, delay to death on-set and reductive division affect bacterial foraging efficiency. This thesis provides a unique point of view on foraging time scales by quantifying multiple parameters governing successful encounter rates. Experimental results were assayed over time, which enables a dynamic trait description of the bacterial population. The contrast between population and individual level measurements also provided unique insight

into the potential emergence of population heterogeneities. Within this experimental system, nutrient limitation leads to an homogenization of the bacterial population. The results regarding cell attachment to chitin beads call into question the accepted trend that cell stickiness increases with the time spent in a nutrient-limited environment. Here, heterotrophic bacteria balance the disadvantage from motility loss and stickiness deficit with a higher viability. This work also presents new stochastic modeling frameworks that contribute to a better understanding of bacterial persistence within a patchy landscape. This provides a well-defined baseline for the minimal particulate requirement for a bacterial population to survive, while also constraining the space of bacterial traits needed to survive in a given environment.

One exciting avenue to explore is an extension of the experimental results onto other bacterial strains foraging in the oceans. Such phenotypic assays could generalize the experimental results observed in chapter 3. If they are combined with genetic tools, it could identify key players in those phenotypic changes and thus gain predictive power on the dynamical changes experienced by foraging bacteria in the global oceans.

Another open question remains about the influence of different types of nutrient limitations on bacterial phenotypes. As mentioned in the introduction, the growth of microbes in the oceans is indeed limited by different chemicals such as iron, vitamins, and also phosphorus. The resolution of the patches bacteria navigate could happen at the mesoscale, where particles concentrate some of those nutrients. Exploring the commonalities and discrepancies between the phenotypic responses to the deprivation of a variety of chemicals could help identify new bacterial niches and further our understanding of the marine microbial ecosystem.

This work contributes to linking the ecological roles of a bacterial strain with its physiology, as it reacts to its surrounding environment. By taking into account the stressor of nutrient limitation during particle foraging, this work aims at contextualizing microbial ecological dynamics within their resource landscape. It also contributes to addressing open questions about the role of bacterial dormancy in marine systems [101] and the complex study of bacterial populations with a low metabolic activity

[56]. In a boarder context, precise physiological measurements on the microscale have outsize effects on our understanding of the microbial ecosystem and the global carbon cycle.

Appendix A

Abbreviations

Long Name	**Abbreviation**
Colony Forming Unit	CFU
Deoxyribonucleic acid	DNA
N-acetyl-D-glucosamine	GlcNAc
High-Performance Liquid Chromatography	HPLC
Optical Density	OD
poly-β-hydroxybutyrate	PHB
Particle Size Distribution	PSD
Polyvinylpyrrolidone	PVP40
International System of Units	SI
Suspended Microchannel Resonator	SMR

Appendix B

Media Recipes

B.1 Tibbles-Rawlings Media

The recipe for this media based on a paper by Tibbles and Rawlings [172] is described extensively in the appendix B of Manoshi Datta's PhD thesis [35] as a minimal medium without carbon source.

B.2 Minimal Artificial Seawater Media

The recipe for this media was optimized collectively, notably by Julia Schwartzman, Tolga Calgar and Kapil Amarmath.

B.2.1 Stock solutions

4X Salt Water

This is the base for all defined media

Table B.1: 4X Salt Water recipe - 1L to filter sterilize through $0.2\mu m$

Component	Amount (per L)	Formula Weight (g/mol)	Concentration (mM)
$NaCl$	80 g	58.44	1369
$MgCl_2 * 6H_2O$	12 g	203.20	59
$CaCl_2 * 2H_2O$	0.60g	147.02	4
KCl	2.0 g	74.56	26

HEPES Buffer

For 1L of 1M HEPES buffer (20X), dissolve 260.29g HEPES sodium salt in 750 mL distilled water before adjusting the pH to 8.2 with concentrated HCl and constant stirring. After storing at 4°C, bring to a final volume 1L with distilled water and filter sterilize through $0.2\mu m$.

PVP40

The stock solution of polyvinylpyrrolidone (with an average molecular weight of 40000) is a 1% w/v solution, which means dissolving 2.5g of PVP40 in 250mL of distilled water. This needs to be filter-sterilized through $0.2\mu m$.

1000x Trace Minerals

This solution contributes to mimicking the ionic composition of seawater. It is possible to make some substitutions in the same oxidation state but with a different counterion for some metals. All dissolutions must happen in 20mM HCl to avoid precipitate and contamination. It is necessary to use single-plastic use material and to thoroughly wash any other instruments with 20mM HCl.

Table B.2: 1000X Trace Minerals

Substance	Final Concentration (mg/L)	Comments
$FeSO_4 * 7H_2O$	2100	
H_3BO_3	30	
$MnCl_2 * 4H_2O$	100	
$CoCl_2 * 6H_2O$	190	
$NiCl_2 * 6H_2O$	24	
$CuCl_2 * 2H_2O$	2	
$ZnSO_4 * 7H_2O$	144	
$Na_2MoO_4 * 2H_2O$	36	
$NaVO_3$	25	Toxic, handle in hood
$NaWO_4 * 2H_2O$	25	Toxic, handle in hood
Na_2SeO_3	4	Toxic, handle in hood

After filter-sterilizing it through $0.2\mu m$, this solution is stable for a couple months when stored at 4°C. For longer term storage, it is possible to keep aliquots at -20°C.

1000X Vitamins

This solution needs to be dissolved in 10mM MOPS at pH 7.2.

Table B.3: 1000X Vitamins

Substance	Final Concentration (mg/L)	Comments
Riboflavin	100	
D-Biotin	30	Stored at 4°C
Thiamine hydrochloride	100	
L-ascorbic acid	100	
Ca-d-pantothenate	100	
Folate	100	
Nicotinate	100	Stored at 4°C
4-aminobenzoic acid	100	Stored at 4°C
Pyridoxine HCl	100	
Lipoic acid	100	
NAD	100	Stored at 4°C
Thiamin pyrophosphate	100	Stored at -20°C
Cyanocobalamin	10	Stored at 4°C

This solution needs to be titrated with a couple of drops of 5M NaOH to avoid precipitate and filter-sterilized through $0.2\mu m$. It is stable for a couple months when stored at 4°C. For longer term storage, it is possible to keep aliquots at -20°C.

10X CNP-Seawater

This solution is an intermediate mix of the final minimal media that can be frozen at -20°C (for faster preparation).

Table B.4: 10X CNP-Seawater

Substance	Volume (mL)
1000X Trace Minerals	10
1000X Sodium Sulfate	10
20X HEPES Buffer, pH 8.2	500
Distilled water	480

Sources of C, N, S and P

This table presents the different options to add on carbon, nitrogen, sulfur and phosphorus to the media. Each line is a different solution, which needs to be filter-sterilized through a $0.2\mu m$ filter.

Table B.5: Possible sources of carbon, nitrogen, phosphorus and sulfur

Solution Name	Providing	Substance	Amount (g) to be dissolved in 40mL of distilled water
1M sodium sulfate (1000X)	S	Na_2SO_4	5.68
0.5M phosphate dibasic (500X)	P	Na_2HPO_4 anhydrous	2.84
0.5M phosphate dibasic (500X)	P	$Na_2HPO_4 * 7H_2O$	10.72
0.4M GlcNAc (20X)	C, N	$C_8H_{15}NO_6$	3.54
1M GlcNAC (50X)	C, N	$C_8H_{15}NO_6$	2.21
1M Ammonium Chloride (100X)	N	NH_4Cl	2.14
0.4M Glucose (20X)	C	$C_6H_{12}O_6$	2.88

B.2.2 Original Media

Here is the recipe for the media with the original concentrations of carbon, nitrogen, and phosphorus.

Table B.6: Original Seawater media recipe (final volume: 40mL)

Volume (mL)	Stock Solution
0.04	1000X Vitamins
0.08	500X 0.5M Phosphate Dibasic
0.4	100X 1M Ammonium Chloride
2	20X 0.4M GlcNAc
10	4X Seawater
4	10X CNP-Seawater
23.5	autoclaved distilled water

B.2.3 Base Media

Table B.7: Base Media Recipe (final volume: 100mL)

Volume (mL)	Stock Solution
5	1% PVP40
0.02	500X 0.5M Phosphate Dibasic
0.2	500X 1M GlcNAc
25	4X Seawater
10	10X CNP-Seawater
59.8	autoclaved distilled water

B.2.4 Starvation Media

Table B.8: Starvation Media Recipe (final volume: 100mL)

Volume (mL)	Stock Solution
5	1% PVP40
0.02	500X 0.5M Phosphate Dibasic
25	4X Seawater
10	10X CNP-Seawater
60	autoclaved distilled water

B.2.5 Rich Media

Table B.9: Rich Media Recipe (final volume: 10mL)

Volume (mL)	Stock Solution
9	Base Media
1	Marine Broth 2216

Appendix C

Physics-based prediction of biopolymer degradation

Context

The degradation of chitin particles by bacteria is a physical phenomenon mediated by biological entities secreting chemical agents. On the one hand, bacteria produce enzymes that mediate the degradation of the chitin polymer. On the other hand, a chitin particle is a matrix of cross-linked polymers that get cleaved by enzymes. In other words, chitin is a biogel that chemical agents can degrade. On-going research about biogels focuses on their degradation, swelling, and also accretion. All in all, the dynamics of particle degradation are at the intersection of biology, chemistry, and physics.

This appendix presents the work done in collaboration with Rami Abi-Akl for the paper [1]. This project explores how the physical modeling of biogel degradation can explain a surprising experimental observation for bacterial particle degradation. This write-up focuses on my contribution.

Detailed Contribution

The idea of the collaboration between Rami Abi-Akl and me emerged after a presentation of Rami Abi-Akl 's research at a departmental seminar. As Rami Abi-Akl had the expertise in biogel physics, my role was to introduce him to the experimental design and results and also to the current biological model of particle degradation. We worked together to design a model bridging the current understanding of biogels and bacterial degradation. Rami Abi-Akl did all the subsequent model analyses. Tim Enke collected the data used for the published paper. It is to note that I also gathered similar data during my thesis, as shown in this appendix. We also wrote a proposal to the MIT Civil and Environmental Engineering cross disciplinary seed fund award with the help of our principal investigators Professor Otto Cordero and Professor Tal Cohen.

Abstract

In the natural environment, insoluble biomatter provides a preeminent source of carbon for bacteria. Its degradation by microbial communities thus plays a major role in the global carbon-cycle. The prediction of degradation processes and their sensitivity to changes in environmental conditions can therefore provide critical insights into globally occurring environmental adaptations. To elucidate and quantify this macro-scale phenomenon, we conduct micro-scale experiments that examine the degradation of isolated biopolymer particles and observe highly nonlinear degradation kinetics. Since conventional scaling arguments fail to explain these observations, it is inferred that the coupled influence of both the physical and biochemical processes must be considered. Hence, we develop a theoretical model that accounts for the bio-chemo-mechanically coupled kinetics of polymer degradation, by considering the production of bio-degraders and their ability to both dissociate the material from its external boundaries and to penetrate it to degrade its internal mechanical properties. This change in mechanical properties combined with the intake of solvent or moisture from

the environment leads to chemo-mechanically coupled swelling of the material and, in-turn, influences the degradation kinetics. We show that the model quantitatively captures our experimental results and reveals distinct signatures of different bacteria that are independent of the specific experimental conditions (i.e. particle volume and initial concentrations). Finally, after validating our model against the experimental data we extend our predictions for degradation processes across various length and time scales that are inaccessible in a laboratory setting.

Citation

Abi-Akl, Rami, **Elise Ledieu**, Tim N. Enke, Otto X. Cordero, and Tal Cohen. "Physics-based prediction of biopolymer degradation." *Soft Matter* 15, no. 20 (2019): 4098-4108.

Appendix D

Bacterial Growth on a Patchy Landscape

Context

This appendix reproduces the paper for the second part of my general exam defended in 2017. It explores the event of sudden particle decolonization.

D.1 Abstract

Bacteria grow on nutrients that are spatially distributed in their natural environments. Nature is characterized by its resource scarcity and its uneven resource distribution that impact different aspects of population growth. In the ocean, heterotrophic bacteria can attach to complex biopolymer particles that act as hotspots of bacterial activity due to their high carbon content. These hotspots, also considered as patches, are distributed in seawater and form a patchy landscape of nutrients. This paper aims to address the dynamics of a bacterial population on a patchy landscape by using the experimental model system consisting of bacterial growing on heterogeneous landscapes made of biopolymer particles in an otherwise carbon-depleted medium. This work describes how the growth of a clonal bacterial population on one particle depends on the initial bacterial concentration and on the density of patches on the

landscape. This growth is a non-linear phenomenon, which suggests the existence of bacterial strategies that trade-off growth on a patch with foraging behaviors on a landscape.

In the ocean, heterotrophic bacteria live in a spatially structured landscape of nutrients. Organic matter in this environment can either be aggregated in particles, in what is known as marine snow, or can be dissolved in seawater. [11, **?**] Particulate organic matter constitutes a form of highly concentrated carbon resources and acts as a hotspot for bacterial activity. [150, 9] Since these particles are rich in complex biopolymers like chitin and alginate, they sink into deeper oceanic layers leading to the sequestration of carbon in sediments. [28] If bacteria capable of dissolving complex biopolymers colonize these particles, they can transform particulate organic matter into dissolved organic matter and biomass, thus recycling essential nutrients back into the marine food web. It is therefore crucial to rationalize the dynamics of such a process in order to understand carbon cycling in the ocean.

Degradation of particulate matter in the ocean is intimately linked to the dynamics of bacterial growth, as degradation is dependent on bacteria producing enzymes that dissolve particulate organic matter. [154] However, the intrinsic spatial structure of the particle environment influences bacterial behavior, as microbes must adapt to conditions of alternating nutrient richness and nutrient depletion. Conditions of nutrient richness are found on and around particles, whereas conditions of nutrient depletion are characteristic of the bulk seawater. Given this difference in the abiotic environment, it follows that bacteria that are categorized as free-living (i.e. found in bulk seawater) are in a very different physiological state than those found attached to particles. [38] Bacteria adapt to attach to particles in order to grow but they also adapt to disperse in search of new particles and to sense chemical gradients. [53] Therefore, organisms must decide whether to remain attached to a particle surface or to swim in pursuit of new resources. This microbial cycle of famine and feast [157] influences the persistence and growth dynamics of a bacterial population and thus its efficiency to occupy and degrade a landscape of several particles. Below, I will expand on each of these two phases of the life-cycle of bacteria on particle landscapes.

(Fig. D-1)

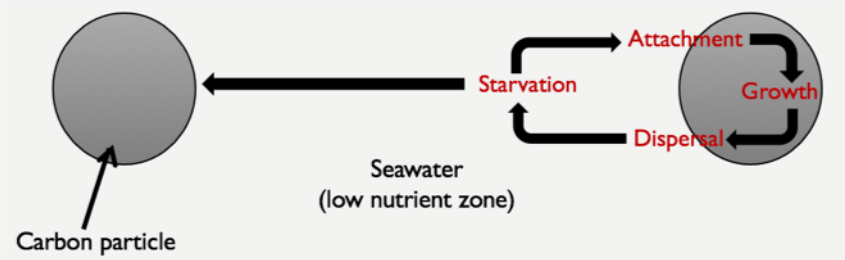

Figure D-1: Life cycle of bacteria on a patchy landscape. This cycle can locally happen at a particular particle or it can involve different particles, as bacteria can disperse from one particle to another.

Firstly, as free-living organisms in the seawater, bacteria are in an environment significantly depleted in nutrients compared to particles. This means that bacteria can undergo starvation while foraging for new resources. [186] Starvation influences the physiological state of individual bacteria through size reduction, membrane changes [73, 92] and motility. [118, 165] All these factors have an impact on microbial foraging strategy, because foraging for new resources depends on intrinsic bacterial properties such as microbial diffusivity and attachment propensity. [36] Kiorboe estimated the median search duration to be less than a day in oceans without considering possible physiological changes of bacteria due to starvation. [87] However, effects of starvation can appear within a couple hours, which is a relevant time scale to influence foraging behaviors. [181] The longer cells search for nutrients, the more affected they are by starvation. Since the interplay between starvation and foraging appears at the microbial scale, it can therefore influence the dynamics of the degradation of a landscape.

Secondly, once a bacterium encounters a particle, it attaches to it and bacterial growth begins. Growth on particles requires the production extracellular enzymes that are able to break down the long polysaccharide chains found in biopolymers into smaller by-products. [196, 182] These smaller molecules can be imported into the cell and used as a carbon and energy source for growth. The enzymes secreted by bacteria and the monomers can be described as public goods, as they are a shared resource from which both the cell that produces the enzymes and its neighbors benefit. [40].

The role of such an interaction on the process of particle colonization remains an important open problem in the field, as it is unclear how it promotes competitive or cooperative behaviors between cells around a particle. [70]

Transitions between the previously described particle-adhered and free-living states are referred to as attachment and detachment. To characterize this phenomenon, it can be hypothesized that as soon as a cell encounters a particle there is attachment. [87] If attachment is defined by the initial contact of a bacteria with a particle, then the detachment rate completely controls the stability of the attached state. This rate is parameterized by intrinsic cellular properties, such as membrane integrity or presence of binding molecules on the cell surface. These properties interplay with the nature of the substrate and its chemical properties such as electronegativity. [69] Detachment also depends on biotic factors, for example the presence of an extracellular matrix, the distribution of cells on the surface of the particle, quorum sensing molecules, and the physiological state. The variety of processes involved in triggering detachment makes it a complex problem that remains poorly understood. The free-living and attached states, as well as the transition between them, have implications for the aggregate behavior of bacterial at the landscape level, where biopolymer particles define discrete patches of nutrients in an otherwise nutrient depleted aquatic environment.

In a homogeneous well-mixed environment, bacterial biomass is expected to follow Monod's equation. However, the growth dynamics at the landscape level, which generally can be characterized by biomass increase on the patches within the landscape, are unknown, as growth dynamics on a patch are connected to the growth dynamics on other patches via bacterial dispersal. [59] A colonized patch is an open system that exchanges fluxes of bacteria but also chemical cues due to bacterial activity with its surroundings. [163] Even before linking patches together, it is unclear how free-living bacteria invade a patch de novo because of feedback loops between the attached and free-living states. Information between growing cells and free-living cells can indeed be transferred through the secretion of chemical cues by attached cells such as byproducts from biopolymer particle degradation. These chemical signals can

in turn change the behavior of free-living cells, as they adapt their motility patterns in response to those chemical gradients. This behavior, known as chemotaxis, has been observed around particles in seawater. [47, 162] Because of the interdependence between cellular states and the dynamical chemical landscape, it remains challenging to predict the growth dynamics of a bacterial population with an initially given spatially heterogeneous pool of resources.

In order to study the emergence of population dynamics on a patchy landscape from a top-down perspective, we investigate how a clonal bacterial population colonizes patches and grows on them. Global properties of the landscape such as particle density are expected to influence fluxes of bacteria between patches and thus to cause non-linearity in bacterial growth. The closer particles are to each other, the more likely it is for bacteria that have detached from a patch to reach another particle. Bacteria experience shorter phases of starvation, which may influence their recovery time to grow. [12] Moreover, biotic properties of the landscape such as the initial concentration of free-living cells are likely to have an influence on growth patterns as well. The more concentrated the bacteria are, the less likely it is that the population collapses because at least some individual bacteria will be able to encounter a particle and grow on it. [87] By changing those different biotic and abiotic conditions in a controlled manner, we aim to identify modifications in growth dynamics that could clarify trade-offs between foraging and growth on a patchy landscape. [189]

D.2 Experimental Design

D.2.1 Rationale

To study growth processes specific to a patchy landscape, we employ paramagnetic chitin particles as a simplified version of patches in the ocean. While particulate organic matter consists of multiple biopolymers [**?**], the particles used in this experiment are composed of only one substrate – chitin - which is the second most abundant biopolymer on Earth, namely chitin. [81] Chitin is insoluble and can be degraded to

smaller monomers of GlcNAc by chitinases. Micrometer-scaled chitin beads are incubated in artificial seawater, in which every nutrient (i.e. P, N, S, vitamins, trace minerals) is in excess and no other carbon sources are provided. In this way, the chitin beads serve as a discrete spatial distribution of nutrient patches. [34, 30] In this experimental system, not only is the resource landscape reduced in complexity to a single carbon source, but the microbial community is also approximated by a single clonal bacterial population. While the behavior of one particular strain does not represent the diversity of bacterial behaviors in nature, it identifies single-species growth mechanisms which could happen at a higher scale within a population. This reductionist approach is a starting point for the identification of ecological processes that balance growth and foraging in a bacterial population living on a patchy landscape.

D.2.2 Bacterial cultures

DsRed-labelled *Vibrio coralliilyticus* was streaked from a glycerol stock onto a Marine Broth (Difco 2216) plate with a 1.5% agar concentration supplemented with 50µg/µl kanamycin. After 72 hours of growth, a single colony was used to inoculate Marine Broth liquid medium supplemented with 40µg/µl kanamycin; incubations at room temperature lasted for 12 hours shaking at 200 rpm. Subsequently, the exponential phase culture was washed two times by gentle spinning and suspended in Tibbes-Rawling medium (recipe in [34]) supplemented with 20µg/µl kanamycin. Based on optical density (correlated with cell counts by flow cytometry), the cell concentration was diluted down to 104 CFU/µl. This culture, as well as a series of six, serial, four-fold dillutions of it, were then incubated with washed paramagnetic chitin beads - New England Biolabs (E8036L) - (pre-washed in Tibbes-Rawling medium) in a 96-well plate. Each cell concentration was incubated with each of three different concentrations of chitin particles (100, 50 or 10 beads per well) in a final well volume of 200 µl.

D.2.3 Imaging

Throughout 72-hour incubation of V. coralliilyticus cultures with chitin beads, the samples were imaged at 20X magnification was performed using the Evos FL Autoimaging System. Both phase-contrast and red fluorescence images were recorded every two hours. For each experimental condition, six to nine replicate particles were imaged. Each well of the plate was also scanned at 10X magnification in the Evos FL Autoimaging System at the end of incubation. The images were processed using Matlab. To detect the beads, the OTSU algorithm was used on the phase-contrast pictures. Only the largest bead in each well was considered for further investigation. We quantify both the amount of fluorescence on the bead and in the surrounding media.

D.3 Results

High-throughput time lapse imaging and image analysis was performed in order to track the dynamics of bacterial colonization on artificial chitin particles. On most of the tracked particles, the number of bacteria varies with time, whereas particle size remains constant (mean coefficient of variation < 0.01). Most of the outliers detected after image processing can mainly be explained by two phenomena. The collision of two particles, or of a particle with a crystal explains a detected steep increase in particle size while the movement of a particle outside the image frame corresponds to a detected decrease in size. These outliers are removed for subsequent analysis (Fig. D-2) by setting a threshold of variation to 0.1.

The footprint of bacterial colonization on particles, measured using a constitutively expressed fluorescent reporter, follows a distinctive pattern, surprisingly not monotonous (Fig. D-3). At an unsaturated initial concentration of bacteria (i.e. any concentration lower than the highest one - 104 CFU/µl), the density of bacteria on a particle first sharply increases until it reaches a peak (phase later referred to as first colonization wave). In some of the conditions reported later, we notice that this increase in fluorescence on the particle happens after a delay. The bacterial density

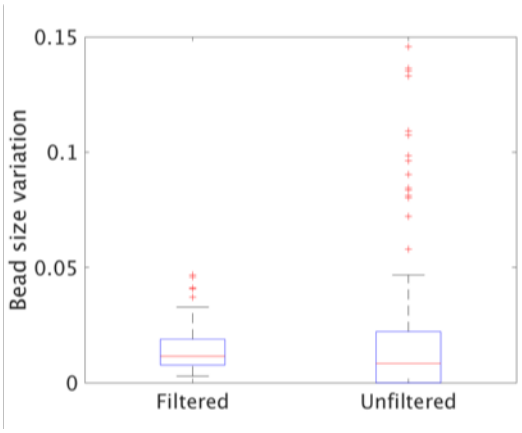

Figure D-2: Boxplot of the variation over time of the particle area (standard deviation normalized to the mean value over the time course of the experiment)

on a particle then drops down at a similar rate and, after some lag time, the bacterial density slowly increases again until it reaches a plateau. These dynamics are consistently found across particles being colonized at unsaturated initial concentration. When the inoculation concentration of bacteria is high (104 CFU/µl), the surface of the particle is already fully colonized when the time-lapse begins and therefore leading to an immediate drop in the bacterial density on the particle.

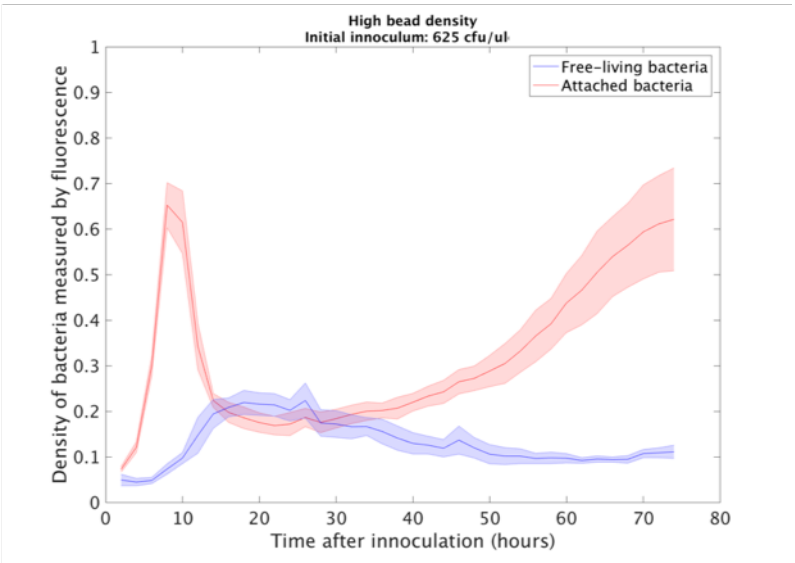

Figure D-3: Dynamics of attached and free-living bacterial density over 72 hours with the third highest bacterial inoculum and the highest particle density. It is aggregated data from 9 replicates, where the central line is the mean over those replicates and the gray area is the standard deviation.

Some properties of these colonization trajectories remain unchanged when initial conditions in bacterial and particle density vary. For example, the maximum density reached during the first colonization wave is not correlated with any of those conditions. However, this maximal colonization peak is inversely correlated with the size of the particle, as shown in Figure D-4. ($p < 10\text{-}10$) If this maximum density were linked to the attachment rate, one could have expected the exact opposite. This is because bacteria are more likely to collide with, and attach to, larger particles. Moreover, the intensity of this first colonization process is not correlated with the initial inoculum of bacteria (data not shown). This dramatic shift in growth could then be triggered by intrinsic changes in the population behavior or in the environment due to the metabolic activity of the cells.

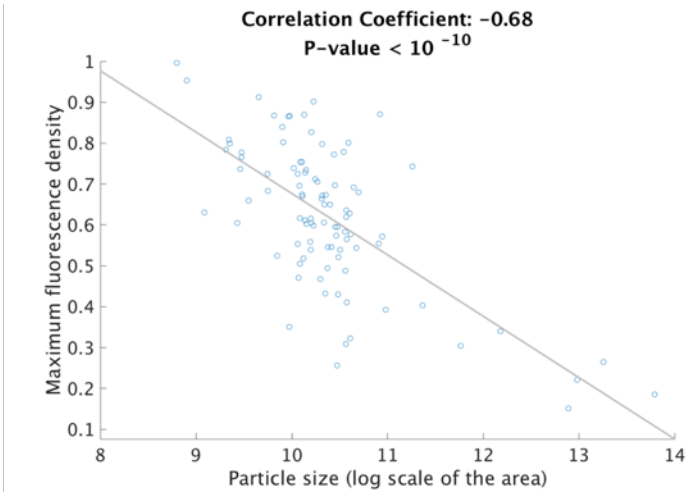

Figure D-4: Maximal bacterial peak density of the first colonization wave in function of the particle size. The size of the particle here is proportional to the square radius.

The initial amount of bacteria significantly influences the dynamics of colonization at early stages. The time needed for bacteria to reach their maximum density of bacteria on the particle during the first colonization is significantly correlated with the microbial inoculum ($p < 10\text{-}10$). Figure D-5 displays the observed trend, which confirms a result previously observed with other strains isolated from a natural community on chitin particles (unpublished data by Tim Enke).

The initial density of particles does not affect the dynamics of the first colonization wave, when the particle is colonized. However, it gains importance during the second

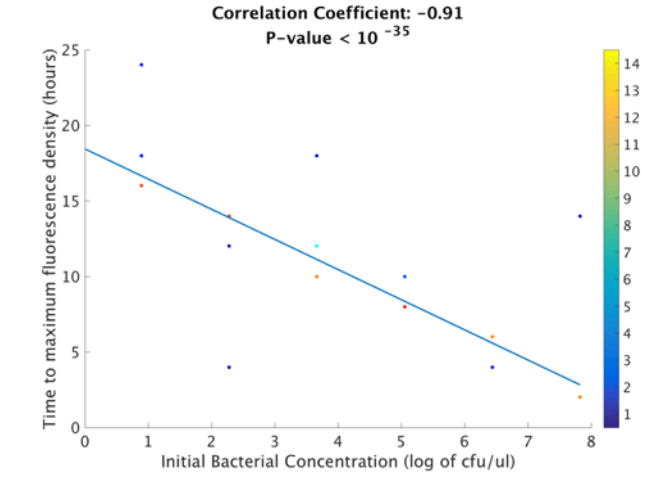

Figure D-5: Delay to reach the maximum bacterial density on particles given the initial bacterial concentration. Point colors represent the number of occurrences of a particular point in the data. The highest initial bacterial concentration has been excluded from this analysis, as the first colonization wave is not observable in the given time scale.

colonization wave. Figure D-6 depicts the dynamics of bacterial density on a particle when inoculated at the highest initial bacterial concentration. It seems relevant to consider this particular subset of initial inoculum, as it is the only occurrence where a stationary phase was reached at the end of the second colonization wave. This is explained by the faster dynamics when inoculated at a higher concentration. Under these conditions, there is a longer delay in recolonization of the particle when the density of beads is lower. It could be explained by a higher nutrient availability in the case of the highest particle density, which is corroborated by the fact that there are more free-living cells when particles are at higher densities. (data not shown)

Free-living cells also follow a non-intuitive pattern, as they do not exhibit a linear increase in bacterial density. Figure D-2 displays a typical trajectory of the free-living cells density. The density stays constant before increasing and reaching a maximum density, which remains stable before decreasing again. This behavior correlates with the behavior of attached cell density ($p=0.06$), as the increase in free-living bacteria happens at the same time point of the decrease in attached cell density. This trend between attached and free-living states suggests a massive detachment event. The difference in intensity between attached and free-living cell densities may be explained

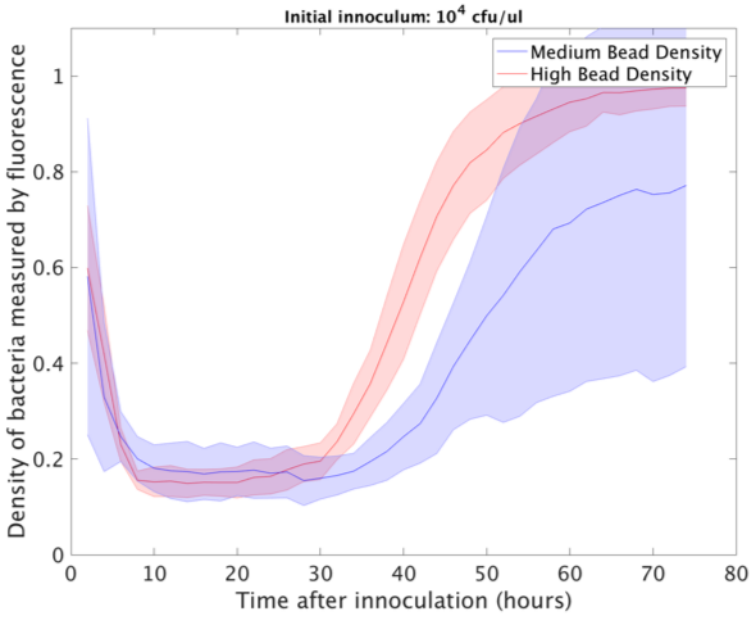

Figure D-6: Attached bacterial density over time in different particle concentrations for a saturated initial bacterial inoculum. The second particle colonization wave begins later when the particle concentration is smaller.

by the three-dimensional nature of the liquid media, in which cells can spread out of the focal plane.

It is worth noticing that some particles remain uncolonized. This failure mode to colonize happens more frequently at the lowest particle concentration (of the order of magnitude of 10 particles per well). In these experiments, at the lowest particle concentration, 15% of the 20 observed particles were not colonized, whereas at the intermediate particle concentration only 4% of the 46 particles failed to show growth. Finally, there is no occurrence of colonization failure at the highest particle concentration. Particle concentration may play a crucial role in the growth dynamics of a microbial community.

D.4 Discussion

Bacterial growth on a patchy landscape can be non-monotonous at a patch level, i.e. that colonization of a patch follows two phases. Two waves of colonization can

be identified on each colonized particle: the first wave of colonization on a particle depends on the initial bacterial concentration, while the second phase of colonization is linked to the density of particles. The data set collected during these experiments casts light on unexpected growth patterns potentially due to the coexistence of two environments and fluxes of bacteria between these two environmental conditions. However, these experiments present some shortcomings.

The total duration of the study was too short to fully observe the second wave of particle colonization under all the different experimental conditions. Furthermore, replicates show evidence of more variation towards the end of the incubation than at its beginning (Fig. D-3 and D-6). On average, the standard deviation of the bacterial density on a patch is more than 20-fold higher at the end of the observation than at the inoculation under the same conditions. Since growth variation is more important at the end of the observation, it suggests that replicates take different paths hinting towards some variability in the experimental set-up. This difference within the *a priori* same initial conditions could be explained by the lack of control over the spatial layout of particles within each well. While the concentration of particles is known at the scale of a well, the local density of particles could be widely different, as paramagnetic particles tend to aggregate. Using the scan of each well, each replicate could be associated with the distance to its nearest neighboring particle. Adding this level of information could explain the variation between replicates.

From an experimental design standpoint, it then becomes important to precisely pre-determine the spatial layout of patches. Such spatial constraints can be imposed by using microfluidic devices with traps. In this case, a trap (a hole of the size of a particle) immobilizes a chitin particle at a fixed spot. [82] Designing multiple microfluidic chips with predetermined local and global densities of particles would be an asset to evaluate the effect of the spatial layout of particles onto growth processes at a landscape scale. The precision of such an approach can help refine how properties of a patchy landscape, such as the distance to the nearest patch or the number of patches within a certain distance, influence growth dynamics. These two landscape properties illustrate the trade-off between growth, which can be linked to the density of nutrients,

hence the number of reachable patches, and dispersal that can be correlated with the need to reach at least one patch to persist, thus the distance to the nearest neighbor. Since this study presents some evidence of the influence of the layout of the particle landscape on bacterial growth dynamics, developing a more controlled device for spatial structure is one direction to be explored more deeply.

During the first wave of particle colonization, the density of particles and thus the spatial layout of those particles don't influence the growth dynamics. Nevertheless, this first phase of colonization still connects what happens on the particle with the surrounding liquid environment, as a massive an abrupt detachment event occurs. This phenomenon is surprising because it implies that growth on a particle is not purely exponential, as expected when resources are in abundance. Since the maximal bacterial density of this first colonization phase does not depend on the initial bacterial concentration but on the particle size, this decrease in bacterial density could be triggered by bacterial metabolism associated to growth on chitin. It is known that some by-products of chitin degradation, such as GlcNAc, provoke detachment. [191] Therefore, the increase of GlcNAc concentration around the particle could lead to a massive detachment event. To test this hypothesis, during at early stages of the incubation, GlcNAc could be added at different time points of the experiment in various concentrations. After the GlcNAc boost, observations could unravel if a threshold of GlcNAc needs to be reached in order to provoke detachment. Another hypothesis is that, as cells are more packed on the surface of the particle, they could run out of other nutrients abundant in seawater, such as oxygen, but unable to diffuse through the bacterial population. [58]

In conclusion, the colonization dynamics of a particle in a patchy landscape are complex, even when colonized by a single clonal bacterial population. It is a non-linear process which involves both growth and dispersal. This study is a first step towards a better understanding of possible trade-offs emerging between the attached and free-living bacterial states.

Bibliography

[1] Rami Abi-Akl, Elise Ledieu, Tim N Enke, Otto X Cordero, and Tal Cohen. Physics-based prediction of biopolymer degradation. *Soft Matter*, 15(20):4098–4108, 2019.

[2] Julius Adler. A method for measuring chemotaxis and use of the method to determine optimum conditions for chemotaxis by escherichia coli. *Microbiology*, 74(1):77–91, 1973.

[3] Julius Adler and Bonnie Templeton. The effect of environmental conditions on the motility of escherichia coli. *Microbiology*, 46(2):175–184, 1967.

[4] Tanvir Ahmed, Thomas S Shimizu, and Roman Stocker. Microfluidics for bacterial chemotaxis. *Integrative biology*, 2(11-12):604–629, 2010.

[5] Uria Alcolombri, François J Peaudecerf, Vicente I Fernandez, Lars Behrendt, Kang Soo Lee, and Roman Stocker. Sinking enhances the degradation of organic particles by marine bacteria. *Nature Geoscience*, 14(10):775–780, 2021.

[6] DB Allan, T Caswell, NC Keim, Casper M van der Wel, and RW Verweij. soft-matter/trackpy: Trackpy v0. 5.0. *Genève: Zenodo*, 2021.

[7] Alice L Alldredge and Mary W Silver. Characteristics, dynamics and significance of marine snow. *Progress in oceanography*, 20(1):41–82, 1988.

[8] M Ardré, G Doulcier, N Brenner, and PB Rainey. Exit from lag phase in populations of pseudomonas fluorescens is determined by strong interactions among cells. 2022.

[9] Carol Arnosti. Microbial extracellular enzymes and the marine carbon cycle. *Annual review of marine science*, 3:401–425, 2011.

[10] F Azam and DC Smith. Bacterial influence on the variability in the ocean's biogeochemical state: a mechanistic view. In *Particle analysis in oceanography*, pages 213–236. Springer, 1991.

[11] Farooq Azam. Microbial control of oceanic carbon flux: the plot thickens. *Science*, 280(5364):694–696, 1998.

[12] RONALD M Baker, FL Singleton, and MA Hood. Effects of nutrient deprivation on vibrio cholerae. *Applied and Environmental Microbiology*, 46(4):930–940, 1983.

[13] Catherine Bannon, Insa Rapp, and Erin M Bertrand. Community interaction co-limitation: Nutrient limitation in a marine microbial community context. *Frontiers in Microbiology*, 13:Art–Nr, 2022.

[14] Luis M Bautista, Joost Tinbergen, and Alejandro Kacelnik. To walk or to fly? how birds choose among foraging modes. *Proceedings of the National Academy of Sciences*, 98(3):1089–1094, 2001.

[15] Yael Ben-Haim, FL Thompson, CC Thompson, MC Cnockaert, Bart Hoste, Jean Swings, and E Rosenberg. Vibrio coralliilyticus sp. nov., a temperature-dependent pathogen of the coral pocillopora damicornis. *International journal of systematic and evolutionary microbiology*, 53(1):309–315, 2003.

[16] HC Berg. Random walks in biology, expanded edition, princeton u, 1993.

[17] Howard C Berg and Edward M Purcell. Physics of chemoreception. *Biophysical journal*, 20(2):193–219, 1977.

[18] Nicholas Blackburn and Tom Fenchel. Influence of bacteria, diffusion and shear on micro-scale nutrient patches, and implications for bacterial chemotaxis. *Marine Ecology Progress Series*, 189:1–7, 1999.

[19] PG Blackwell. Random diffusion models for animal movement. *Ecological Modelling*, 100(1-3):87–102, 1997.

[20] Alexander B Bochdansky and Gerhard J Herndl. Ecology of amorphous aggregations (marine snow) in the northern adriatic sea. v. role of fecal pellets in marine snow. *Marine Ecology-Progress Series*, 89:297–297, 1992.

[21] Pierre Bovet and Simon Benhamou. Spatial analysis of animals' movements using a correlated random walk model. *Journal of theoretical biology*, 131(4):419–433, 1988.

[22] Gary Bradski and Adrian Kaehler. Opencv. *Dr. Dobb's journal of software tools*, 3:120, 2000.

[23] Douglas R Brumley, Francesco Carrara, Andrew M Hein, Yutaka Yawata, Simon A Levin, and Roman Stocker. Bacteria push the limits of chemotactic precision to navigate dynamic chemical gradients. *Proceedings of the National Academy of Sciences*, 116(22):10792–10797, 2019.

[24] Yannick Buijs, Sheng-Da Zhang, Karen Marie Jørgensen, Thomas Isbrandt, Thomas Ostenfeld Larsen, and Lone Gram. Enhancement of antibiotic production by co-cultivation of two antibiotic producing marine vibrionaceae strains. *FEMS Microbiology Ecology*, 97(4):fiab041, 2021.

[25] Tim Bushnell. What is flow cytometry light scatter and how cell size and particle size affects it, Mar 2021.

[26] Nathan Cermak, Jamie W Becker, Scott M Knudsen, Sallie W Chisholm, Scott R Manalis, and Martin F Polz. Direct single-cell biomass estimates for marine bacteria via archimedes' principle. *The ISME journal*, 11(3):825–828, 2017.

[27] Chih-Ching Chien, Chang-Chieh Chen, Meng-Hui Choi, Shieh-Shiuh Kung, and Yu-Hong Wei. Production of poly-β-hydroxybutyrate (phb) by vibrio spp. isolated from marine environment. *Journal of Biotechnology*, 132(3):259–263, 2007.

[28] Byung C Cho and Farooq Azam. Major role of bacteria in biogeochemical fluxes in the ocean's interior. *Nature*, 332(6163):441–443, 1988.

[29] Natalie R Cohen, Matthew R McIlvin, Dawn M Moran, Noelle A Held, Jaclyn K Saunders, Nicholas J Hawco, Michael Brosnahan, Giacomo R DiTullio, Carl Lamborg, John P McCrow, et al. Dinoflagellates alter their carbon and nutrient metabolic strategies across environmental gradients in the central pacific ocean. *Nature Microbiology*, 6(2):173–186, 2021.

[30] Otto X Cordero and Roman Stocker. A particularly useful system to study the ecology of microbes. *Environmental microbiology reports*, 9(1):16–17, 2017.

[31] Wallace H Coulter. Means for counting particles suspended in a fluid, October 20 1953. US Patent 2,656,508.

[32] John C Crocker and David G Grier. Methods of digital video microscopy for colloidal studies. *Journal of colloid and interface science*, 179(1):298–310, 1996.

[33] Xiongfeng Dai, Manlu Zhu, Mya Warren, Rohan Balakrishnan, Vadim Patsalo, Hiroyuki Okano, James R Williamson, Kurt Fredrick, Yi-Ping Wang, and Terence Hwa. Reduction of translating ribosomes enables escherichia coli to maintain elongation rates during slow growth. *Nature microbiology*, 2(2):1–9, 2016.

[34] Manoshi S Datta, Elzbieta Sliwerska, Jeff Gore, Martin F Polz, and Otto X Cordero. Microbial interactions lead to rapid micro-scale successions on model marine particles. *Nature communications*, 7(1):1–7, 2016.

[35] Manoshi Sen Datta. *Microbial community structure and dynamics on patchy landscapes*. PhD thesis, Massachusetts Institute of Technology, 2016.

[36] M Patricia Dawson, Beverley A Humphrey, and Kevin C Marshall. Adhesion: a tactic in the survival strategy of a marine vibrio during starvation. *Current Microbiology*, 6(4):195–199, 1981.

[37] Paul A Del Giorgio and Jonathan J Cole. Bacterial growth efficiency in natural aquatic systems. *Annual Review of Ecology and Systematics*, pages 503–541, 1998.

[38] Edward F DeLong, Diana G Franks, and Alice L Alldredge. Phylogenetic diversity of aggregate-attached vs. free-living marine bacterial assemblages. *Limnology and oceanography*, 38(5):924–934, 1993.

[39] John E Dore, Roger Lukas, Daniel W Sadler, Matthew J Church, and David M Karl. Physical and biogeochemical modulation of ocean acidification in the central north pacific. *Proceedings of the National Academy of Sciences*, 106(30):12235–12240, 2009.

[40] Knut Drescher, Carey D Nadell, Howard A Stone, Ned S Wingreen, and Bonnie L Bassler. Solutions to the public goods dilemma in bacterial biofilms. *Current Biology*, 24(1):50–55, 2014.

[41] Glen G D'Souza, Vanessa R Povolo, Johannes M Keegstra, Roman Stocker, and Martin Ackermann. Nutrient complexity triggers transitions between solitary and colonial growth in bacterial populations. *The ISME journal*, 15(9):2614–2626, 2021.

[42] Ali Ebrahimi, Akshit Goyal, and Otto X Cordero. Particle foraging strategies promote microbial diversity in marine environments. *Elife*, 11:e73948, 2022.

[43] Ali Ebrahimi, Julia Schwartzman, and Otto X Cordero. Cooperation and spatial self-organization determine rate and efficiency of particulate organic matter degradation in marine bacteria. *Proceedings of the National Academy of Sciences*, 116(46):23309–23316, 2019.

[44] Tim N Enke, Manoshi S Datta, Julia Schwartzman, Nathan Cermak, Désirée Schmitz, Julien Barrere, Alberto Pascual-García, and Otto X Cordero. Modular assembly of polysaccharide-degrading marine microbial communities. *Current Biology*, 29(9):1528–1535, 2019.

[45] Tim N Enke, Gabriel E Leventhal, Matthew Metzger, José T Saavedra, and Otto X Cordero. Microscale ecology regulates particulate organic matter turnover in model marine microbial communities. *Nature communications*, 9(1):1–8, 2018.

[46] Tom Fenchel. Motility and chemosensory behaviour of the sulphur bacterium thiovulum majus. *Microbiology*, 140(11):3109–3116, 1994.

[47] Tom Fenchel. Microbial behavior in a heterogeneous world. *Science*, 296(5570):1068–1071, 2002.

[48] Tom Fenchel. The microbial loop–25 years later. *Journal of Experimental Marine Biology and Ecology*, 366(1-2):99–103, 2008.

[49] Vicente I Fernandez, Yutaka Yawata, and Roman Stocker. A foraging mandala for aquatic microorganisms. *The ISME Journal*, 13(3):563–575, 2019.

[50] Kristina M Fontanez, John M Eppley, Ty J Samo, David M Karl, and Edward F DeLong. Microbial community structure and function on sinking particles in the north pacific subtropical gyre. *Frontiers in microbiology*, 6:469, 2015.

[51] FERRAN Garcia-Pichel. Rapid bacterial swimming measured in swarming cells of thiovulum majus. *Journal of Bacteriology*, 171(6):3560–3563, 1989.

[52] Ana Gasperotti, Sophie Brameyer, Florian Fabiani, and Kirsten Jung. Phenotypic heterogeneity of microbial populations under nutrient limitation. *Current opinion in biotechnology*, 62:160–167, 2020.

[53] Sonia Giubergia, Christopher Phippen, Kristian Fog Nielsen, and Lone Gram. Growth on chitin impacts the transcriptome and metabolite profiles of antibiotic-producing vibrio coralliilyticus s2052 and photobacterium galatheae s2753. *Msystems*, 2(1):e00141–16, 2017.

[54] Michel Godin, Andrea K Bryan, Thomas P Burg, Ken Babcock, and Scott R Manalis. Measuring the mass, density, and size of particles and cells using a suspended microchannel resonator. *Applied physics letters*, 91(12):123121, 2007.

[55] Casey M Godwin and James B Cotner. Aquatic heterotrophic bacteria have highly flexible phosphorus content and biomass stoichiometry. *The ISME Journal*, 9(10):2324–2327, 2015.

[56] Declan A Gray, Gaurav Dugar, Pamela Gamba, Henrik Strahl, Martijs J Jonker, and Leendert W Hamoen. Extreme slow growth as alternative strategy to survive deep starvation in bacteria. *Nature communications*, 10(1):1–12, 2019.

[57] Ard Jan Grimbergen, Jeroen Siebring, Ana Solopova, and Oscar P Kuipers. Microbial bet-hedging: the power of being different. *Current opinion in microbiology*, 25:67–72, 2015.

[58] Hans-Peter Grossart, Thomas Kiørboe, Kam Tang, and Helle Ploug. Bacterial colonization of particles: growth and interactions. *Applied and Environmental Microbiology*, 69(6):3500–3509, 2003.

[59] HP Grossart, Thomas Kiørboe, KW Tang, M Allgaier, EM Yam, and Helle Ploug. Interactions between marine snow and heterotrophic bacteria: aggregate formation and microbial dynamics. *Aquatic microbial ecology*, 42(1):19–26, 2006.

[60] Sebastian Gude, Erçağ Pinçe, Katja M Taute, Anne-Bart Seinen, Thomas S Shimizu, and Sander J Tans. Bacterial coexistence driven by motility and spatial competition. *Nature*, 578(7796):588–592, 2020.

[61] Lionel Guidi, Samuel Chaffron, Lucie Bittner, Damien Eveillard, Abdelhalim Larhlimi, Simon Roux, Youssef Darzi, Stéphane Audic, Léo Berline, Jennifer R Brum, et al. Plankton networks driving carbon export in the oligotrophic ocean. *Nature*, 532(7600):465–470, 2016.

[62] Lionel Guidi, Lars Stemmann, George A Jackson, Frédéric Ibanez, Hervé Claustre, Louis Legendre, Marc Picheral, and Gabriel Gorskya. Effects of phytoplankton community on production, size, and export of large aggregates: A world-ocean analysis. *Limnology and Oceanography*, 54(6):1951–1963, 2009.

[63] Florian Hahne, Nolwenn LeMeur, Ryan R Brinkman, Byron Ellis, Perry Haaland, Deepayan Sarkar, Josef Spidlen, Errol Strain, and Robert Gentleman. flowcore: a bioconductor package for high throughput flow cytometry. *BMC bioinformatics*, 10(1):1–8, 2009.

[64] D Hammill. Cytoexplorer: interactive analysis of cytometry data. *R package version*, 1(8), 2020.

[65] Leigh K Harris and Julie A Theriot. Relative rates of surface and volume synthesis set bacterial cell size. *Cell*, 165(6):1479–1492, 2016.

[66] Noelle A Held, Matthew R McIlvin, Dawn M Moran, Michael T Laub, and Mak A Saito. Unique patterns and biogeochemical relevance of two-component sensing in marine bacteria. *MSystems*, 4(1):e00317–18, 2019.

[67] Louise Holmquist and Staffan Kjelleberg. Changes in viability, respiratory activity and morphology of the marine vibrio sp. strain s14 during starvation of individual nutrients and subsequent recovery. *FEMS microbiology ecology*, 12(4):215–223, 1993.

[68] Sung-Ha Hong, Jean-Baptiste Gorce, Horst Punzmann, Nicolas Francois, Michael Shats, and Hua Xia. Surface waves control bacterial attachment and formation of biofilms in thin layers. *Science advances*, 6(22):eaaz9386, 2020.

[69] MA Hood and PA Winter. Attachment of vibrio cholerae under various environmental conditions and to selected substrates. *FEMS microbiology ecology*, 22(3):215–223, 1997.

[70] Hans-Georg Hoppe, Carol Arnosti, and GJ Herndl. Ecological significance of bacterial enzymes in the marine environment. *Enzymes in the environment: activity, ecology, and applications*, pages 73–107, 2002.

[71] Dana E Hunt, Dirk Gevers, Nisha M Vahora, and Martin F Polz. Conservation of the chitin utilization pathway in the vibrionaceae. *Applied and environmental microbiology*, 74(1):44–51, 2008.

[72] Juan Iriberri, Marian Unanue, Isabel Barcina, and Luis Egea. Seasonal variation in population density and heterotrophic activity of attached and free-living bacteria in coastal waters. *Applied and Environmental Microbiology*, 53(10):2308–2314, 1987.

[73] Garth A James, DR Korber, DE Caldwell, and J William Costerton. Digital image analysis of growth and starvation responses of a surface-colonizing acinetobacter sp. *Journal of bacteriology*, 177(4):907–915, 1995.

[74] Christopher W Jones and Judith P Armitage. Positioning of bacterial chemoreceptors. *Trends in microbiology*, 23(5):247–256, 2015.

[75] Markéta Julinová, Jan Kupec, Josef Houser, Roman Slavík, Hana Marušincová, Lenka Červeňáková, and Stanislav Klívar. Removal of polyvinylpyrrolidone from wastewater using different methods. *Water environment research*, 84(12):2123–2132, 2012.

[76] Christian E Junge. Air: Chemistry and radioactivity. *Int Geophys. Ser*, 1963.

[77] Yevgeniy Kalinin, Silke Neumann, Victor Sourjik, and Mingming Wu. Responses of escherichia coli bacteria to two opposing chemoattractant gradients depend on the chemoreceptor ratio. *Journal of bacteriology*, 192(7):1796–1800, 2010.

[78] Markus Karner and Gerhard J Herndl. Extracellular enzymatic activity and secondary production in free-living and marine-snow-associated bacteria. *Marine biology*, 113(2):341–347, 1992.

[79] Johannes M Keegstra, Francesco Carrara, and Roman Stocker. The ecological roles of bacterial chemotaxis. *Nature Reviews Microbiology*, pages 1–14, 2022.

[80] Nathan Keyfitz and Hal Caswell. Markov chains for individual life histories. *Applied Mathematical Demography*, pages 245–267, 2005.

[81] Nemat O Keyhani and Saul Roseman. Physiological aspects of chitin catabolism in marine bacteria. *Biochimica et Biophysica Acta (BBA)-General Subjects*, 1473(1):108–122, 1999.

[82] Jae Jung Kim, Ki Wan Bong, Eduardo Reátegui, Daniel Irimia, and Patrick S Doyle. Porous microwells for geometry-selective, large-scale microparticle arrays. *Nature materials*, 16(1):139–146, 2017.

[83] Yeong-Chul Kim. Diffusivity of bacteria. *Korean Journal of Chemical Engineering*, 13(3):282–287, 1996.

[84] Nikole E Kimes, Christopher J Grim, Wesley R Johnson, Nur A Hasan, Ben D Tall, Mahendra H Kothary, Hajnalka Kiss, A Christine Munk, Roxanne Tapia, Lance Green, et al. Temperature regulation of virulence factors in the pathogen vibrio coralliilyticus. *The ISME journal*, 6(4):835–846, 2012.

[85] Thomas Kiørboe. Formation and fate of marine snow: small-scale processes with large-scale implications. *Scientia marina*, 65(S2):57–71, 2001.

[86] Thomas Kiørboe. A mechanistic approach to plankton ecology. *ASLO Web Lectures*, 1(2):1–91, 2009.

[87] Thomas Kiørboe, Hans-Peter Grossart, Helle Ploug, and Kam Tang. Mechanisms and rates of bacterial colonization of sinking aggregates. *Applied and Environmental Microbiology*, 68(8):3996–4006, 2002.

[88] Thomas Kiørboe and George A Jackson. Marine snow, organic solute plumes, and optimal chemosensory behavior of bacteria. *Limnology and Oceanography*, 46(6):1309–1318, 2001.

[89] Thomas Kiørboe, Kam Tang, Hans-Peter Grossart, and Helle Ploug. Dynamics of microbial communities on marine snow aggregates: colonization, growth, detachment, and grazing mortality of attached bacteria. *Applied and Environmental Microbiology*, 69(6):3036–3047, 2003.

[90] Thomas J Kirn, Brooke A Jude, and Ronald K Taylor. A colonization factor links vibrio cholerae environmental survival and human infection. *Nature*, 438(7069):863–866, 2005.

[91] Staffan Kjelleberg, Nan Albertson, Klas Flärdh, Louise Holmquist, Åsa Jouper-Jaan, Rita Marouga, Jörgen Östling, Björn Svenblad, and Dieter Weichart. How do non-differentiating bacteria adapt to starvation? *Antonie Van Leeuwenhoek*, 63(3):333–341, 1993.

[92] Staffan Kjelleberg and Malte Hermansson. Starvation-induced effects on bacterial surface characteristics. *Applied and Environmental Microbiology*, 48(3):497–503, 1984.

[93] Arthur L Koch, Betsy R Robertson, and Don K Button. Deduction of the cell volume and mass from forward scatter intensity of bacteria analyzed by flow cytometry. *Journal of microbiological methods*, 27(1):49–61, 1996.

[94] Seiji Kojima, Koichiro Yamamoto, Ikuro Kawagishi, and Michio Homma. The polar flagellar motor of vibrio cholerae is driven by an na+ motive force. *Journal of bacteriology*, 181(6):1927–1930, 1999.

[95] TS Kostadinov, DA Siegel, and S Maritorena. Retrieval of the particle size distribution from satellite ocean color observations. *Journal of Geophysical Research: Oceans*, 114(C9), 2009.

[96] TS Kostadinov, DA Siegel, and S Maritorena. Global variability of phytoplankton functional types from space: assessment via the particle size distribution. *Biogeosciences*, 7(10):3239–3257, 2010.

[97] Kento Koyama, Hidekazu Hokunan, Mayumi Hasegawa, Shuso Kawamura, and Shigenobu Koseki. Modeling stochastic variability in the numbers of surviving salmonella enterica, enterohemorrhagic escherichia coli, and listeria monocytogenes cells at the single-cell level in a desiccated environment. *Applied and Environmental Microbiology*, 83(4):e02974–16, 2017.

[98] Bennett S Lambert, Vicente I Fernandez, and Roman Stocker. Motility drives bacterial encounter with particles responsible for carbon export throughout the ocean. *Limnology and Oceanography Letters*, 4(5):113–118, 2019.

[99] Alyse A Larkin, Catherine A Garcia, Nathan Garcia, Melissa L Brock, Jenna A Lee, Lucas J Ustick, Leticia Barbero, Brendan R Carter, Rolf E Sonnerup, Lynne D Talley, et al. High spatial resolution global ocean metagenomes from bio-go-ship repeat hydrography transects. *Scientific data*, 8(1):1–6, 2021.

[100] Marianne H Larsen, Nicholas Blackburn, Jens L Larsen, and John E Olsen. Influences of temperature, salinity and starvation on the motility and chemotactic response of vibrio anguillarum. *Microbiology*, 150(5):1283–1290, 2004.

[101] Jay T Lennon and Stuart E Jones. Microbial seed banks: the ecological and evolutionary implications of dormancy. *Nature reviews microbiology*, 9(2):119–130, 2011.

[102] Sydney Levitus. Sea level changes results from the ipcc 2007 report and subsequent results. In *Sea Level Rise and Coastal Infrastructure: Prediction, Risks, and Solution*, pages 20–27. ASCE, 2012.

[103] Bruce E Logan, Uta Passow, Alice L Alldredge, Hans-Peter Grossartt, and Meinhard Simont. Rapid formation and sedimentation of large aggregates is predictable from coagulation rates (half-lives) of transparent exopolymer particles (tep). *Deep Sea Research Part II: Topical Studies in Oceanography*, 42(1):203–214, 1995.

[104] Richard A Long, David C Rowley, Eric Zamora, Jiayuan Liu, Douglas H Bartlett, and Farooq Azam. Antagonistic interactions among marine bacteria impede the proliferation of vibrio cholerae. *Applied and Environmental Microbiology*, 71(12):8531–8536, 2005.

[105] Karin Malmcrona-Friberg, Amanda Goodman, and Staffan Kjelleberg. Chemotactic responses of marine vibrio sp. strain s14 (ccug 15956) to low-molecular-weight substances under starvation and recovery conditions. *Applied and Environmental Microbiology*, 56(12):3699–3704, 1990.

[106] Anders Mårell, John P Ball, and Annika Hofgaard. Foraging and movement paths of female reindeer: insights from fractal analysis, correlated random walks, and lévy flights. *Canadian Journal of Zoology*, 80(5):854–865, 2002.

[107] Linda L McCarter. Dual flagellar systems enable motility under different circumstances. *Microbial Physiology*, 7(1-2):18–29, 2004.

[108] Dalit Meron, Rotem Efrony, Wesley R Johnson, Amy L Schaefer, Pamela J Morris, Eugene Rosenberg, E Peter Greenberg, and Ehud Banin. Role of flagella in virulence of the coral pathogen vibrio coralliilyticus. *Applied and environmental microbiology*, 75(17):5704–5707, 2009.

[109] Mireia Mestre and Juan Höfer. The microbial conveyor belt: connecting the globe through dispersion and dormancy. *Trends in Microbiology*, 29(6):482–492, 2021.

[110] Gail Lorenz Miller. Use of dinitrosalicylic acid reagent for determination of reducing sugar. *Analytical chemistry*, 31(3):426–428, 1959.

[111] RONALD W Mink and RB Hespell. Long-term nutrient starvation of continuously cultured (glucose-limited) selenomonas ruminantium. *Journal of Bacteriology*, 148(2):541–550, 1981.

[112] James G Mitchell. The influence of cell size on marine bacterial motility and energetics. *Microbial ecology*, 22(1):227–238, 1991.

[113] James G Mitchell, Lynette Pearson, Simon Dillon, and Katerina Kantalis. Natural assemblages of marine bacteria exhibiting high-speed motility and large accelerations. *Applied and environmental microbiology*, 61(12):4436–4440, 1995.

[114] Michael T Montgomery and David L Kirchman. Role of chitin-binding proteins in the specific attachment of the marine bacterium vibrio harveyi to chitin. *Applied and environmental microbiology*, 59(2):373–379, 1993.

[115] CM Moore, MM Mills, KR Arrigo, I Berman-Frank, L Bopp, PW Boyd, ED Galbraith, RJ Geider, C Guieu, SL Jaccard, et al. Processes and patterns of oceanic nutrient limitation. *Nature geoscience*, 6(9):701–710, 2013.

[116] Luiza P Morawska, Jhonatan A Hernandez-Valdes, and Oscar P Kuipers. Diversity of bet-hedging strategies in microbial communities—recent cases and insights. *WIREs Mechanisms of Disease*, 14(2):e1544, 2022.

[117] Bernard Moussian. Chitin: structure, chemistry and biology. *Targeting chitin-containing organisms*, pages 5–18, 2019.

[118] Robert F Mueller. Bacterial transport and colonization in low nutrient environments. *Water Research*, 30(11):2681–2690, 1996.

[119] Tim Müller, Britta Walter, Astrid Wirtz, and Andreas Burkovski. Ammonium toxicity in bacteria. *Current microbiology*, 52(5):400–406, 2006.

[120] Trang TH Nguyen, Emily J Zakem, Ali Ebrahimi, Julia Schwartzman, Tolga Caglar, Kapil Amarnath, Uria Alcolombri, François J Peaudecerf, Terence Hwa, Roman Stocker, et al. Microbes contribute to setting the ocean carbon flux by altering the fate of sinking particulates. *Nature communications*, 13(1):1–9, 2022.

[121] Bin Ni, Remy Colin, Hannes Link, Robert G Endres, and Victor Sourjik. Growth-rate dependent resource investment in bacterial motile behavior quantitatively follows potential benefit of chemotaxis. *Proceedings of the National Academy of Sciences*, 117(1):595–601, 2020.

[122] Toshiyuki Nikata, Ken Sumida, Junichi Kato, and Hisao Ohtake. Rapid method for analyzing bacterial behavioral responses to chemical stimuli. *Applied and Environmental Microbiology*, 58(7):2250–2254, 1992.

[123] Noele Norris, Uria Alcolombri, Johannes M Keegstra, Yutaka Yawata, Filippo Menolascina, Emilio Frazzoli, Naomi M Levine, Vicente I Fernandez, and Roman Stocker. Bacterial chemotaxis to saccharides is governed by a trade-off between sensing and uptake. *Biophysical Journal*, 121(11):2046–2059, 2022.

[124] James A Novitsky and Richard Y Morita. Survival of a psychrophilic marine vibrio under long-term nutrient starvation. *Applied and Environmental Microbiology*, 33(3):635–641, 1977.

[125] T Nyström, RM Olsson, and STAFFAN Kjelleberg. Survival, stress resistance, and alterations in protein expression in the marine vibrio sp. strain s14 during starvation for different individual nutrients. *Applied and Environmental microbiology*, 58(1):55–65, 1992.

[126] Thomas Nyström, Nan H Albertson, Klas Flärdh, and Staffan Kjeileberg. Physiological and molecular adaptation to starvation and recovery from starvation by the marine vibrio sp. s14. *FEMS Microbiology Letters*, 74(2-3):129–140, 1990.

[127] Thomas Nyström, Klas Flärdh, and Staffan Kjelleberg. Responses to multiple-nutrient starvation in marine vibrio sp. strain ccug 15956. *Journal of bacteriology*, 172(12):7085–7097, 1990.

[128] Nikola Ojkic, Diana Serbanescu, and Shiladitya Banerjee. Surface-to-volume scaling and aspect ratio preservation in rod-shaped bacteria. *Elife*, 8:e47033, 2019.

[129] Jörgen Östling, Louise Holmquist, Klas Flärdh, Björn Svenblad, Åsa Jouper-Jaan, and Staffan Kjelleberg. Starvation and recovery of vibrio. In *Starvation in bacteria*, pages 103–127. Springer, 1993.

[130] M Paoluzzi, R Di Leonardo, and L Angelani. Effective run-and-tumble dynamics of bacteria baths. *Journal of Physics: Condensed Matter*, 25(41):415102, 2013.

[131] Kevin M Passino. Bacterial foraging optimization. *International Journal of Swarm Intelligence Research (IJSIR)*, 1(1):1–16, 2010.

[132] Olga E Petrova and Karin Sauer. Sticky situations: key components that control bacterial surface attachment. *Journal of bacteriology*, 194(10):2413–2425, 2012.

[133] Andy Phaiboun, Yiming Zhang, Boryung Park, and Minsu Kim. Survival kinetics of starving bacteria is biphasic and density-dependent. *PLoS computational biology*, 11(4):e1004198, 2015.

[134] Cynthia H Pilskaln, TA Villareal, M Dennett, C Darkangelo-Wood, and G Meadows. High concentrations of marine snow and diatom algal mats in the north pacific subtropical gyre: Implications for carbon and nitrogen cycles in the oligotrophic ocean. *Deep Sea Research Part I: Oceanographic Research Papers*, 52(12):2315–2332, 2005.

[135] P Pletnev, I Osterman, P Sergiev, A Bogdanov, and O Dontsova. Survival guide: Escherichia coli in the stationary phase. *Acta Naturae ( )*, 7(4 (27)):22–33, 2015.

[136] Helle Ploug, Hans-Peter Grossart, Farooq Azam, and Bo Barker Jørgensen. Photosynthesis, respiration, and carbon turnover in sinking marine snow from surface waters of southern california bight: implications for the carbon cycle in the ocean. *Marine Ecology Progress Series*, 179:1–11, 1999.

[137] Shaul Pollak, Matti Gralka, Yuya Sato, Julia Schwartzman, Lu Lu, and Otto X Cordero. Public good exploitation in natural bacterioplankton communities. *Science Advances*, 7(31):eabi4717.

[138] Carla Pruzzo, Alessandra Crippa, Stefania Bertone, Luigi Pane, and Annamaria Carli. Attachment of vibrio alginolyticus to chitin mediated by chitin-binding proteins. *Microbiology*, 142(8):2181–2186, 1996.

[139] Carla Pruzzo, Renato Tarsi, Maria Del Mar Lleò, Caterina Signoretto, Massimiliano Zampini, Luigi Pane, Rita R Colwell, and Pietro Canepari. Persistence of adhesive properties in vibrio cholerae after long-term exposure to sea water. *Environmental Microbiology*, 5(10):850–858, 2003.

[140] Edward M Purcell. Life at low reynolds number. *American journal of physics*, 45(1):3–11, 1977.

[141] Graham H Pyke, H Ronald Pulliam, and Eric L Charnov. Optimal foraging: a selective review of theory and tests. *The quarterly review of biology*, 52(2):137–154, 1977.

[142] Eugene Rosenberg, Kenneth H Keller, and Martin Dworkin. Cell density-dependent growth of myxococcus xanthus on casein. *Journal of Bacteriology*, 129(2):770–777, 1977.

[143] Brandon M Satinsky, Byron C Crump, Christa B Smith, Shalabh Sharma, Brian L Zielinski, Mary Doherty, Jun Meng, Shulei Sun, Patricia M Medeiros, John H Paul, et al. Microspatial gene expression patterns in the amazon river plume. *Proceedings of the National Academy of Sciences*, 111(30):11085–11090, 2014.

[144] Severin J Schink, Elena Biselli, Constantin Ammar, and Ulrich Gerland. Death rate of e. coli during starvation is set by maintenance cost and biomass recycling. *Cell systems*, 9(1):64–73, 2019.

[145] Thomas Schweder, Stephanie Markert, and Michael Hecker. Proteomics of marine bacteria. *Electrophoresis*, 29(12):2603–2616, 2008.

[146] Alan L Shanks and Jonathan D Trent. Marine snow: microscale nutrient patches 1. *Limnology and Oceanography*, 24(5):850–854, 1979.

[147] Alan L Shanks and Jonathan D Trent. Marine snow: sinking rates and potential role in vertical flux. *Deep Sea Research Part A. Oceanographic Research Papers*, 27(2):137–143, 1980.

[148] Orr H Shapiro, Esti Kramarsky-Winter, Assaf R Gavish, Roman Stocker, and Assaf Vardi. A coral-on-a-chip microfluidic platform enabling live-imaging microscopy of reef-building corals. *Nature communications*, 7(1):1–10, 2016.

[149] Kazuyuki Shimizu. Regulation systems of bacteria such as escherichia coli in response to nutrient limitation and environmental stresses. *Metabolites*, 4(1):1–35, 2013.

[150] Mary Wilcox Silver, Alan L Shanks, and Jonathan D Trent. Marine snow: microplankton habitat and source of small-scale patchiness in pelagic populations. *Science*, 201(4353):371–373, 1978.

[151] Meinhard Simon, Alice L Alldredge, and Farooq Azam. Bacterial carbon dynamics on marine snow. *Marine Ecology Progress Series*, pages 205–211, 1990.

[152] Meinhard Simon, Hans-Peter Grossart, Bernd Schweitzer, and Helle Ploug. Microbial ecology of organic aggregates in aquatic ecosystems. *Aquatic microbial ecology*, 28(2):175–211, 2002.

[153] Jonasz Słomka, Uria Alcolombri, Eleonora Secchi, Roman Stocker, and Vicente I Fernandez. Encounter rates between bacteria and small sinking particles. *New Journal of Physics*, 22(4):043016, 2020.

[154] David C Smith, Meinhard Simon, Alice L Alldredge, and Farooq Azam. Intense hydrolytic enzyme activity on marine aggregates and implications for rapid particle dissolution. *Nature*, 359(6391):139–142, 1992.

[155] Steven Smriga, Vicente I Fernandez, James G Mitchell, and Roman Stocker. Chemotaxis toward phytoplankton drives organic matter partitioning among marine bacteria. *Proceedings of the National Academy of Sciences*, 113(6):1576–1581, 2016.

[156] Kwangmin Son, Filippo Menolascina, and Roman Stocker. Speed-dependent chemotactic precision in marine bacteria. *Proceedings of the National Academy of Sciences*, 113(31):8624–8629, 2016.

[157] Sujatha Srinivasan and Staffan Kjelleberg. Cycles of famine and feast: the starvation and outgrowth strategies of a marinevibrio. *Journal of biosciences*, 23(4):501–511, 1998.

[158] Lars Stemmann, Marc Picheral, Lionel Guidi, Fabien Lombard, Franck Prejger, Hervé Claustre, and Gabriel Gorsky. Assessing the spatial and temporal distributions of zooplankton and marine particles using the underwater vision profiler. *Sensors for ecology*, page 119, 2012.

[159] Lars Stemmann, Marsh Youngbluth, Kevin Robert, Aino Hosia, Marc Picheral, Harriet Paterson, Frederic Ibanez, Lionel Guidi, Fabien Lombard, and Gabriel Gorsky. Global zoogeography of fragile macrozooplankton in the upper 100–1000 m inferred from the underwater video profiler. *ICES Journal of Marine Science*, 65(3):433–442, 2008.

[160] Roman Stocker. Reverse and flick: Hybrid locomotion in bacteria. *Proceedings of the National Academy of Sciences*, 108(7):2635–2636, 2011.

[161] Roman Stocker. Marine microbes see a sea of gradients. *science*, 338(6107):628–633, 2012.

[162] Roman Stocker and Justin R Seymour. Ecology and physics of bacterial chemotaxis in the ocean. *Microbiology and Molecular Biology Reviews*, 76(4):792–812, 2012.

[163] Roman Stocker, Justin R Seymour, Azadeh Samadani, Dana E Hunt, and Martin F Polz. Rapid chemotactic response enables marine bacteria to exploit ephemeral microscale nutrient patches. *Proceedings of the National Academy of Sciences*, 105(11):4209–4214, 2008.

[164] Max A Stockslager, Selim Olcum, Scott M Knudsen, Robert J Kimmerling, Nathan Cermak, Kristofor R Payer, Vincent Agache, and Scott R Manalis. Rapid and high-precision sizing of single particles using parallel suspended microchannel resonator arrays and deconvolution. *Review of Scientific Instruments*, 90(8):085004, 2019.

[165] Serina Stretton, Stephen J Danon, Staffan Kjelleberg, and Amanda E Goodman. Changes in cell morphology and motility in the marine vibrio sp. strain s14 during conditions of starvation and recovery. *FEMS microbiology letters*, 146(1):23–29, 1997.

[166] Scott Sutton. Accuracy of plate counts. *Journal of validation technology*, 17(3):42, 2011.

[167] Pavel Svoboda, Eva S Lindström, Omneya Ahmed Osman, and Silke Langenheder. Dispersal timing determines the importance of priority effects in bacterial communities. *The ISME journal*, 12(2):644–646, 2018.

[168] Rachel E. Szabo, Sammy Pontrelli, Jacopo Grilli, Julia A. Schwartzman, Shaul Pollak, Uwe Sauer, and Otto X. Cordero. Ecological stochasticity and phage induction diversify bacterioplankton communities at the microscale. *bioRxiv*, 2021.

[169] Johannes Taktikos, Holger Stark, and Vasily Zaburdaev. How the motility pattern of bacteria affects their dispersal and chemotaxis. *PloS one*, 8(12):e81936, 2013.

[170] Simon Tavaré. The linear birth–death process: an inferential retrospective. *Advances in Applied Probability*, 50(A):253–269, 2018.

[171] JS Terracciano and E Canale-Parola. Enhancement of chemotaxis in spirochaeta aurantia grown under conditions of nutrient limitation. *Journal of bacteriology*, 159(1):173–178, 1984.

[172] Brian J Tibbles and Douglas E Rawlings. Characterization of nitrogen-fixing bacteria from a temperate saltmarsh lagoon, including isolates that produce ethane from acetylene. *Microbial ecology*, 27(1):65–80, 1994.

[173] Mark C Urban and Luc De Meester. Community monopolization: local adaptation enhances priority effects in an evolving metacommunity. *Proceedings of the Royal Society B: Biological Sciences*, 276(1676):4129–4138, 2009.

[174] Lucas J Ustick, Alyse A Larkin, Catherine A Garcia, Nathan S Garcia, Melissa L Brock, Jenna A Lee, Nicola A Wiseman, J Keith Moore, and Adam C Martiny. Metagenomic analysis reveals global-scale patterns of ocean nutrient limitation. *Science*, 372(6539):287–291, 2021.

[175] Amy Veprauskas and Jim M Cushing. A juvenile–adult population model: climate change, cannibalism, reproductive synchrony, and strong allee effects. *Journal of biological dynamics*, 11(sup1):1–24, 2017.

[176] Natalie Verstraeten, Wouter Joris Knapen, Cyrielle Ines Kint, Veerle Liebens, Bram Van den Bergh, Liselot Dewachter, Joran Elie Michiels, Qiang Fu, Charlotte Claudia David, Ana Carolina Fierro, et al. Obg and membrane depolarization are part of a microbial bet-hedging strategy that leads to antibiotic tolerance. *Molecular cell*, 59(1):9–21, 2015.

[177] Jonathan E Visick and Steven Clarke. Repair, refold, recycle: how bacteria can deal with spontaneous and environmental damage to proteins. *Molecular microbiology*, 16(5):835–845, 1995.

[178] George H Wadhams and Judith P Armitage. Making sense of it all: bacterial chemotaxis. *Nature reviews Molecular cell biology*, 5(12):1024–1037, 2004.

[179] Navish Wadhwa and Howard C Berg. Bacterial motility: machinery and mechanisms. *Nature Reviews Microbiology*, 20(3):161–173, 2022.

[180] Maureen A Walling, Jennifer A Novak, and Jason R E Shepard. Quantum dots for live cell and in vivo imaging. *International journal of molecular sciences*, 10(2):441–491, 2009.

[181] Xueming Wei and Wolfgang D Bauer. Starvation-induced changes in motility, chemotaxis, and flagellation of rhizobium meliloti. *Applied and environmental microbiology*, 64(5):1708–1714, 1998.

[182] Matthias Wietz, Bernd Wemheuer, Heike Simon, Helge-Ansgar Giebel, Maren A Seibt, Rolf Daniel, Thorsten Brinkhoff, and Meinhard Simon. Bacterial community dynamics during polysaccharide degradation at contrasting sites in the southern and atlantic oceans. *Environmental Microbiology*, 17(10):3822–3831, 2015.

[183] Tiffany C Williams, Mesrop Ayrapetyan, and James D Oliver. Molecular and physical factors that influence attachment of vibrio vulnificus to chitin. *Applied and environmental microbiology*, 81(18):6158–6165, 2015.

[184] Karina M Winn, David G Bourne, and James G Mitchell. Vibrio coralliilyticus search patterns across an oxygen gradient. *PLoS One*, 8(7):e67975, 2013.

[185] Imke F Wulsten, Alibek Galeev, and Kerstin Stingl. Underestimated survival of campylobacter in raw milk highlighted by viability real-time pcr and growth recovery. *Frontiers in Microbiology*, 11:1107, 2020.

[186] Emily M Yam and Kam W Tang. Effects of starvation on aggregate colonization and motility of marine bacteria. *Aquatic microbial ecology*, 48(3):207–215, 2007.

[187] Yutaka Yawata, Francesco Carrara, Filippo Menolascina, and Roman Stocker. Constrained optimal foraging by marine bacterioplankton on particulate organic matter. *Proceedings of the National Academy of Sciences*, 117(41):25571–25579, 2020.

[188] Yutaka Yawata, Otto X Cordero, Filippo Menolascina, Jan-Hendrik Hehemann, Martin F Polz, and Roman Stocker. Competition–dispersal tradeoff ecologically differentiates recently speciated marine bacterioplankton populations. *Proceedings of the National Academy of Sciences*, 111(15):5622–5627, 2014.

[189] Yutaka Yawata, Otto X. Cordero, Filippo Menolascina, Jan Hendrik Hehemann, Martin F. Polz, and Roman Stocker. Competition-dispersal tradeoff ecologically differentiates recently speciated marine bacterioplankton populations. *Proceedings of the National Academy of Sciences of the United States of America*, 111(15):5622–5627, 2014.

[190] Jinki Yeom and Eduardo A Groisman. Reduced atp-dependent proteolysis of functional proteins during nutrient limitation speeds the return of microbes to a growth state. *Science Signaling*, 14(667):eabc4235, 2021.

[191] C. Yu, A. M. Lee, B. L. Bassler, and S. Roseman. Chitin utilization by marine bacteria: A physiological function for bacterial adhesion to immobilized carbohydrates. *Journal of Biological Chemistry*, 266(36):24260–24267, 1991.

[192] Emily J Zakem, BB Cael, and Naomi M Levine. A unified theory for organic matter accumulation. *Proceedings of the National Academy of Sciences*, 118(6):e2016896118, 2021.

[193] Jonathan P Zehr, Joshua S Weitz, and Ian Joint. How microbes survive in the open ocean. *Science*, 357(6352):646–647, 2017.

[194] Zhong Zhao, Lansun Chen, and Xinyu Song. Extinction and permanence of chemostat model with pulsed input in a polluted environment. *Communications in Nonlinear Science and Numerical Simulation*, 14(4):1737–1745, 2009.

[195] Xiang-Yu Zhuang and Chien-Jung Lo. Construction and loss of bacterial flagellar filaments. *Biomolecules*, 10(11):1528, 2020.

[196] Amy E. Zimmerman, Adam C. Martiny, and Steven D. Allison. Microdiversity of extracellular enzyme genes among sequenced prokaryotic genomes. *ISME Journal*, 7(6):1187–1199, 2013.